



8-2012

Inkjet Printability of Electronic Materials Important to the Manufacture of Fully Printed OTFTs

Sooman Lim

Western Michigan University, sooman.lim@gmail.com

Follow this and additional works at: <https://scholarworks.wmich.edu/dissertations>



Part of the Chemical Engineering Commons, and the Other Engineering Commons

Recommended Citation

Lim, Sooman, "Inkjet Printability of Electronic Materials Important to the Manufacture of Fully Printed OTFTs" (2012). *Dissertations*. 61.

<https://scholarworks.wmich.edu/dissertations/61>

This Dissertation-Open Access is brought to you for free and open access by the Graduate College at ScholarWorks at WMU. It has been accepted for inclusion in Dissertations by an authorized administrator of ScholarWorks at WMU. For more information, please contact wmu-scholarworks@wmich.edu.



INKJET PRINTABILITY OF ELECTRONIC MATERIALS
IMPORTANT TO THE MANUFACTURE OF
FULLY PRINTED OTFTS

by

Sooman Lim

A Dissertation
Submitted to the
Faculty of The Graduate College
in partial fulfillment of the
requirements for the
Degree of Doctor of Philosophy
Department of Paper Engineering, Chemical Engineering, and Imaging
Advisor: Margaret Joyce, Ph.D.

Western Michigan University
Kalamazoo, Michigan
August 2012

THE GRADUATE COLLEGE
WESTERN MICHIGAN UNIVERSITY
KALAMAZOO, MICHIGAN

Date June 4, 2012

WE HEREBY APPROVE THE DISSERTATION SUBMITTED BY

Sooman Lim

ENTITLED Inkjet Printability of Electronics Materials Important to the Manufacture of
Fully Printed OTFTs

AS PARTIAL FULFILLMENT OF THE REQUIREMENTS FOR THE


DEGREE OF Doctor of Philosophy

Paper Engineering, Chemical Engineering, and Imaging
(Department)

Paper and Imaging Science and Engineering
(Program)


Dr. Margaret Joyce
Dissertation Review Committee Chair


Dr. Paul D. "Dan" Fleming
Dissertation Review Committee Member


Dr. Bradley J. Bazán
Dissertation Review Committee Member


Dr. Alexandra Pekarovicova
Dissertation Review Committee Member

APPROVED


Dean of The Graduate College

Date

August 2012

INKJET PRINTABILITY OF ELECTRONIC MATERIALS IMPORTANT TO THE MANUFACTURE OF FULLY PRINTED OTFTS

Sooman Lim, Ph.D.

Western Michigan University, 2012

In this study, the inkjet printability of materials important to fabricating OTFTs was researched. In order to understand the jetting evolution of inkjet printed inks, simulations were performed with a nano copper and nano particle silver ink. To predict the inkjettability of the nano copper ink, Z and Oh numbers at different temperatures were determined. The results from the simulation studies were compared to experimental results obtained using a Dimatix inkjet printer. For the semiconductor ink, the inkjet printability of two organic semiconductors, P2TDC17FT4 (poly[(3,7-diheptadecylthieno[3,2-b]thieno[2',3':4,5]thieno[2,3-d]thiophene-2,6-diyl)[2,2'-bithiophene]-5,5'-diyl] dissolved in 1,2-dichlorobenzene and P3HT (poly-3 hexylthiophene) were compared to determine the relationship between drop speed, drop volume and firing voltage, as well as the influence of drop spacing and substrate temperature on print quality. From these studies, the printability and print quality were sufficient to realize a fully inkjet printed top gate OTFT. The performance of the P2TDC17FT4, printed under ambient conditions, has important implications to the realization of low cost fully printed OTFTs.

As a post processing study, the sintering of a nano copper ink, a promising replacement for silver ink, with IPL (Intensive Pulsed Light) was researched. The relationship between ink film thickness and energy required for sintering was determined. A comparison of the energy levels required for sintering on glass and PET in relationship to ink film thickness is reported and the thermal contribution of the substrate to the processing requirements of this ink is revealed. The findings advance the current understanding of the material property needs and challenges to attaining a fully inkjet printed OTFT.

Copyright by
Sooman Lim
2012

ACKNOWLEDGMENTS

First of all, I praise God's mercy on me. I wish to express my sincere thanks to my advisor Dr. Margaret Joyce for her guidance and help. I am for sure that I could not meet this glorious moment in my life without her supporting. My special gratitude goes to Dr. Paul D. Fleming for his instruction and valuable insight during discussion for my topics. I would like to also express my thanks to Dr. Bradley J. Bazuin and Alexandra Pekarovicova for reviewing my work.

In addition, I would like to say thank to my friends Ahmed, Hemant, Ali and Dania for their help on my researches. And, I thank to all the other friends, especially Ting Chen, and people at Department Paper Engineering, Chemical Engineering and Imaging for making it enjoyable time. Furthermore, I owe my gratitude to all my friends in Korean Student Union and church families in Kalamazoo Korean Church. And, I send many thanks to Dr. Jongtae Youn who introduced me abroad studying and stayed with me whenever I was in trouble.

Finally, I am so happy to see my parents with bright laughter. I hope this dissertation could be a small piece of repayment for their sacrifices for me. I love you.

Sooman Lim

TABLE OF CONTENTS

ACKNOWLEDGMENTS	ii
LIST OF TABLES	vi
LIST OF FIGURES	vii
CHAPTER	
I. INTRODUCTION	1
References	5
II. LITERATURE REVIEW	6
Fundamentals of Inkjet Printing	6
Equation Governing Drop Formation	13
The Jetting Evolution of Inkjet	14
Deposition Dynamics of Colloidal Drops on Non-Porous Media	20
The Intensive Pulsed Light Sintering System	23
UV/Ozone Treatment	24
Inkjetability of an Ambient Stable Organic Semiconductor	25
The Use of OTFTs	25
OTFT Technologies.....	27
Organic Materials used in OTFTs and Deposition Methods .	34
Photolithography.....	39

Table of Contents—continued

CHAPTER

References.....	42
III. STATEMENT OF THE PROBLEM AND OBJECTIVES	47
IV. A STUDY ON THE JETTING EVOLUTION OF NANO COPPER INK AND NANO PARTICLE SILVER INK WITH INKJET	49
Abstract	49
Introduction	50
Experiment	54
Results and Discussion	58
Conclusion	70
References	71
V. INKJET PRINTABILITY ON AN AMBIENT STABLE ORGANIC SEMICONDUCTOR	73
Abstract	73
Introduction	74
Experiment	77
Properties of Materials	77
Design of Experiment for Inkjettability of OSCs	78
Printed OTFTs	79

Table of Contents—continued

CHAPTER	
Results and Discussion	80
Conclusion	97
References	99
VI. INKJET PRINTING AND SINTERING OF NANO COPPER INK	102
Abstract	102
Introduction	103
Experiment	106
Results and Discussion	110
Conclusion	127
References	128
VII. CONCLUSION	130
APPENDIX.....	132

LIST OF TABLES

1. Comparison of Surface Tension Properties of the Inks Used and Surface Energies of the Printed Ink Films	81
2. Parameters of Cross Model and Carreau Models	83
3. The Results of Cross-Model Analysis	114
4. Surface Energy Values of Substrates	115
5. The Experimental Design Followed for Altering the Amount of Energy Applied to the Nano Copper Printed PET Film	117
6. Thermal Properties of Materials	126

LIST OF FIGURES

1. Illustration of different inkjet printing technologies	7
2. Schematic design showing the principles of operation of a continuous inkjet (CIJ) printer.....	8
3. Illustration of single acoustic ejector print head	9
4. Illustration of the piezo movement under an applied voltage.....	10
5. Illustration of a push-mode piezoelectric inkjet print head	11
6. Construction of a traditional piezoelectric squeeze type print head	12
7. Illustration of shear mode drop ejection technology.....	12
8. Influence of the Z number on drop volume, normalized to the volume displaced by the actuator at different driving voltages	14
9. Illustration of ink ejection from a bend type piezo inkjet print head.....	15
10. Examples of different printed line behaviors	17
11. Typical printed line behavior at an intermediate substrate temperature	17
12. The relationship between waveform, piezo element movement and ink ejection with time.....	18
13. Pinned contact line resulting in coffee ring deposits (a). Constant contact angle and mixed mode resulting in moderately more uniform deposits (b).....	21
14. Marangoni effect, where T_c is the CT line temperature, T_a is the drop apex temperature, σ_c is the CL surface tension and σ_a is the drop apex surface tension.....	22

List of Figures—continued

15. History of organic and inorganic semiconductor mobility improvement...	26
16. Schematic of an n-type enhancement MOSFET.....	28
17. Charge transfer characteristics of a FET.....	29
18. Diagram of a bottom-gate OTFT device showing the path of charge carriers from source to drain	31
19. Bottom gate (a and b) and Top gate structure based on p-type semiconductor (c and d).....	33
20. Common semiconductor materials used for the production of OTFTs	35
21. Structure of P3HT after spin-casting	37
22. Illustration of the photolithography patterning process	40
23. Illustration of the inkjet head design created using <i>Flow-3D</i>	57
24. 2D Piezo – inkjetting modeling in accordance with DMP used in this experiment (left, by <i>Flow-3D</i>) and the structural, bottom and cut view of PIJ print head	57
25. Influence of temperature on the calculated Z number (a) and Oh number (b) for the nano copper ink and nano particle silver inks	59
26. Influence of temperature on the $We_{critical}$ for nano copper (a) and nano particle silver inks (b)	60
27. Change in drop ejection speed, V, and Z number with temperature for the nano copper (a) and nano particle silver inks (b).....	62
28. Experimentally applied jetting waveform (a) and simulated pressure in the ink chamber with time (b) for the nano copper ink	64

List of Figures—continued

29. Comparison of drop evolution and drop ejection pictures droplet obtained experimentally and using CFD software for the nano copper ink	65
30. Experimentally applied jetting waveform (a) and simulated pressure in the ink chamber with time (b) for nano particle silver ink	67
31. The evolution of an ejected droplet compared experiment with CFD for nano particle silver ink	68
32. The comparison of simulation results with experimental data obtained by exchanging the waveforms used on each ink.....	69
33. Schematic design of a top gate structure of an OTFT where, light blue, orange, purple, pink, indicate the copper plate, PET, nano particle silver and semiconductor, respectively	80
34. Comparison of the steady state flow sweep profiles for the OSC and P3HT inks	82
35. Waveforms and specific parameters used in each waveform to optimize the jetting of the OSC (a) and P3HT (b) semiconductors inks	86
36. The influence of the firing voltage driving the piezoelectric actuator on the ejected drop volume and velocity. Data for the OSC (a) and P3HT (b) inks jetted at a frequency of 20 kHz are shown.....	87
37. Results from the TGA testing of the OSC ink	89
38. The result of second TGA test with constant temperature 130°C	90
39. Comparison of drop diameters measured after printing the OSC and P3HT inks with different drop speeds	91
40. Line widths for different drop spacings at 6 m/s.	92

List of Figures—continued

41. Captured pictures for OSC (left) and P ₃ HT (right) printed at a drop spacing 30 μm and a drop speed of 6 m/s.....	93
42. Line widths and pictures of P3HT and OSC printed lines.....	95
43. Interdigitated Channel S/D (Line width 238 μm , Channel width 10mm, Channel length 79.7 μm)	96
44. Output characteristics of OTFT printed with OSC ink.....	97
45. Schematic of intensive pulsed light sintering system (a), spectral distribution of the Xenon lamp at 3600 V - 15 Hz setup (b)	108
46. Change in surface tension and viscosity (a), Z number and Oh number (b). 111	
47. The waveform and ink ejection for nano copper ink	113
48. The result of rheological behavior for nano copper ink.....	114
49. Influence of UV/Ozone treatment on PET with time (a) and pictures of printed nano copper ink films (b)	116
50. Optical micrographs of nano copper ink sintered at different applied Xenon lamp energy intensities.....	119
51. SEM micrographs of sintered samples (Magnification $\times 100$).....	120
52. Energy mapping of the 4.2 inch spiral Xenon lamp used	121
53. XRD patterns of nano copper ink printed with different drop spacing (D.S).....	122
54. Surface morphology of unsintered ink film (a) and sintered film (b). All films were printed using at a drop spacing of 10 μm	123

List of Figures—continued

55. Relation between average ink film thickness and required energy for sintering nano copper ink on PET	124
56. Adhesion testing for the sintered nano copper film on PET (a) and glass (b)	125

CHAPTER I

INTRODUCTION

Printed Organic Thin Film Transistors (OTFTs) are appealing to large-area electronic applications such as low cost active-matrix displays, electronic paper and flexible microelectronics.¹ The reason for increased interest in these applications is largely due to the cost advantages of printing, an additive process, over expensive silicon technology, a subtractive process.²

Traditional silicon manufacturing is a subtractive process, hence it is wasteful. It also requires the investment into expensive capital equipment, and due to its complexity, it is a low throughput process. On the other hand, printing is an additive process, which enables high throughput.

In order to determine the feasibility of using solution processable electronic materials to fabricate active and passive electronic devices, various printing techniques have been investigated; inkjet³, flexography⁴, offset⁵. Among the printing processes explored, inkjet printing offers the advantages of not requiring a physical image carrier, because it is a non-impact process.

For Drop-on-Demand (DOD) inkjet printers, droplets are only placed where desired, leading to a decrease in material costs and waste. This makes inkjet printing a

higher throughput, environmentally friendly process, requiring fewer fabrication steps in comparison to traditional photolithography. In addition, inkjet printing provides the opportunity to design and print a product on demand using common graphic software such as Illustrator and Photoshop (Adobe).⁶ The disadvantage to inkjet in comparison to other printing processes is that it requires inks of high fluidity (low viscosity), low specific surface tension, specific particle size ($\leq \sim 150 \text{ nm}$)⁷ and certain drying characteristics to jet and print well. These properties must all be balanced to obtain a desired ink film uniformity, thickness and spreading for a given application. All of these factors affect the electrical performance of the printed ink. However, adjusting the applied voltage, waveform, drop height, drop spacing, and temperature of the substrate and nozzle enable these factors to be altered. Thus, inkjet printing could offer an economically attractive alternative to photolithography.³

In micro-electro-mechanical system (MEMS) processing, a DOD inkjet printer is a suitable device for the manufacture of electronic devices, which require a high print resolution, uniform surface and a thin ink film. Since all these requirements are related to the properties and quality of the droplets fired from the nozzles, an understanding of drop evolution is important for the successful patterning of electronic devices. Since, however, the comprehension of the fluid dynamic behavior of inks during drop ejection is difficult, the use of numerical simulations is of interest as a means to predict drop formation and reduce the experimental time and funds

required to achieve success. In chapter four, commercially available simulation software (*Flow-3D*, Flow Science, Inc.) is used to study the relationship between the jetting evolution of inks and the applied pressure into the ink chamber. By changing the waveform, the displacement of the piezoelectric element in the ink cartridge is altered. This results in different pressures within the ink chamber being applied, which affects the jetting of the inks. The simulation data were compared to experimental data gathered for a nano particle silver ink and nano particle copper ink printed with a Dimatix inkjet printer (DMP 2800, Fujifilm).

Organic semiconductor materials have been researched as alternative materials to inorganic semiconductors and silicon based materials. The interest in organic semiconductors is their solubility in various solvents, making them solution processable and printable⁸. Piezo inkjet is an attractive print method for the fabrication of OTFTs, because it is low cost, applicable to large area processing, compatible with various materials, is a closed system requiring little ink for make-ready and generates little or no waste⁹. The focus of the research described in chapter five was to compare the inkjet printability of an ambient stable semiconductor material (Thiophene-Fused Thiophene Copolymer, OSC) to P3HT (poly-3 hexylthiophene). The properties of both inks were characterized by measuring their surface tension, surface energy and viscosity. The, Z (Oh) number derived from the Re and We numbers was calculated for each material to predict the jetting

performance through the orifice of a Dimatix inkjet printer (DMP-2800, Fujifilm). The relationship between drop speed, drop volume and firing voltage was studied, as well as, the influence of drop spacing and substrate (PET) temperature on print quality. This research shows that the printability and print quality of the OSC is sufficient to realize a fully inkjet printed top gate OTFT.

An alternative, low cost replacement, for silver and gold conductive inks is of great interest to the printed electronics industry. Nano particle copper inks and silver coated nano copper inks are some of the alternative materials of interest, especially in applications where low temperature, low cost, flexible substrates are favored.

Although the inkjettability of nano copper inks and influence on print quality have been reported^{10,11} information regarding the relationship between ink film thickness and the energy required for sintering by intensive pulse light are not yet understood.

An inkjettable nano copper ink was printed on PET and glass and the samples sintered using bursts of high intensity pulsed light. The amount of energy applied determined the degree of sintering among particles. The greater the number of sintered nanoparticles, the higher is the conductivity of the printed traces. A comparison of energy levels required for sintering on glass and PET in relationship to ink film thickness is reported and the thermal contribution of the substrate to the processing requirements of this ink is revealed in chapter four.

References

- 1 C.D. Dimitrakopoulos, D.J. Masearo, IBM J. Res. Dev. 45 11 (2001).
- 2 Ioannis Kyriassis, Organic Field Effect Transistors (Theory, Fabrication and Characterization), ISBN 978-0-387-92133-4, Springer Science Business Media, LLC, (2009).
- 3 H. Sirringhaus, T. Kawase, R.H. Friend, T. Shimoda, M. Inbasekaran, W. Wu, E.P Woo, Science 290 2123 (2009).
- 4 T. Mäkelä, S. Jussila, H. Kosonen, T.G. Bäcklund, H.G.O. Sandberg, H. Stubb, Synt. Met. 153, 285, (2005).
- 5 D. Zielke, A.C. Hübler, U. Hahn, N. Brandt, M. Bartsch, U. Fügmann, T. Fischer, J. Veres, S. Ogier, Appl. Phys. Lett., 87, 123508. (2005).
- 6 Stephan Busato, Alberto Belloli, Paolo Ermanni, Inkjet printing of palladium catalyst patterns on polyimide film for electroless copper plating, Vol 123, pp. 40-846, (2007).
- 7 Veronika Chovancova, Paul Howell, Paul D. Fleming III and Adam Rasmusson, "Color and Lightfastness of Different Epson Ink Jet Ink Sets", J. Imaging Sci. Technol., 49 (6), November/December 2005, 652-659.
- 8 T. R. Hebner, C. C. Wu, D. Marcy, M. H. Lu, and J. C. Sturm, Ink-jet printing of doped polymers for organic light emitting devices, Appl. Phys. Lett., 72, 519, (1998).
- 9 K.E. Paul, W.S. Wong, S.E. Ready and R.A. Street, "Additives jet printing of polymer thin-film transistors", Appl. Phys. Lett. , 0003-6951, 83(10), (2003).
- 10 B. K. Park, D. J. Kim, S. H. Jeong, J. H. Moon, J. S. Kim, Thin Solid Films 515, 7706-7711, (2007).
- 11 H. S. Kim, S. R. Dhage, D. E. Shim, Appl. Phys., A 97: 791-798 (2009).

CHAPTER II

LITERATURE REVIEW

Fundamentals of Inkjet Printing

Printed electronic applications require a higher level of print standards than graphic printing applications. For inkjet printing, there are multiple factors regarding drop properties that must be controlled to obtain good print quality; drop speed, drop volume, drop spacing and drop shape. Drop speed is controlled by the waveform applied. The waveform controls the movement of the piezo element, the duration of the movement and the frequency. Drop speed is reported in m/s. Since a higher drop speed results in a shorter time of flight, the possibility of the drop being disturbed during its travel from the print head to substrate is less. Thus, drop position errors are reduced at high drop speeds. Drop volume is the amount of ink ejected. It is controlled by the waveform and the orifice size of the nozzle. The ideal drop volume depends on the application under consideration, since the volume must meet the performance requirements of the printed layer. Drop volumes for most printed electronic applications typically vary from 2 to 32 picoliters.¹ Drop volume is related to the drop size. For large areas where coverage is needed, large drops (high volume) are desired, whereas for high resolution printing small drops (low volume) are desired.

The variations in drop volume and speed need to stay within a certain percentage of each other, typically around 2 percent, in order to avoid irregularities in the printed object.² In order to achieve a high image quality, it is important that the dot shape on the substrate be uniform. The shape of the dot is influenced by the formation of tails or satellite drops, which are highly undesirable. Furthermore, the droplets must fall in a straight path towards the substrate, typically within 10 mrad accuracy.² Thus, overall, the productivity of a high quality image depends on the stability and setup of the jetting process.

Generally, inkjet printing technology can be classified into continuous (CIJ) and DOD systems as shown in Figure 1.

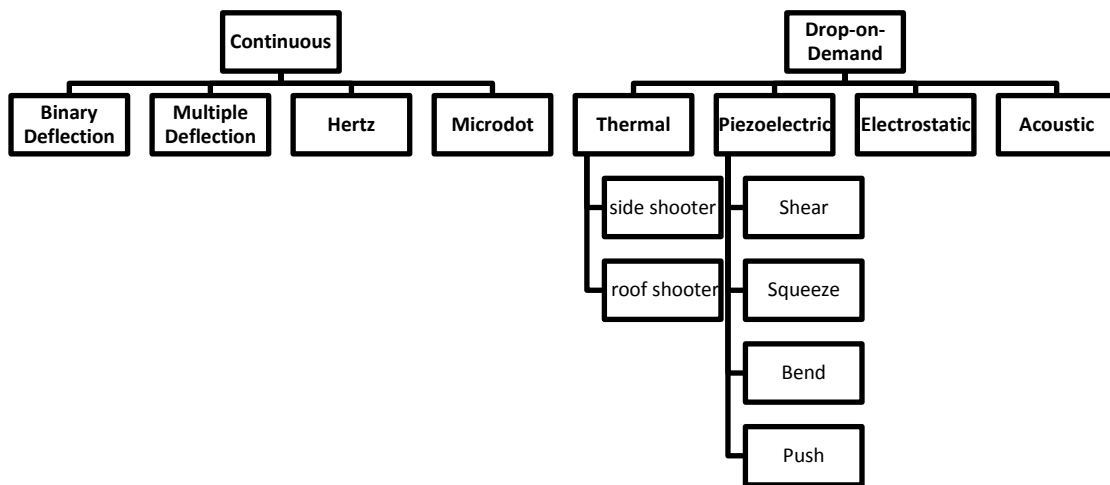


Figure 1. Illustration of different inkjet printing technologies.

Both methods of drop generation are able to produce fluid drops with diameters in the range of 10 to 150 μm . CIJ printing is mainly used in applications where a drop diameter of approximately 40 μm is desired i.e., coding and marking applications, whereas DOD printing is dominant in graphics and printed electronics due to its ability to produce drops of a smaller diameter, typically 20–50 μm . CIJ printing generates a continuous stream of liquid drops even when no printing is taking place. Only uncharged drops fall onto the substrate while the other drops are deflected by an electric field to a gutter to be recycled (Figure 2).

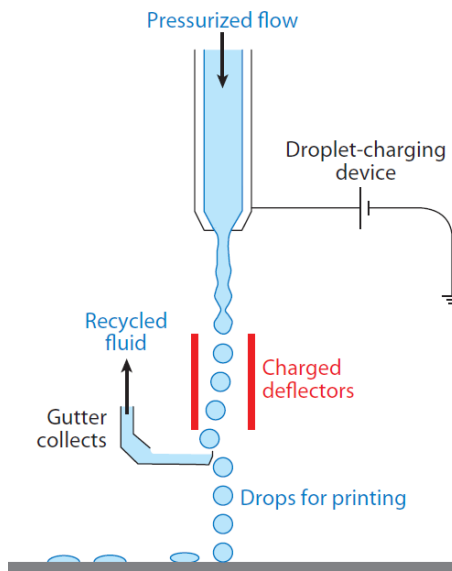


Figure 2. Schematic design showing the principles of operation of a continuous inkjet (CIJ) printer.³

DOD inkjet technology can be divided into thermal, piezo, electrostatic and acoustic technology types. The basic principle of an electrostatic inkjet system is to

generate an electrical field between the inkjet writing system and the substrate. Ink drops are generated by sending image-dependent controlled impulses to the nozzles. These impulses cause a drop to be released and routed through the electrical field onto the substrate. For an acoustic inkjet printer, sound waves are generated, which move toward an acoustic lens when a transducer is excited with RF energy. The lens, attached on the tip of the transducer, focuses the sound waves toward the liquid surface. The impact of the sound burst causes a radiation pressure from the sound wave, resulting in ink drop formation (Figure 3).⁴

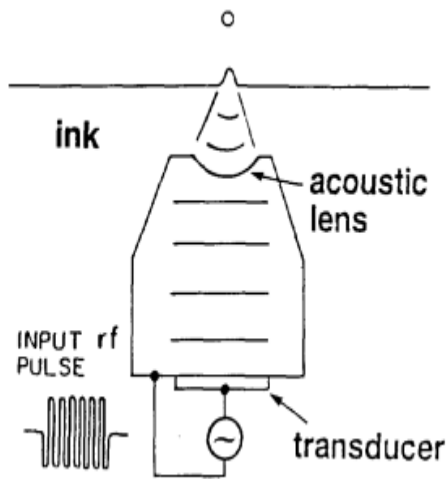


Figure 3. Illustration of single acoustic ejector print head.⁴

Piezo DOD inkjet printers utilized the piezoelectric effect to generate a drop through the mechanical displacement of a piezo element in the ink chamber when a digital image signal is received.

Figure 4 describes the piezoelectric effect, which is the relationship between a mechanical stress and an electrical voltage that can be found for certain materials. When a voltage (signal) is applied to the piezo material, the material distorts according to the level of voltage applied. This mechanical stress generates a pressure in the ink chamber causing the ink to be ejected.

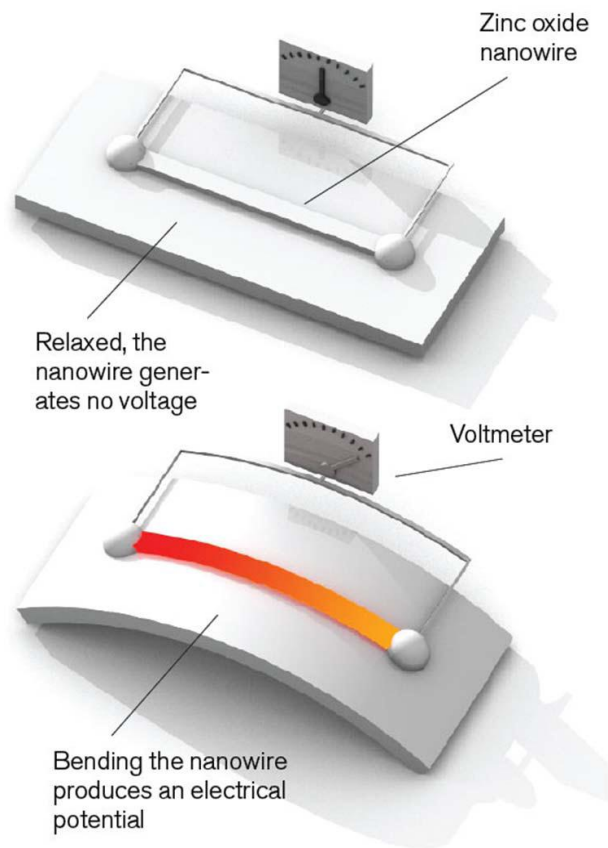


Figure 4. Illustration of the piezo movement under an applied voltage.⁵

In a push-mode design, shown in Figure 5, a piezoceramic rod expands to push against the ink and eject a droplet. In theory, piezodrivers can directly contact and push against the ink. However in practice, a thin diaphragm is incorporated between the piezodriver and ink to prevent any undesirable interactions between the ink and piezodriver materials.

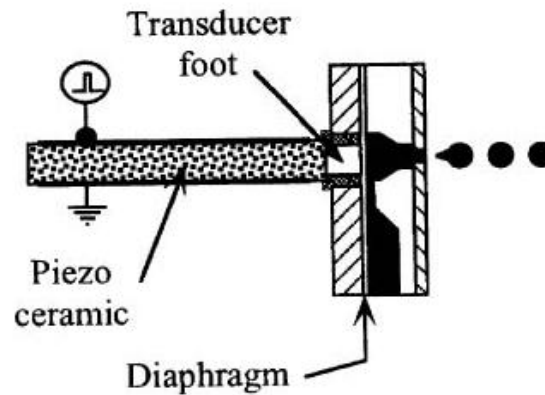


Figure 5. Illustration of a push-mode piezoelectric inkjet print head.⁶

For the squeeze mode shown in Figure 6, a piezoelectric element is fastened to a glass tube with an orifice at one end. When an electrical pulse is received, the piezoelectric element contracts inward. Upon contraction, the glass tube as well as the liquid inside is pressed, resulting in the ejection of droplets.

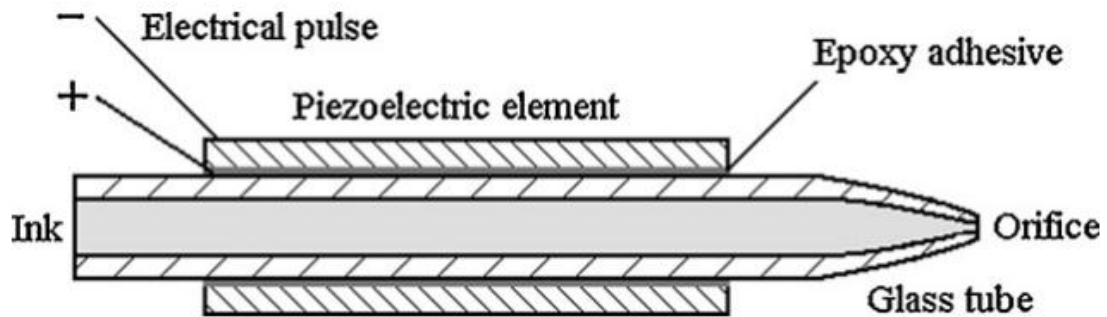


Figure 6. Construction of a traditional piezoelectric squeeze type print head.⁷

A shear-mode print head is shown in Figure 7. The applied electric field is designed to be perpendicular to the polarization of the PZT (Lead Zirconate Titanate) piezo electrical material. Since the PZT elements are uniquely driven in this mode, both pumping and suction actions will occur simultaneously. This means that in this configuration, there is always an effect on the adjacent channels. So, adjacent chambers cannot be used at the same time.

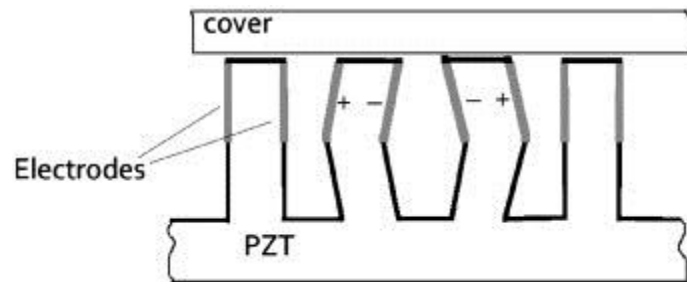


Figure 7. Illustration of shear mode drop ejection technology.⁸

Equation Governing Drop Formation

Fromm⁹ attained an approximate solution to the Navier – Stokes equations to explain droplet formation. As part of the solution, he introduced the dimensionless Z number, defined in Equation 1.

$$Z = \frac{Re}{We} = (d\rho\sigma)^{\frac{1}{2}}/\eta = Oh^{-1} \text{ (Ohnesorge number)} \quad \text{Eq. (1)}$$

where η , ρ , and γ are the viscosity, density, and surface tension of the liquid, respectively, and d is the diameter of the nozzle aperture. According to his study, if the Z number is over 2 then drop formation for a DOD system is possible. Reis et al.¹⁰ demonstrated that if the Z number is between 1 and 10, then drop formation is also possible (Figure 8). The lower limit is controlled by viscosity and the upper limit represents satellite drop formation. In practice, systems where the Z number is much larger than 10 are printable as long as the satellite drops merge with the main droplet before contacting the substrate. Both works showed the main factor appearing to affect printability to be the solvent's vapor pressure.

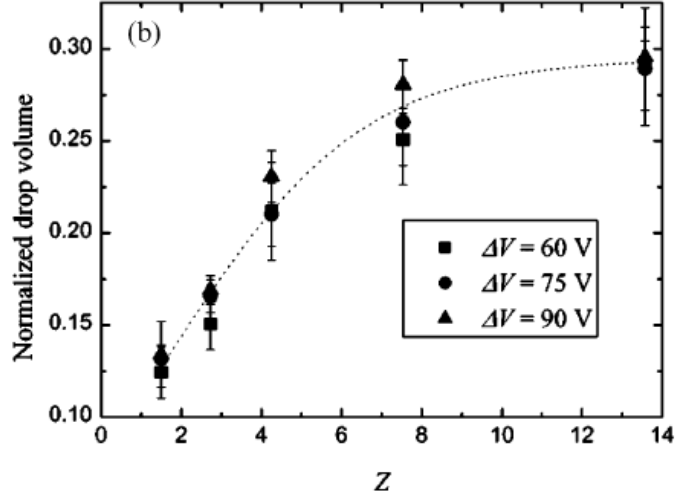


Figure 8. Influence of the Z number on drop volume, normalized to the volume displaced by the actuator at different driving voltages.¹⁰

The Jetting Evolution of Inkjet

Figure 9 illustrates the bend mode piezoelectric effect. The applied voltage signal from a computer distorts the piezo material, which is located in the ink chamber. This action results in the expulsion of ink from the nozzle. The ejected drops follow a ballistic trajectory toward the substrate after leaving the nozzles.

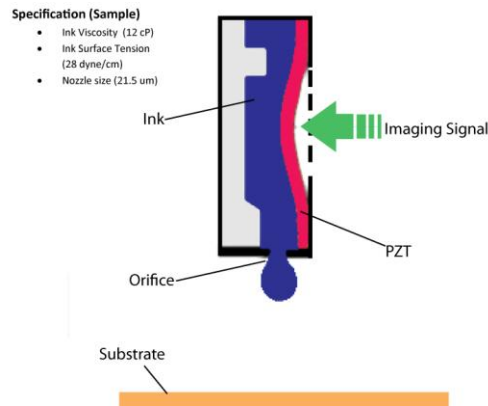


Figure 9. Illustration of ink ejection from a bend type piezo inkjet print head.

There are several advantages in using a piezo inkjet printer. First, there is a high ejection frequency (print speed) and less waste generated than with liquid thermal inkjet. It is also possible to more precisely control the size and shape of the droplet by adjusting the waveform in the software. These are some of the advantages that make inkjet printing a very attractive process for the manufacture of printed electronics.^{11,12,13,14} Liou et al.,¹⁵ showed reasonably good agreement between the drop evolution at the nozzle of a piezo inkjet printer (Epson C45) and computational fluid dynamics (CFD) simulation results. The work focused on how the waveform affects drop formation as the computed droplet volume and velocity were increased with a rise in driving voltage. In order to obtain fine lines, it was found that a reduction in drop speed and nozzle size was needed to decrease ink volume. Moreover, it was shown that adjustments to drop speed eliminated the formation of satellite droplets and that ink puddle formation could be avoided by adjusting the waveform. Ink puddle formation results when the ink covers the orifice, decreasing

the cycle repeatability of inkjet droplet ejection. Air bubbles generated around the nozzles were also found to be an issue affecting the proper ejection of droplets. Jong et al.,¹⁶ using commercial simulation software (*FLOW-3D*), found that reducing the size of the ink particles and lowering the ink film thickness around the orifice prevented the growth of air bubbles. Ink viscosity and surface tension were determined to be the main properties in the inkjet process for good jetting. Through this work, it was shown that all energy is transferred into viscous flow, the surface tension of the drop, and kinetic energy as a drop is expelled.¹⁷ Therefore, for proper ink ejection, it was concluded that the viscosity must be low enough to allow the ink to fill the ink chamber, and the pressure low enough to hold the ink back at the nozzle, without dripping from the nozzle occurring. Nozzle clogging due to ink drying around the orifice was a major concern so it was recommended that a humectant (low-volatility water miscible liquid such as ethylene glycol) be added to the ink at 10-20 % to prevent clogging.

Soltman et al.,¹⁸ found that there is a proper condition in relationship to the temperature of the substrate and the drop spacing of materials (PEDOT/PSS) to obtain a fine and uniform line (Figure 10 and Figure 11). Moreover, they found that there was a greater tendency for a coffee ring effect to occur when droplets are printed onto a heated substrate, as a result of the greater evaporation of the ink at the edges of the printed droplets.

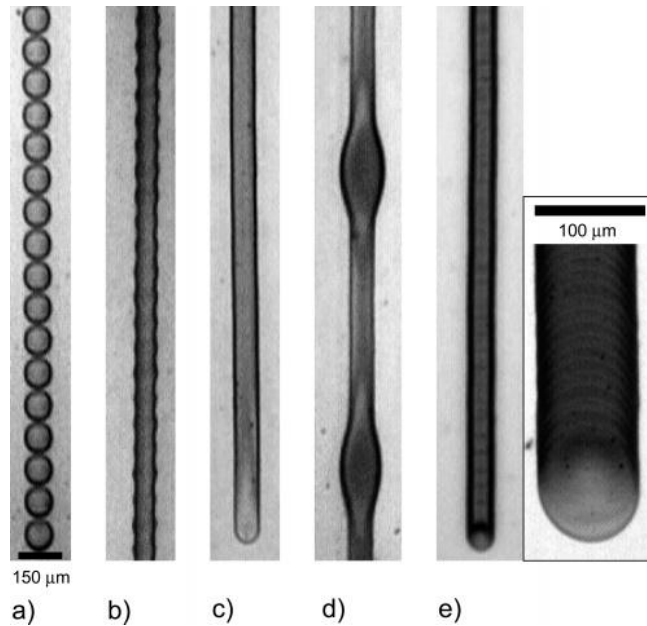


Figure 10. Examples of different printed line behaviors: (a) individual drops, (b) scalloped, (c) uniform, (d) bulging, and (e) stacked coins when the substrate is heated and delayed drop. Drop spacing decreases from left to right.¹⁸

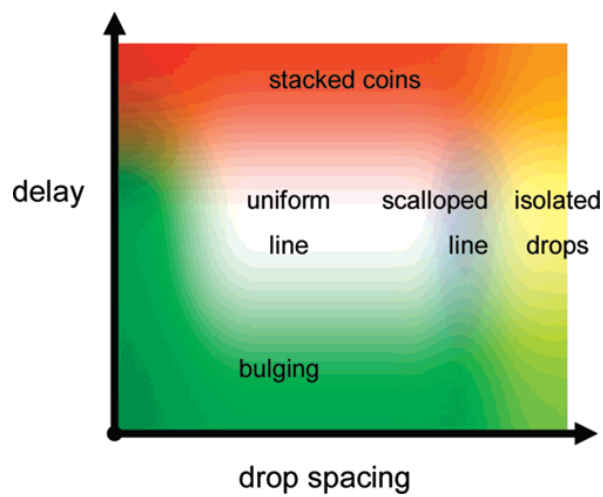


Figure 11. Typical printed line behavior at an intermediate substrate temperature.¹⁸

Sayama¹⁹, et al. studied the relationship between the applied formation waveform and the pressure caused by the waveform as shown in Figure 12. The graph depicts a structured bipolar voltage waveform driving a piezo- electrical material and the computed transient pressure resulting during each of the six time intervals (T1 to T6) shown and separated by colors. In this study, the print head remains 1 mm above a targeted substrate expelling droplets downward under the pressure of the waveforms being sent at a 10 kHz rate.

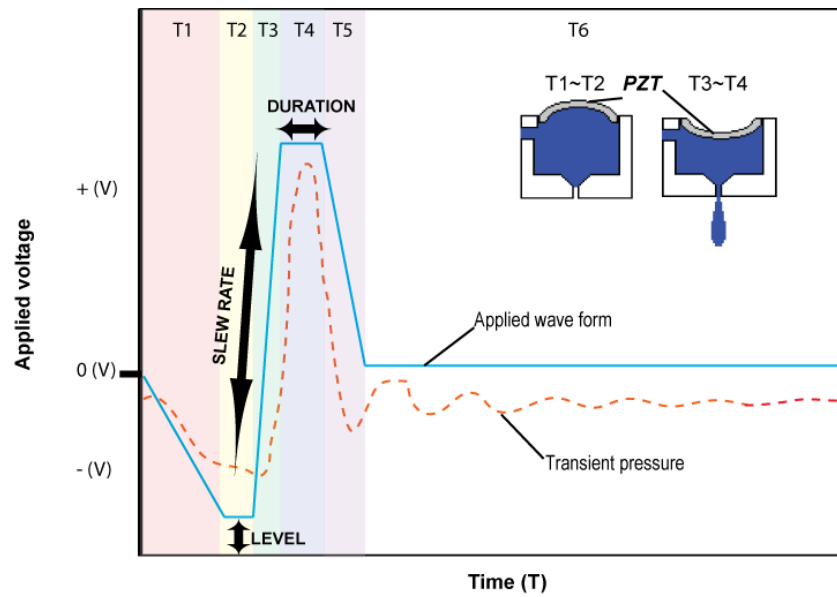


Figure 12. The relationship between waveform, piezo element movement and ink ejection with time.

The six time intervals are classified as follows: 1st recharging (T₁), holding (T₂), discharging (T₃), second holding (T₄), second recharging (T₅), and dissipation time (T₆) with applied voltage (V). The T₁ and T₂ time intervals are the negative

displacement time zones of the PZT that draws fluid into the pumping chamber. Then, the firing pulse (positive displacement) is applied (T_3 and T_4) to the PZT, resulting in the ejection of the ink drop from the nozzle. When the pulse is applied to the PZT, pressure waves inside the channel are created in accordance with the voltage and slew rate of the pulse, leading to the ejection of the ink from the chamber. The pressure waves at first come together toward the middle of the ink chamber from the end of each channel. After the ejection of the ink, a residual pressure variation exists (T_6) that should be dissipated prior to the next waveform and drop formation. There are three main functions that control the PZT; they are the so-called level, slew rate and duration. The voltage level determines how far the piezo material is bent. The slew rate and duration determines how fast the material is bent and how long it stays in that position, respectively. By adjusting those parameters, the ink ejection can be properly controlled.

Since all the issues introduced above are dependent on the controlling waveform, nozzle size and ink properties, theoretically analyzing the drop formation from a print head is necessary in order to understand the process. Therefore, modeling and simulation are useful tools for lowering the cost of experiments and saving time. *FLOW-3D19* modeling software has been used to simulate drop formation processes. It uses VOF (Volume of Fluid) methods to track the location of fluid and solid

surfaces and enables the proper dynamic boundary conditions at those surfaces to be applied and calculated^{20,21,22}

Deposition Dynamics of Colloidal Drops on Non-Porous Media

Since most inks used in printed electronics are colloidal drops printed on non-porous media, drop impingement on the substrate should be considered. When a printed drop makes contact with the surface of a non-porous substrate, rapid drop deformation occurs, followed by spreading to a maximum diameter, followed by either oscillations or complete rebound, which depends on the surface energy of the substrate^{23,24}. Generally, there are two different drop deposition phenomena after drop impingement on the substrate. In the pinned contact line mode, formation of a pinned contact angle initially starts with substrate heterogeneities (mostly for hydrophilic substrates) or roughness. This type of wetting may cause a coffee ring effect to occur due to differences in the evaporation fluxes between the center and edges of the pinned contact line. Differences in the evaporation fluxes result in convection flow of the fluid which carries particles to the edge of the contact line contributing to the coffee ring effect (Figure 13a). In the constant contact angle mode (most common for hydrophobic surfaces), the drop contact line decreases, but the contact angle remains roughly the same because of the similar evaporation rates over the entire drop (Figure 13b).

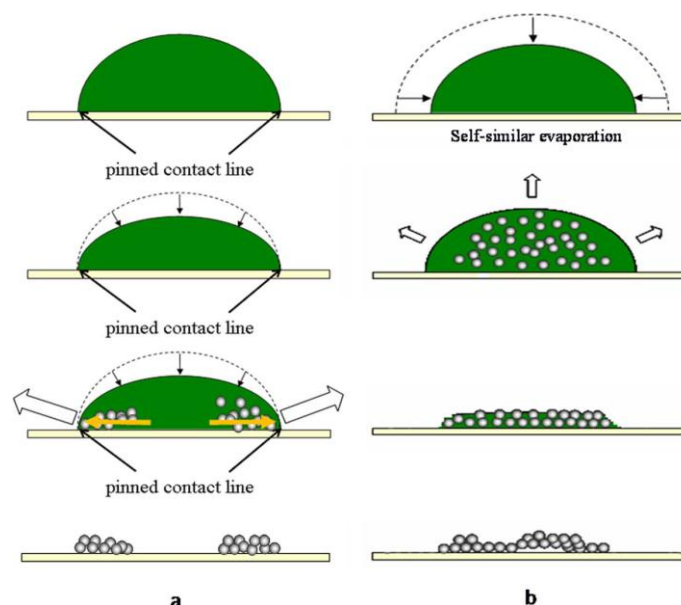


Figure 13. Pinned contact line resulting in coffee ring deposits (a). Constant contact angle and mixed mode resulting in moderately more uniform deposits (b).²⁴

In a dual solvent system, where a mixture of low and high boiling-point liquids is used, the Marangoni effect (Figure 14) is the dominant contributor to the coffee ring effect.^{23,25} Since surface tension is a function of temperature, a non-uniform temperature profile along the drop surface during evaporation sets up corresponding surface tension gradients to drive fluid flow. A Marangoni force establishes itself when there is a gradient in surface tension along a liquid-gas interface, where regions of higher surface tension “pull” the liquid along the interface. Mixing different materials with a large difference in boiling points or vapor pressures is a way to reduce coffee ring effects due to the Marangoni force.²⁵

Functional inkjet inks for printed electronics applications typically consist of two or more solvents. Thus, to prevent coffee ring effects, monitoring and adjustments are necessary, particularly when fluids are printed on PET.

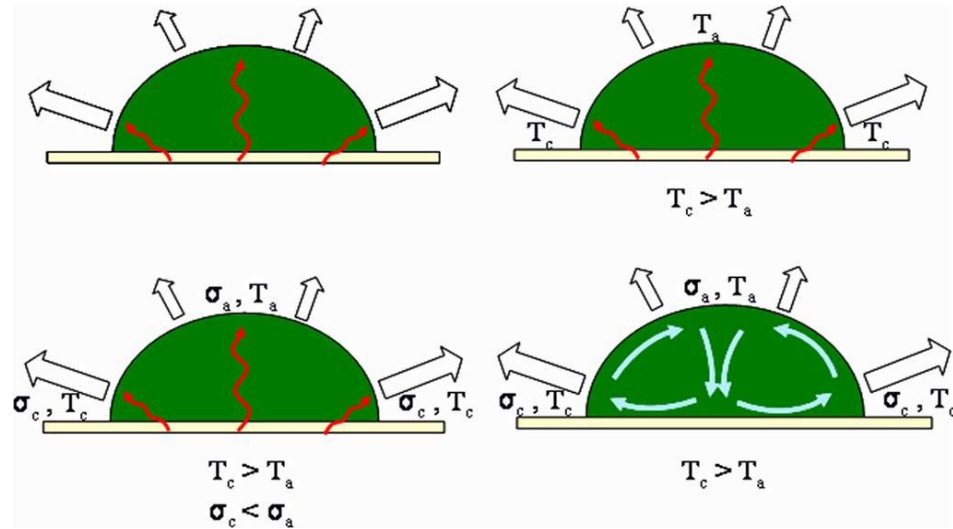


Figure 14. Marangoni effect, where T_c is the CT line temperature, T_a is the drop apex temperature, σ_c is the CL surface tension and σ_a is the drop apex surface tension.²⁴

The Intensive Pulsed Light Sintering System

Inkjet printing has received considerable attention in the field of printed electronics, because of its compatibility with various materials, it being a non-impact additive print method requiring no mask patterning, the low volume of material required (minimal waste) and the low temperature process requirements. This enables a lower cost of fabrication for passive components in comparison to other methods of deposition.²⁶²⁷²⁸ Although novel materials for the fabrication of the electronic devices, such as silver and gold, can be applied by this process, their price, being precious metals, prevents them from being used in low cost, high volume applications.²⁹ This has led to interest in the formulation and development of solution processable copper inks for printing.²⁹ Alternatively, copper metallization has found use in both MEMS and large area electronics, due to its low electrical resistivity $\sim 1.7 \mu\Omega\cdot\text{cm}$ and cost. This has made the use of ultraviolet-curing copper inkjet inks (UV ink) attractive.³⁰ New developments in copper ink technology have resulted in the commercial availability of copper oxide inks, which reportedly transform into a true copper thin-film upon processing with special near UV curing systems in air.²⁹ Depending on the ink manufacturer, inks that can be applied by either screen or piezo-type inkjet print methods have become available for testing.³¹ Kim, et al. studied the use of nano copper ink with Intensive Pulse Light (IPL) to avoid long thermal drying times and the need for high temperature processing.²⁹ The nano copper was deposited on polymer substrates such as Polyethylene (PE) and

Polypropylene (PP) then exposed to a Xenon lamp (PerkinElmer QXA. UK). The effect of various exposure energies to the grain size and resistivity of the ink were studied. With proper exposure energy, the nano copper features had one-third the resistivity as compared to thermal drying, without damage to the substrate.

UV/Ozone Treatment

UV/ozone is a well-known method for cleaning contaminated organic surfaces through the oxidation of functional groups residing on the surface, while also resulting in a change to the energy of the surface.³² This treatment has been applied to various fields. Ton-That et al.³³, and Jo et al.³⁴ demonstrated the ability to increase the spreading and leveling of an organic semiconductor (pentacene) over a printed dielectric treated with UV/ozone. By improving the wetting (coverage) of the semiconductor over the dielectric layer a higher mobility was achieved.³⁴ Besides pentacene, various types of other organic semiconductors were treated with similar results. The common result induced by the use of the UV/ozone treatment was an increase in surface energy^{32,35}, resulting in a lower contact angle (improved wetting and adhesion). Based on these findings, it is expected that the application of a UV/ozone treatment could improve the wetting and leveling of subsequent printed layers possibly leading to the elimination of pinholes or surface non-uniformities that could adversely impact the performance of some printed electronic components.

Inkjetability of an Ambient Stable Organic Semiconductor

The Use of OTFTs

Thin film transistors (TFT) are of importance to various electronic applications such as displays, RFID tags and sensors.³⁶ In displays, TFTs are especially critical to display performance. Traditionally, amorphous or polycrystalline silicon is used for these applications. Though the performance of both materials meet current demands, more desirable alternative materials are being sought, which are lower in cost to manufacture, less rigid and more readily available. For many applications where TFTs are used, the final costs depend more on manufacturing costs than the price of the materials used.²⁸ Thus, materials capable of simplifying the manufacturing process or reducing the number of steps required in the fabrication process would be of great economic benefit. A new generation of materials that do not require chemical or physical vapor deposition processing, but instead could be printed would fill this need. The ability to print OTFTs with high throughput is a prime motivation for examining inkjet printing as a manufacturing process.³⁷

As an alternative to traditional silicon technology, various organic materials have been developed and are being used. Due to improvements in organic material performance over the last two decades (Figure 15), the use of OTFTs has expanded

into areas where beneficial properties such as low temperature processing and low elastic modulus have made them suitable for use with flexible substrates.³⁸

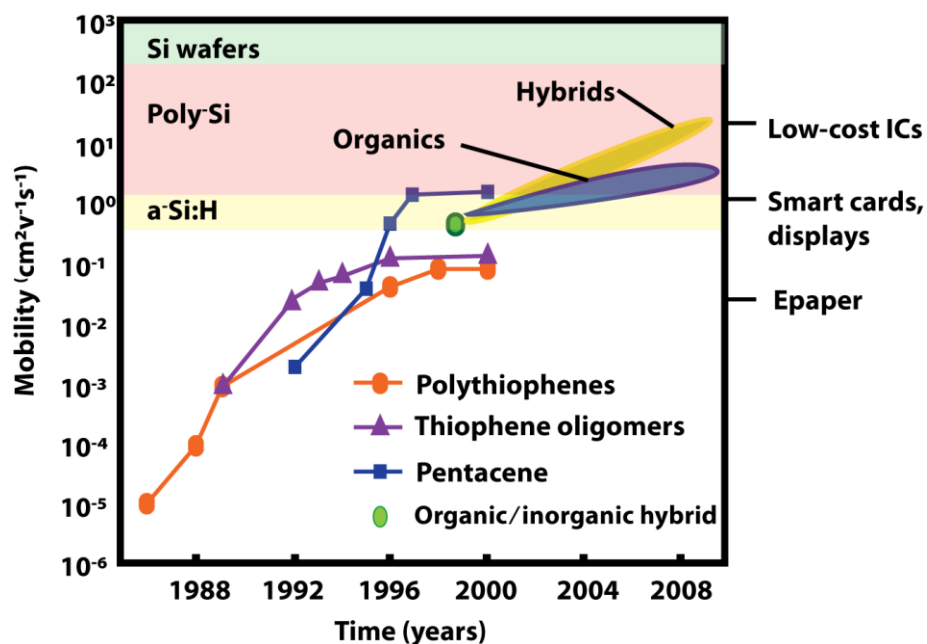


Figure 15. History of organic and inorganic semiconductor mobility improvement.³⁹

Furthermore, the simplicity of additive deposition processing and the improvements in mobility (flow of current, at first, it was $10^{-5} \text{ cm}^2/\text{Vs}$ but now over $1 \text{ cm}^2/\text{Vs}$) have increased the use of OTFTs.⁴⁰ However, despite the benefits described, the number of applications employing OTFTs is still low. This is because the currently available organic semiconductors are very expensive (application volumes are not yet high enough to drive down costs) and the materials lack stability under ambient conditions, which restrict their use to semi-batch or batch manufacturing processes where inert gases or vacuum processing can be employed. As a

consequence, a complete low cost (fully printed) manufacturing process capable of high yields has not been demonstrated, except for a few specialty areas (e.g., OPV). In the absence of large volume consumption, material costs remain unfavorably high. Overall, it is desired to have an ambient stable organic semiconductor suitable for OTFT use that can be deposited efficiently (pinhole free and uniform) at high speeds. The advent of ambient stable, solution processable, high performance semiconductive materials compatible with previous and succeeding printed layers would enable a new generation of low cost roll-to-roll manufacturing technologies to be realized.

OTFT Technologies

The most common types of transistors are the Field Effect Transistors (FET).^{41,42,43,44} An MIS (Metal, Insulator, Semiconductor) capacitor is the main structure in this application. If an oxide is used as the insulator in this type of application, it is called a MOSFET (Metal-Oxide-Semiconductor Field Effect Transistor). The best way to imagine how a FET works is to picture a person holding a magnet behind a piece of paper and moving a piece of iron placed on the other side of the paper with the magnet.³⁷ By this example, when a positive voltage is applied to the gate in an n-channel MOSFET, positive charges are induced on the gate, leading to the push of the majority carrier positive holes contained in the p-substrate (Figure 16) by the repulsive force and the attraction of electron minority carriers.

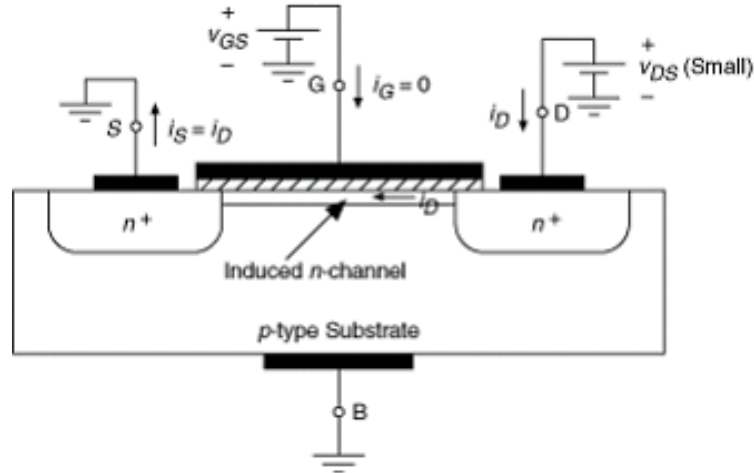
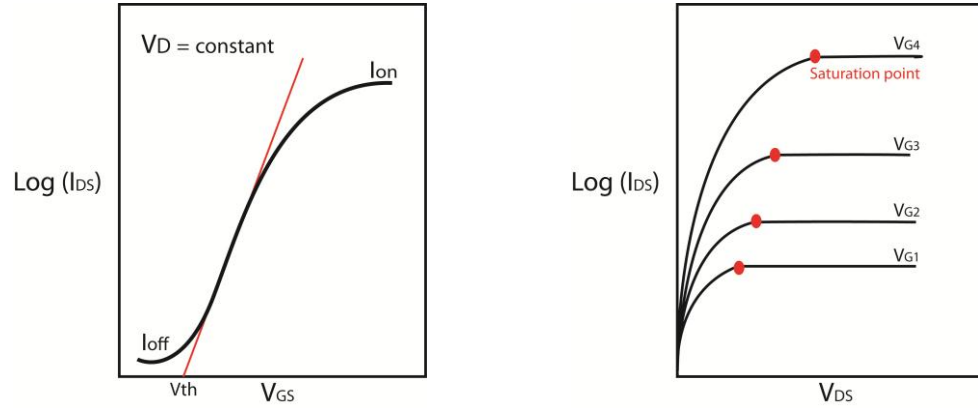


Figure 16. Schematic of an n-type enhancement MOSFET.⁴⁵

This results in an n-channel at the insulator interface, which more readily allows electron passage. The source and drain regions on either side of the channel provide electron majority carriers that can be injected for flow through the channel. The amount of current flow can be adjusted by altering the voltage applied to the gate as it modifies the channel depth and carrier concentration. This is the simple principle for a FET.

In Figure 17, the current flowing between the source and drain, I_{DS} , is expressed in terms of the voltage of the source and drain, V_{DS} , and gate voltage V_{GS} as shown in equation (2)⁴⁶.



(a) transfer characteristic (b) output characteristic

Figure 17. Charge transfer characteristics of a FET.

$$I_{DS} = \frac{W\mu C_i}{2L} (V_{GS} - V_{th})^2 \quad \text{Eq.(2)}$$

where L is the channel length, W is the channel width, C_i is the capacitance per unit area of the insulating layer, V_{th} is the threshold voltage, and μ is an effective field-effect mobility of the semiconductor.

The two electronic characteristics important to the performance of a FET are: transfer characteristics and output characteristics. First is to consider the relation between I_{DS} and V_{GS} , like Figure 17 (a), with fixed V_{DS} . In this process, the effect of gate voltage is transferred to the channel as a field effect. The second graph, Figure 17 (b), shows the change in V_{GS} caused by changes in V_{DS} and I_{DS} . By measuring these characteristics, the performance of a FET can be estimated.⁴⁶ For the transfer characteristics, an understanding of how effectively the V_{GS} can make charges to the

channel is important. By applying a negative or positive charge to the gate, the amount of I_{DS} can be adjusted. This also shows the controllability of V_{GS} to the channel, meaning that a higher slope characteristic is better. However, equation (2) can only be applied if the insulating layer at the channel works properly. Thus, the V_{GS} , which should be over the threshold voltage, may be changed without this assumption. For the output characteristics, it is important that the I_{DS} is saturated over a certain area of V_{DS} , due to the pinch-off effect in which the channel is closed to the drain electrode. It shows that no matter how the V_{DS} is increased, the I_{DS} is maintained. Thus, a constant flow of current can be maintained.

TFTs work similar to MOSFETs. For both, the current between the source and the drain electrodes can be modulated by the gate voltage. However for the TFT, the metal electrodes, source and drain, directly attach to the semiconductor. Also, TFTs do not use a dopant (no p-n junctions)⁴⁵. Instead, the carriers are effectively injected into the electrodes and passes through an accumulation layer channel.

Figure 18 shows the workings of a semiconductor in a TFT. If no voltage is applied, the semiconductor is slightly conductive (considered the off current level). If a negative voltage is applied to the gate, for a p-type semiconductor as shown, holes in the semiconductor are drawn to the interface of the insulator and semiconductor by the field effect, leading to the generation of an accumulation layer. The accumulation layer (channel) allows the holes applied by the source to move more readily through it

resulting in current flow (considered the on current level). Therefore, the gate voltage controls the on/off current flow levels (or on/off ratio) of the TFT in a similar way to a MOSFET gate, but the TFT cannot be fully turned-off like the MOSEFT.

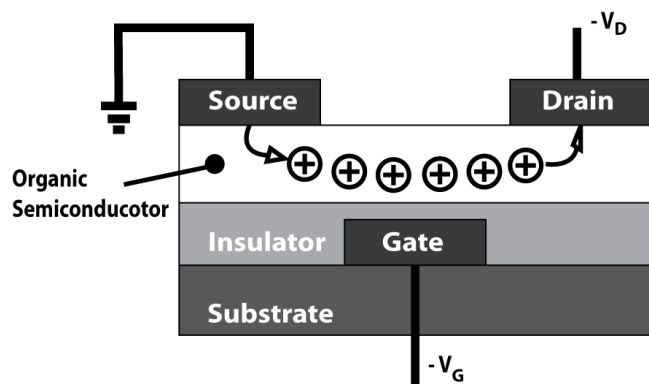


Figure 18. Diagram of a bottom-gate OTFT device showing the path of charge carriers from source to drain.

TFTs can be made with various semiconductor materials. A common material is silicon (a-si, poly-si, micro-si, etc.) Since the primary commercial application of TFTs is in low cost LCDs, it is typically deposited on glass. Although TFTs can be used in many applications because they are thin, it has been shown that the substrate and TFT should have the same crystal structure for highest mobility.^{47,48} In general, OTFTs are TFTs in which the inorganic materials are replaced with organic materials. Although both materials are used, the physical properties by which current flows differ. For organic semiconductors, weak intermolecular van der Waals interactions

($10^{-3} \sim 10^{-2}$ eV), causes an energy gap between the HOMO (highest occupied energy orbitals) and LUMO (lowest occupied energy orbitals) orbitals. This requires the charge carriers to hop between the orbitals for energy transfer, resulting in low mobility. The mobility in an OTFT for polymer and small molecule semiconductors range from $10^{-4} \sim 10^{-2}$ cm²/V s and $10^{-2} \sim 1$ cm²/V s, respectively. For inorganic semiconductors such as Si and Ge, the atoms are held together with very strong covalent bonds (2 ~4 eV), so an energy gap is small enough for transporting charge carriers from the valence band to the conduction band like a free electron, which is called band transport, rather than hopping. As a result, inorganic TFTs have significantly higher mobility (1300 cm²/V s) than OTFTs.

Despite the low mobility in OTFTs, they are still used in many fields because of their low boiling points, which are suitable for low temperature processing applications. Also their solubility in organic solvents, enable them to be applied by solution processable methods such as coating and printing. These characteristics are expanding their use into new application areas where these properties are of benefit.

Figure 19 shows two common OTFT device configurations. The region between the source/drain is called the channel (L) and the length along the channel is called the width (W) (Figure 19a). The transistor state is changed to the on and off stage by applying and removing voltage to the gate. One of the structures for the OTFTs shown is a bottom gate structure where the semiconductor is deposited on the

dielectric (Figure 19a and b). In this structure, the surface of the dielectric affects the quality of the dielectric-semiconductor interface, which will impact the OTFT performance.⁴⁹

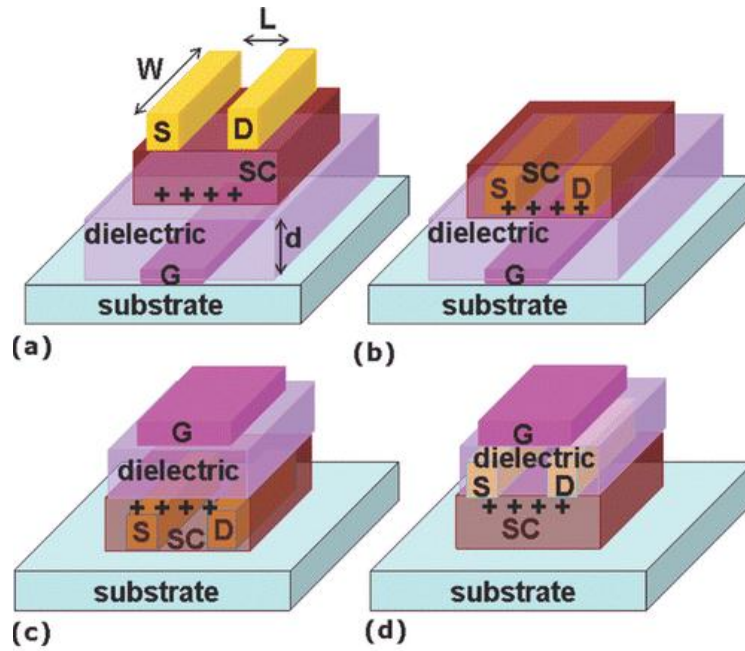


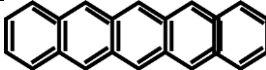
Figure 19. Bottom gate (a and b) and Top gate structure based on p-type semiconductor (c and d).⁵⁰

The other structure shown is a top gate structure where the semiconductor is deposited under the dielectric. This structure can be divided into bottom contact (Figure 19c) and top contact (Figure 19d) structures. In Configuration (d), accumulation in the channel reduces the semiconductor impedance. And, direct contact of the source and drain to the channel minimizes any contact resistance or additional bulk semiconductor (non-channel) impedance. Inherently, the channel

forms at the dielectric/semiconductor boundary. Therefore, the semiconductor material properties at this boundary directly effect performance. Top contact OTFTs typically have the highest performance due to the lower contact resistance between the semiconductor and the insulator. In the bottom contact, however, there is a higher energy barrier because the conjugated organic materials are disordered at the interface with the electrode due to the larger molecular size of the organic material relative to the metal particles (source and drain).⁵¹

Organic Materials Used in OTFTs and Deposition Methods

Figure 20 shows the structures of common semiconductor materials used in transistors. A short description of each type of material is provided below.

Semiconductor	Representative chemical structure	Mobility ($\text{cm}^2\text{V}^{-1}\text{s}^{-1}$)
Silicon	Silicon crystal	300 ~ 900
	Polysilicon	50 ~ 100
	Amorphous silicon	~ 1
Pentacene		10^{-1}

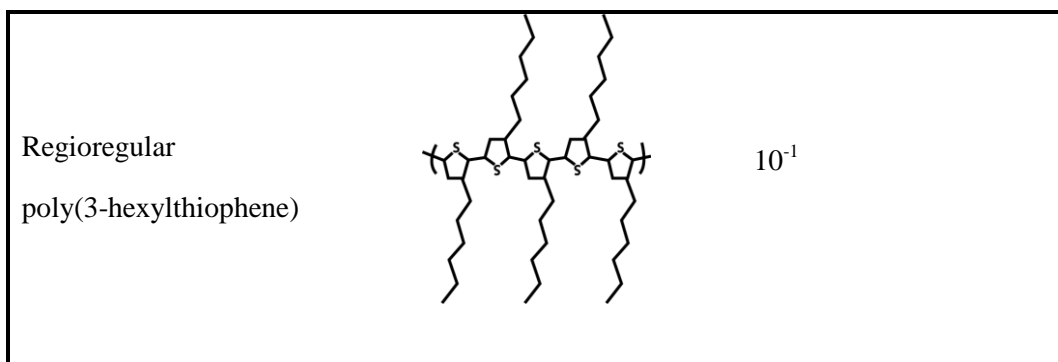


Figure 20. Common semiconductor materials used for the production of OTFTs.³⁹

a. Amorphous silicon (a-Si or α -Si)

Unlike silicon, which is normally bonded to four neighboring silicon atoms, amorphous silicon does not form a continuous crystalline lattice, leading to dangling bonds in the network of the silicon. Since other defects, such as impurities, cannot dramatically affect the overall characteristics of silicon, uniform lines of a-Si can be patterned over large areas.⁵² Another advantage to a-Si is that it can be deposited at very low temperatures (under 75 °C). Thus, a-Si is commonly used for TFT structures in the backplane of displays.

b. Polycrystalline silicon

Polycrystalline silicon is composed of a number of smaller silicon crystals. As a result, the mobility is higher than a-Si and higher doping is possible. However due to its crystalline structure, it is more brittle and requires a higher CVD (Chemical Vapor Deposition) processing temperature than a-Si (at least 300 °C).⁵³

c. Polymer

Polymer semiconductors typically have poor solubility in organic solvents that limit the solvent choices available for solution processing on a commercial scale. The representative material for polymer semiconductors is regioregular poly(3-hexylthiophene) (P3HT). P3HT has relatively good solubility in various solvents, such as tetrahydrofuran (THF), chloroform, chlorobenzene, and p-xylene, which enables its use in small scale laboratory applications, but these solvents are not practical for large-scale industrial use. Another disadvantage to using P3HT is its instability under ambient conditions due to its sensitivity to oxygen and light.⁴⁶ So for best results, P3HT should be processed under inert conditions.⁴⁶

Previous work has shown the ability to reach an On/Off current ratio of 10^6 and mobility of $0.1 \text{ cm}^2/\text{Vs}$ for P3HT.⁵⁴ As for the performance of OTFTs fabricated with P3HT, it was shown that top gate structures had a higher mobility than bottom gate structures where Ta_2O_5 and P3HT were used as the dielectric and semiconductor, respectively. In this structure, the interface between both the dielectric and semiconductor were less disordered in the top gate structure. However, a high off current and the compatibility between semiconductor and insulator were of issue. Depending on how the organic insulator molecules fit next to the polymer structure, organic insulators may be good materials for this structure. This is because the polymer chains align themselves as shown in Figures 21a and 21b.

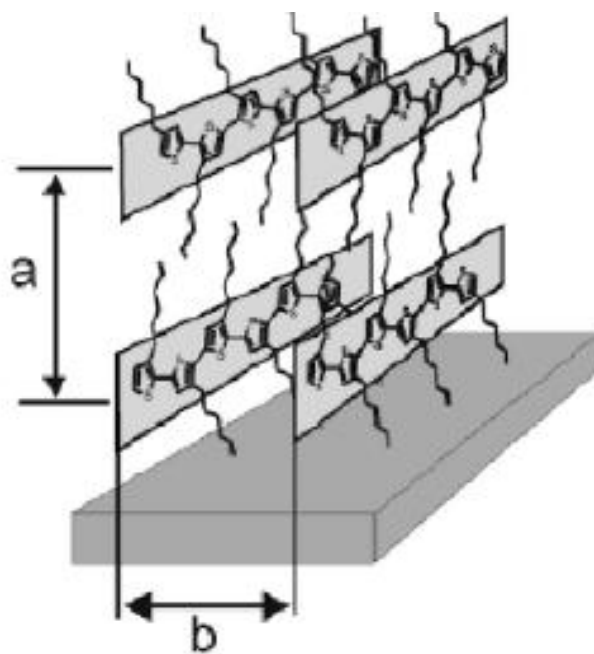


Figure 21. Structure of P3HT after spin-casting.⁵⁵

d. Small molecules

Most of the devices made of small molecules employ pentacene or oligothiophenes and their derivatives⁵⁶. The mobilities of these materials have reached $6 \text{ cm}^2/\text{Vs}$ for pentacene and $1 \text{ cm}^2/\text{Vs}$ for sexithiophene. By improving modifications to the insulator – semiconductor interface. Although a pentacene TFT has a high mobility, it is easily degraded by water vapor, oxygen and various chemical solvents. The solubility of an organic semiconductor in suitable solvents for commercial printing is essential for their use in low cost electronic devices. Unfortunately, all current small molecule semiconductive materials are insoluble, so

their use is limited to application by vapor deposition for thin film production. One other deposition method that can be used is organic vapor phase deposition (OVPD). The principle of OVPD is the same as vapor deposition, except for the use of inactivated N₂ gas for transferring the evaporated molecules to the substrate. OVPD offers good control over film morphology and structural order. However, it is hard to retain a constant film thickness at the surface over a large area and its application time is long.

e. other functional layers

An insulator material serving as a dielectric layer must be of the proper film thickness to prevent shorting, must be pin-hole free, level and smooth, as well as, have the ability to withstand the TFT fabrication process. There are some organic insulators such as PVP (Polyvinylpyrrolidone) and PVAc (Polyvinyl acetate), which have been successfully used for the fabrication of TFTs through application by spin coating.⁵⁷ Electrodes are made of conductive materials such as silver (Ag) and Copper (Cu), which can be deposited by spin coating or directly printing onto substrates. Silver, has been considered as the most effective conductive ink in the field of printed electronics, especially in display applications.^{58,59} In addition, advances in the production of nano Ag particles have made Ag suitable for the printing of micro passive components.⁶⁰ Xue et al.,⁶¹ used Ag as source/drain

electrodes for polymer transistors. The electrode was printed at room temperature using a DOD inkjet printer with an internal nozzle diameter size of 70 μm .

Copper nanoparticle ink is also an attractive material in the fabrication of solution-deposited amorphous semiconductor thin film transistors.⁶² By using two different inks synthesized with PVP of different molecular weights, TFTs were inkjet printed onto a spin-coated tin-doped zinc oxide (ZNO) layer in a bottom gate and top contact structure. It was found that by adjusting the particle size and annealing temperature of the Cu nanoparticle ink the work function could be tuned, resulting in a decrease in energy barrier for electron injection at the interface of electrode and semiconductor.

Photolithography

Traditionally, thermal oxidation or photolithography methods are used for making electronic devices. Photolithography is a technology for transferring patterns onto a substrate. Figure 22 shows an etch-back process in photolithography.⁶³ First, a photoresist is applied over the layer of material to be patterned (Figure 22a). The photoresist is then exposed to light through a photomask that carries the pattern of interest. The exposed portion is then removed by using a developer (Figure 22b). Next, the material is etched away from the unprotected areas (Figure 22c). Finally, the photoresist is stripped off with an appropriate solvent (Figure 22d).

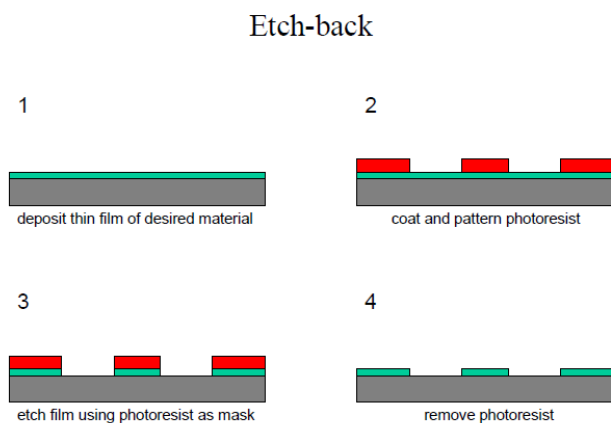


Figure 22. Illustration of the photolithography patterning process.⁶⁴

Although this technique has the advantage of being able to produce high resolution patterning in inorganic materials, the greater number of processing steps and amount of material waste generated in comparison to printing makes this a more costly process than printing. Moreover, the use of solvents in the process can dissolve, crack and swell the organic films being processed.⁶⁵ The overall complexity and wastefulness of the photolithography process has led to the desire to find a lower cost and less wasteful fabrication process. Inkjet printing, being a simple and additive process offers the desired solution. This work seeks to explore the process and material contributions to inkjet printability, print quality and electrical performance of

single and multiple printed layers of functional inks relevant to realizing fully inkjet printed capacitors and OTFTs under ambient conditions.

References

- 1 H. Wijshoff, Océ Technologies B.V., Venlo, Structure- and fluid-dynamics in piezo inkjet print heads, The Netherlands, ISBN 978-90-365-2582-4, (2008).
- 2 R. Derby, J. Appl. Phys., 97, 094903, (2005).
- 3 B. Derby, Annu. Rev. Mater. Res. 40:395–414, (2010).
- 4 B. Hadimioglu, 1051-0117/92/0000-0929 IEEE, (1992).
- 5 K., Bourzac, “Nanopiezoelectronics”, *10 Emerging Technologies*, March/April, 2009 accessed 6/11/12 from:
<http://www.technologyreview.com/article/412192/tr10-nanopiezoelectronics/>.
- 6 H. P. Le, Journal of Imaging Science and Technology 42: 49—62 (1998).
- 7 E.Q. Lia, Q. Xua, J. Suna, J.Y.H. Fuha, Y.S. Wonga, S.T. Thoroddsen, Sensors and Actuators A: Physical, 163 315–322, (2010).
- 8 P. Glynne-Jones, M. Coletti, N.M. White, S.B. Gabriel, C. Bramanti, ActaAstronautica, Vol 67, pp 194–203, (2010).
- 9 J. E. Fromm, “Numerical Calculation of the Fluid Dynamics of Drop-on-Demand Jets”, IBM Journal of Research and Development, , 28, 322, (1984).
- 10 Reis, N.; Ainsley, C.; Derby, B., “Ink-jet delivery of particle suspensions by piezoelectric droplet ejectors”, J. Appl. Phys., 97(9), 094903-6, (2005).
- 11 H. Kipphan, Handbook of Print Media, Springer, (2001).
- 12 H. Sirringhau, T. Kawase, R. H. Friend, T. Shimoda, M. Inbasekaran, Science 290, 2123, (2000).
- 13 J. A. Defranco, B. S. Schmidt, M. Lipson and G. G. Malliaras, Organic electronics 7, 22-28, (2006).
- 14 Li and L. J. Guo, “Organic thin film transistors and polymer light- emitting diodes patterned by polymer inking and stamping”, IOP Publishing Ltd, UK, (2008).

- 15 Tong-Min Liou, Chia-Yen Chan, Kuan-Cheng Shin., Effects of actuating waveform, ink property, and nozzle size on piezo electrically driven inkjet droplets, *Microfluid Nanofluid* DOI 10, 1007/s 10404-009-0488-4, (2009).
- 16 Jong Jos de and Bruin Gerrit de, Air entrapment in piezo-driven inkjet print head, *J. Acoust. Soc. Am.* Volume 120, Issue 3, pp. 1257-1265 (2006).
- 17 Kang, H. R. *J. Imaging Sci.* 35, 179-188, 189-194, 195-201, (1991).
- 18 D. Soltman and V. Subramanian, Inkjet-Printed Morphologies and Temperature Control of the Coffee Ring Effect”, *Langmuir* 24, 2224-2231, (2008).
- 19 Sayama T, Yonekubo S., Device for driving inkjet print head, US Patent 6,074,033, (1998).
- 20 Bogy D. E., Talke F.E., *IBM J Res. Dev.* 28:314–321, (1984).
- 21 Y. Liu, T. Cui, K. Varahramyan, *Solid-State Electronics* 47, 1543-1548, (2003).
- 22 S.M. Bidoki, J. Nouri and A. A. Heidari, IOP Publishing Ltd., 0960-1317, (2010).
- 23 H. Dong, W. W. Carr, and J. F. Morris, “Visualization of drop-on-demand inkjet: Drop formation and deposition,” *Rev. Scientific Instruments*, vol. 77, p. 085101, (2006).
- 24 Abhijit S. Joshi and Ying Sun, “Numerical Simulation of Colloidal Drop Deposition Dynamics on Patterned Substrates for Printable Electronics Fabrication”, *Journal of Display Technology*, Vol. 6, No. 11, 579-585 (2010).
- 25 S. Jeong, D. Kim, and J. Moon, *J. Phys. Chem. C*, 112 (14), pp 5245–5249, (2008)
- 26 C.M. Hong and S. Wagner, “Inkjet Printed Copper/Drain Metallization for Amorphous Silicon Thin-film Transistors”, *IEEE Electron device letter*, Vol, 21, No. 8, pp 384-386, (2000).
- 27 H.J. Lee, S. H. Seo, K.S. Yun, J. W. Joung, I. Y. O and J. G. Yook, “RF performance of CPW Transmission Line Fabricated with Inkjet Printing Technology”, *IEEE*, 978-1-4244-2642-3, pp 1-4, (2008).
- 28 C. D. Dimitrakopoulos, and D. J. Mascaro, “Organic Thin-film Transistors: A review of Recent Advance,” *IBM J. Res. & Dev.*, vol. 45, no. 1, pp 11-27, (2001).

- 29 H.S. Kim, S. R. Dhage and D. E. Shim, “Intense pulsed light sintering of copper nano ink for printed electronics”, Appl. Phys. A 97: 791-798 (2009).
- 30 M. Ishibashi, Y. Hotta, T. Ushiroguchi, R. Akiyama, Y. Kawakami, K. Ohtsu, H. Kiyomoto and C. Tanuma, “Photocurable ink for printing on Metallic and Plastic Substrates”, IEEE Polytronic Conference, 1-4244-1186-6, (2007).
- 31 Intrinsiq Materials, “Products” accessed 6/11/12 from [http://www.intrinsiqmaterials.com/ Products.html](http://www.intrinsiqmaterials.com/Products.html).
- 32 K. Efimenko, W. E. Wallace and J. Genzer, “Surface modification of sylgard-184 poly (dimethyl siloxane) Networks by Ultraviolet and Ultraviolet/Ozone treatment”, Elsevier Science, 0021-9797, (2002).
- 33 C. Ton-That, D.O.H. Teare, P.A. Campbell, R. H. Bradley, “Surface characterization of ultraviolet-ozone treated PET using atomic force microscopy and X-ray photoelectron spectroscopy”, Elsevier Science B.V, 0039-6028, (1999).
- 34 S. J. Jo, C. S. Kim, J. B. Kim, J. H. Kim, M. J. Lee, H. S. Hwang, H. K. Baik and Y. S. Kim, “Surface property controllable multilayered gate dielectric for low voltage organic thin film transistor”, Applied Physics Letters, 93, 083504-1, (2008).
- 35 B. Gongjian, W. Yunxuan and H. Xinghou, “Surface modification of polyolefin by UV light/ozone treatment”, J of Applied Polymer Science, Vol. 60, 2397-2402, (1996).
- 36 Gilles Horowitz, “Organic thin film transistors: From theory to real devices”, J. Mater, Vol. 19, pp 1946-1962, (2004).
- 37 J. K. Song, “Organic film transistor; the main elements for organic electronics”, The Korean Physical Society, Vol. 7, no. 14, pp 21-26, (2005).
- 38 T.H. Huang, H. C. Huang, Z. Pei, Organic Electronics, 11, 618–625, (2010).
- 39 J.M. Shaw, P.F. Seidler, IBM, J. Res. & Dev., Vol. 45, no. 1, (2001).
- 40 B. S. Ong, Y. Wu, P. Liu, S. Gardner, Adv. Mater. 17, 1141, (2005).
- 41 J. Anthony, Chem. Rev. 106, 5028, (2006).

- 42 F. Garnier, R. Hajlaoui, A. Yassar, and P. Srivastava, "All-Polymer Field-Effect Transistors Realized by Printing Techniques," *Science* 265, 1684 (1994).
- 43 J. H. Burroughes, C. A. Jones and R. H. Friend, *Nature* 335,137, (1998).
- 44 T. N. Jackson, American Physical Society Meeting Digest, March (2000).
- 45 "Field Effect Transistors", downloaded from <http://www-ferp.ucsd.edu/najmabadi/CLASS/ECE60L/02-S/NOTES/FET.pdf>, accessed 6/11/2012
- 46 H. E. Katz, "Organic Molecular Solids as Thin Film Transistor Semiconductors, *J. Mater. Chem.* 7, 369, (1997).
- 47 Wang, J., Sun, X., Chen, L. & Chou, S. Y, *Adv. Mater.* 15, 1254 (2003).
- 48 BL Conover and MJ Escuti, "Fabrication and Characterization of an Organic Thin Film Transistor", [http: www.ece.ncsu.edu/oleg/files-wiki/3/33/ModuleFourProcedures.pdf](http://www.ece.ncsu.edu/oleg/files-wiki/3/33/ModuleFourProcedures.pdf)
- 49 Massimo V. Fischetti, Terrance P. O'Regan, "Theoretical Study of Some Physical Aspects of Electronic Transport in n MOSFETs at the 10-nm Gate Length", *IEEE, Transactions on Electron Devices*, Vol. 54, No. 9, (2007).
- 50 T. B. Singh and N. S. Sariciftci, *Annual Review of Materials Research*, Vol. 36: 199-230, (2006).
- 51 H. Klauk, *Organic Electronics: Materials, Manufacturing, and Applications*, ISBN-13: 978-3527312641, Wiley-VCH, (2006).
- 52 Wikipedia, "Amorphous silicon", accessed 6/11/12 from http://en.wikipedia.org/wiki/Amorphous_silicon
- 53 T. Kim, S-M. Suh, S. L. Girshick, M. R. Zachariah, and P. H. McMurry, "Particle formation during low-pressure chemical vapor deposition from silane and oxygen", *J. Vac. Sci. Technol.*, 20, 413-423, (2002).
- 54 Stutzmann, N., Tervoort, T. A., Bastiaansen, K. and Smith, *Nature* 407, 613, (2000).

- 55 H.G.O. Sandberg, G.I. Frey, M.N. Shkunov, H. Sirringhaus, R. H. Friend, M.M. Nielsen and C. Kwnpf, *Langmuir* 18, 10176, (2002).
- 56 D. Li and L. Jay Guo, “Organic thin film transistors and polymer light-emitting diodes patterned by polymer inking and stamping”, IOP Publishing Ltd, (2008).
- 57 J. S. Kim, J. H. Chang, B. Kim, B. K. Ju and J. H. Park, “Characteristics of Organic Thin-Film Transistor with Polymeric Insulator and P3HT by Using Spin-Coating, (2007).
- 58 G. Horowitz, “Organic thin film transistors: From theory to real devices”, *J. Mater.*, Vol. 19 No. 7, (2004).
- 59 J. Doggart, Y. Wu and S. Zhu, “Inkjet printing narrow electrodes with <50 μm line width and channel length for organic thin-film transistors”, *American Institute of Physics*, 94, 163503, (2009).
- 60 M. Mantysalo et al., “Evaluation of Inkjet Technology for Electronic Packaging and System Integration”, *IEEE*, 1-4244-0985-3, (2007).
- 61 Xue, F, Liu Z, Su Y, Varahramyan K, “Inkjet printed silver source/drain electrodes for low-cost polymer thin film Transistor”, *Microelectronics Engineering*, 83, 298-302, (2006).
- 62 Woo, K, Bae C, Jeong Y, Kim D. and Moon J., “Inkjet-printed Cu source/drain electrodes for solution-deposited thin film transistors”, *J. Mater. Chem.*, 20, pp 3877-3882, (2010).
- 63 R. Schoreder, L. A. Majeswski, and M. Grell, *Appl. Phys. Lett.* 83, 3201 (2003).
- 64 R. B. Darling, EE-527: “MicroFabrication”, accessed 6/11/12 from:
<http://www.ee.washington.edu/research/microtech/cam/PROCESSES/PDF%20FILES/Photolithography.pdf>
- 65 J. A. DeFranco, B. S. Schmidt, M. Lipson, G. G. Malliaras, *Organic Electronics*, Vol 7, (1), pp 22–28, (2006).

CHAPTER III

STATEMENT OF THE PROBLEM AND OBJECTIVES

In the manufacturing of OTFTs, inkjet technology is very attractive because solution processable functional materials are suitable for processing by this method. DOD inkjet printing can lower manufacturing costs and the environmental impact of the TFT manufacturing process, because printing, being an additive process is simpler and generates less waste. Since, it doesn't need an imaged plate to carry inks to the substrate like conventional processes, (offset, gravure, flexography, etc.), the time and costs for these materials are saved. In addition, because it is a non-contact print method, ink transfer is not determined by the roughness of the substrate and damage to the printed layers, in the case of multilayer printing, is avoided. Although the throughput of inkjet printers is not as high as roll-to-roll (R2R), gravure or flexography, in applications where high throughput is not needed, its output is suitable. However, there are some disadvantages to inkjet printing; it is relatively hard to deposit thick ink films, nozzle clogging can be a problem, the inks must be low in viscosity (low solids), surface tension must be within an applicable range and coffee ring effects may occur.

The purpose of this study was to analyze the inkjettability and printability of materials used in the fabrication of OTFTs such as electrode, dielectric and organic semiconductor inks. As a first step, the jetting evolution from the nozzle was simulated by using commercial simulation software, resulting in a comprehensive understanding of ink jetting performance on inkjet print quality. From the understanding of the relation between the waveform and drop evolution, the proper waveform for each material to optimize print resolution, surface uniformity and film thickness was determined. In preparation for the deposition of the materials, rheological, surface tension and dynamic contact angle measurements were performed. From these measurements, the drop formation and jetting performance of the inks were simulated using *Flow* - 3D simulation software. During deposition of multiple ink layers, it was determined that a UVO treatment was needed to promote ink adhesion, and improve print quality and compatibility between the layers. From the findings of this research, an understanding of the material and processing challenges to obtaining a fully inkjet printed OTFT was obtained.

CHAPTER IV

A STUDY ON THE JETTING EVOLUTION OF NANO COPPER INK AND NANO PARTICLE SILVER INK WITH INKJET

Sooman Lim, Paul D. Fleming and Margaret Joyce

Department of Paper Engineering, Chemical Engineering, and Imaging,

Western Michigan University

4601 Campus Dr. # A-217

Keyword: Inkjet, Nano copper, Z number, Simulation, Drop formation

Abstract

Drop-on-Demand (DOD) inkjet is considered an important device for MEMS processing. Difficulties in understanding the fluid dynamic behavior of inks during drop ejection have led to the use of numerical simulations to predict drop formation. In this study, simulations were performed to predict and understand the jetting evolution of a nano copper ink and nano particle silver ink. In order to predict the inkjettability of the inks, the Z and Oh numbers were determined at different temperatures. The results from the simulation studies were compared to experimental results obtained using a Dimatix inkjet printer.

Introduction

Recently, as an alternative to conventional R2R contact printing methods, which requires a higher level of process development to overcome the challenges of contact printing at high speeds, various alternative non-contact print methods, especially suitable for micro patterning, have been investigated.¹ Among those being investigated and used is inkjet printing, which has gained acceptance because it does not require a mechanical image carrier, can deposit various materials and is environmental friendly.^{2,3} Inkjet technology has been a part of micro-electro-mechanical system processing (MEMS) for a long time. For these applications, the ejection of fine drops has been well researched.⁴ Thermal and piezoelectric actuation methods are commercially successful technologies among micro drop jetting techniques. However, since thermal actuation may cause changes in the material properties of a functional ink, piezoelectric inkjet (PIJ) technology is preferred for the industrial printing of MEMS.⁵ Piezo DOD inkjet printers are based on the piezoelectric effect. Drops are generated by mechanical displacement brought about by a digital image signal (waveform) sent to the piezo element contained in the ink chamber.

Many researchers have studied the fluid dynamics of DOD printers with numerical methods.^{6,7} Fakhfouri et al.⁸ addressed the propagation of the pressure

wave along the capillary tube and the conversion of the kinetic energy of the liquid jet into surface energy. According to this work, these are the main phenomena governing the jetting process of a piezo type inkjet print head. Both phenomena can be characterized by dimensionless numbers, namely the Ohnesorge number (Oh)⁸ or Z number and the Weber number (We)⁸. With these numbers, the possibility for droplet ejection and the formation of free satellite drops are estimated. In regards to generating a droplet, the calculation of two dimensionless numbers is required to estimate whether proper drop ejection will occur. For proper drop ejection, first, the inertial forces at the orifice of the nozzles must be higher than the surface tension forces of the inks. This corresponds to the definition of the We number, which as shown by Equation 3, is the inertial force over the surface tension force acting on a fluid⁹,

$$We = \text{Inertial force} / \text{Surface tension force} = d \cdot v^2 \cdot \rho \cdot \sigma^{-1} \quad \text{Eq. (3)}$$

where d is the droplet diameter, v is the velocity of the liquid, ρ is the density of the liquid and σ is the surface tension of the liquid. For proper drop ejection, the inertial force should be higher than the surface tension force. Another important rheological parameter is the Reynolds number (Equation 4), Re , which is defined as the kinetic energy over the viscous dissipation energy, where η is the dynamic viscosity of the liquid. For proper drop ejection, this parameter should also be considered,

$$Re = d \cdot v \cdot \rho \cdot \eta^{-1} \quad \text{Eq. (4)}$$

For simplicity, these two numbers are combined into one dimensionless number, the Ohnesorge⁸ number (Equation 5),

$$Oh = \sqrt{We}/Re = \eta \cdot (\rho \cdot \sigma \cdot d)^{-0.5} \quad \text{Eq. (5)}$$

The Z number is the reciprocal of the Oh number (Equation 6),

$$Z = (\rho \cdot \sigma \cdot d)^{0.5} / \eta = Oh^{-1} \quad \text{Eq. (6)}$$

The Z number, introduced by Fromm,⁶ takes a similar approach to the Oh number, providing a valid range for drop formation to occur. Later, Reis et al.,¹⁰ reported that the predicted range for the ejection of concentrated alumina wax suspensions was in the range of $1 < Z < 10$ for a DOD inkjet printing system. At $Z=10$ or higher, satellite drops were formed. In addition, it was demonstrated that the relation between Z number and drop volume was proportional. In regards to the We number, Pilch et al.¹¹ reported that there is no breakup when the We number is smaller than its $We_{critical}$ value (Equation 7),

$$We_{critical} = 12 \cdot (1 + 1.077 \cdot Oh^{1.6}) \quad \text{Eq. (7)}$$

Thus, the required velocity for ejection of an ink from an inkjet head can be calculated.

For many printed electronic applications, silver ink is used, due to its high conductivity and solubility properties in many solvents. However, its expensive price has led to interest in the development of solution processable copper inks for printing. New developments in copper ink technology have resulted in the commercial availability of copper inks, which can be applied by either screen or piezo inkjet print methods. Although both of the inks have gained wide spread use as conductive inks in the field of printed electronics, simulation studies comparing the drop ejection of nano copper ink and nano particle silver ink to experimental inkjetting results have not yet been reported.

In this study, the drop formation of a nano copper (Intrinsiq, CA) and nano silver ink (Inktek, Korea), were simulated and the results compared with experimental data obtained using a laboratory scale piezo type inkjet printer (Dimatix Materials Printer, DMP-2800, Fujifilm). From the ejection mechanism of the ink, the relationships between fluid flow, droplet formation, ejection pressure and motion of the PZT (Lead Zirconate Titanate, a piezoelectric material) element, based upon analysis of the Z number and $We_{critical}$, number were determined. *Flow - 3D*, a commercial simulation software, was used as a simulation tool, because it is a

suitable software package for simulating drop formation processes and printing issues in various engineering applications^{12,13,14 15}.

Experiment

1. Dimensional analysis.

A commercial nano copper ink containing 45 nm diameter particles (10 % Wt, as reported by the supplier) uniformly dispersed in a mixture of Ethane-1,2-diol and n-Butanol and a commercial nano silver ink containing nano silver particles dissolved in alkyl amine were used. In order to predict the inkjettability of the nano copper and nano particle silver ink, Z and Oh numbers for the inks were determined at different temperatures. Since the Z number is a function of temperature, changes in cartridge temperature during the printing process had to be considered. The surface tension at various temperatures was measured using a First Ten Angstrom FTA 200 surface tension analyzer by the pendent drop method. A syringe heater (Newera, NY) was wrapped around the syringe to increase the temperature of the ink, enabling the measurement of surface tensions over a temperature range of 25 to 70 °C. For the viscosity, steady state flow measurements were conducted over the same temperatures range applied during surface tension measurements. A TA instrument RA 2000 rheometer was used to perform temperature ramp studies at a fixed shear rate of 10 s^{-1} . This shear rate was determined to be in the second linear region of the

steady flow curve. The theoretical minimum velocity required for generating drop ejection from a PZT print head was estimated by the dimensional analysis of the $We_{critical}$.

2. Numerical approaches

Flow-3D (Ver. 9.3, Flow science.), commercial software for engineers, was used to solve the numerical equations for simulating the ink ejection from the nozzle of the DMP. The ink was assumed to be incompressible and homogeneous.

Negligible gravity effects were also assumed meaning that the Bond number¹⁶ $\ll 1$ or surface tension was dominant, $Bo = \rho g a^2 / \sigma$, where ρ is the liquid density, γ is the surface tension of the fluid, g is the acceleration of gravity and a is the drop diameter. In this case, fluid properties typically used for inkjet printing were applied such as 1 g/cm³ for density, 100 μ m for drop diameter and 29 dyne/cm for the surface tension, resulting in a Bo number of 0.0033. Non-Newtonian flow was also assumed, with a sharply defined free surface being assumed present during simulation. The governing equations applied were the Navier-Stokes equation and continuity equations (Equation 8) and (Equation 9),¹⁶

$$\rho \frac{D\vec{V}}{D\tau} = \rho \vec{g} - \nabla p + \mu \nabla^2 \vec{V} \quad \text{Eq. (8)}$$

$$\nabla \cdot \vec{V} = 0 \quad \text{Eq. (9)}$$

where $\vec{V} = (u, v, w)$ is the velocity vector, ρ is the mass density, \vec{g} is the acceleration of gravity, p is the pressure, μ is the shear viscosity of the fluid, and τ is a time variable.

In Figure 23, an illustration of the inkjet head design created using *Flow-3D* is shown. Only half of the ink jet geometry was modeled to reduce the computational calculation time because there is a symmetry plane on the left boundary. The top boundary (+ z direction) was a continuative boundary through which the outflow flew out. The bottom boundary (-z direction) was a specified pressure by which various pressures were applied as a function of time. For cylindrical coordinate problems, the mesh is defined in terms of the cylindrical coordinates. An initial maximum time step was set for this case at 100 μs .

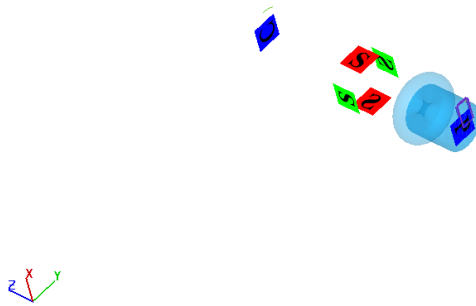


Figure 23. Illustration of the inkjet head design created using *Flow-3D*.

The total ejection length from the nozzle (z direction) used in the simulation was 500 μm and the diameter of the nozzle orifice used was 21 μm , which is the orifice size of the DMP.

Figure 24 shows the 2D modeling (x, z cross sections) designed using the by *Flow 3D* software with the nozzle of the diameter corresponding to the diameter of the nozzle of the DMP. A long channel ink chamber with a nozzle configuration, as shown Figure 24, was the basic geometry used for the inkjet head.

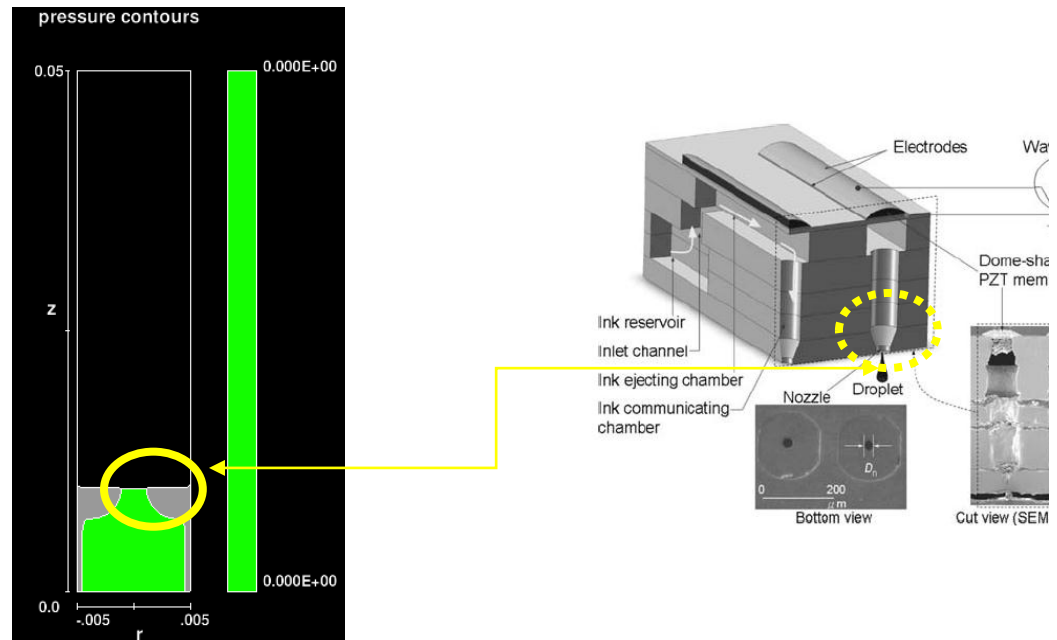


Figure 24. 2D Piezo – inkjetting modeling in accordance with DMP used in this

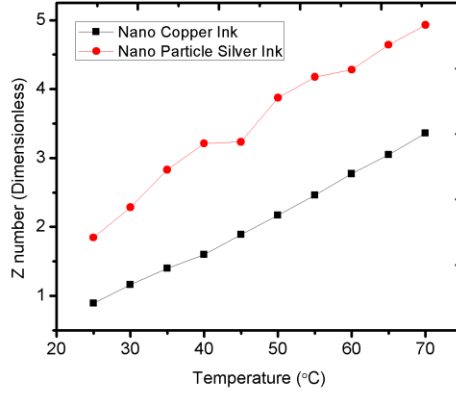
experiment (left, by *Flow-3D*) and the structural, bottom and cut view of PIJ print head.¹⁷

In order to compare the simulation results with the experimental data, the drop evolution progress was recorded using a drop watcher camera on the DMP set to a capture rate of 100 μs . With the recorded images, simulations were performed to determine the set up parameters in the software required to match the experimental results. Specifically, step changes to the applied pressure, which were negative or positive, were followed by waveform adjustments being made. In addition, the changes in the meniscus in the nozzle with time were simulated. These crucial data were then used to prevent the puddling of the ink at the nozzle. From the analysis, it was determined that the evolution and formation of the drops were depicted clearly with the visualized simulation results.

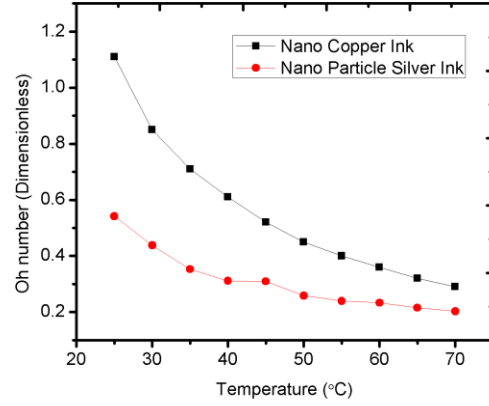
Results and Discussion

1. Dimensional Analysis.

Figure 25 shows the Z and Oh numbers for the nano copper and nano particle silver ink at different temperatures calculated according to Equations 5 and 6 in which a density of 1.0 g/cm^3 and droplet diameter of $21.5 \mu\text{m}$, corresponding to the nozzle diameter, were used.



(a)



(b)

Figure 25. Influence of temperature on the calculated Z number (a) and Oh number (b) for the nano copper ink and nano particle silver inks.

Since the surface tension and viscosity changed with temperature, both of these parameters decreased as the temperature was raised. For the Z number, the range was in between $0.89 < Z < 4.50$ for the nano copper ink and $1.84 < Z < 4.92$ for the nano particle silver ink in the temperature range measured, respectively, as shown in Figure 25. Thus, jetting of the nano copper was predicted to be possible over $25\text{ }^{\circ}\text{C}$ and the nano particle silver ink was predicted to be jettable at $25\text{ }^{\circ}\text{C}$. For the Oh number, since the ratio of We number to Re number was more than 1 at $25\text{ }^{\circ}\text{C}$ for the nano copper ink, it was predicted that it would eject poorly at this temperature. This indeed, was experimentally found.

In Figure 26, the required drop velocity for jetting both inks was calculated using Equation 3. According to the We_{critical} gained by Equation 7, the calculated

minimum velocity was 4.19 m/s and 3.91 m/s at 70 °C and rose to 6.1 m/s and 4.59 m/s at 25 °C for the nano copper and nano particle silver ink, respectively. This change in minimum drop velocity requirement for jetting was caused by the increase in minimum kinetic energy required for drop formation to overcome the stronger intermolecular forces between ink components at the lower temperature.

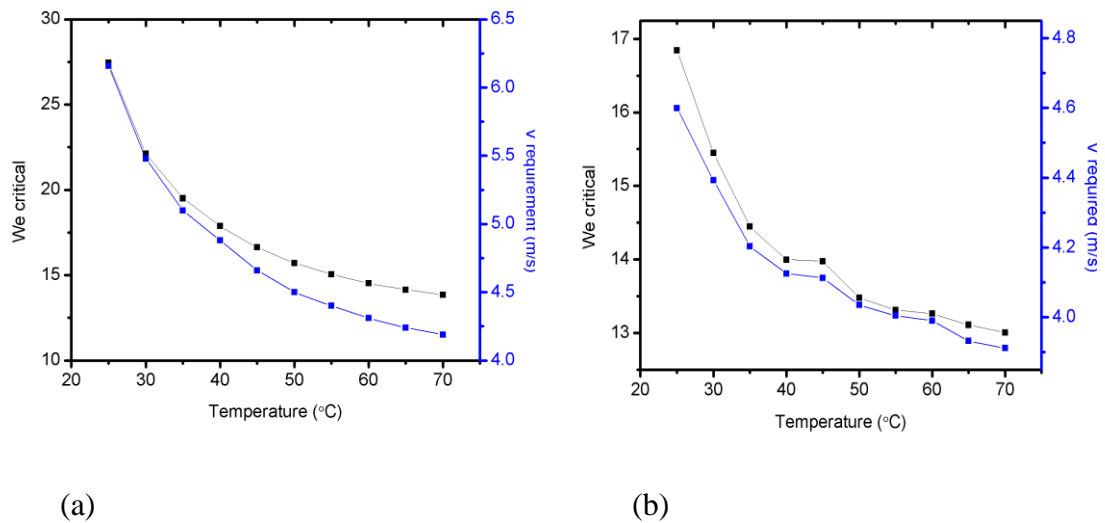
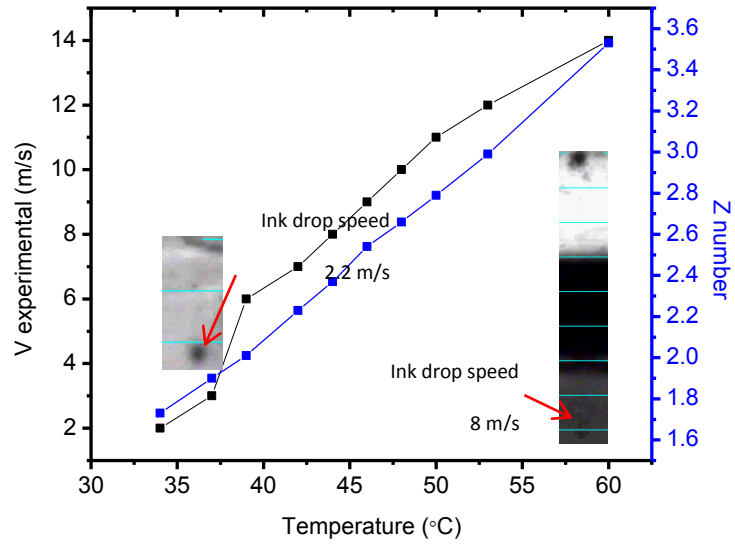


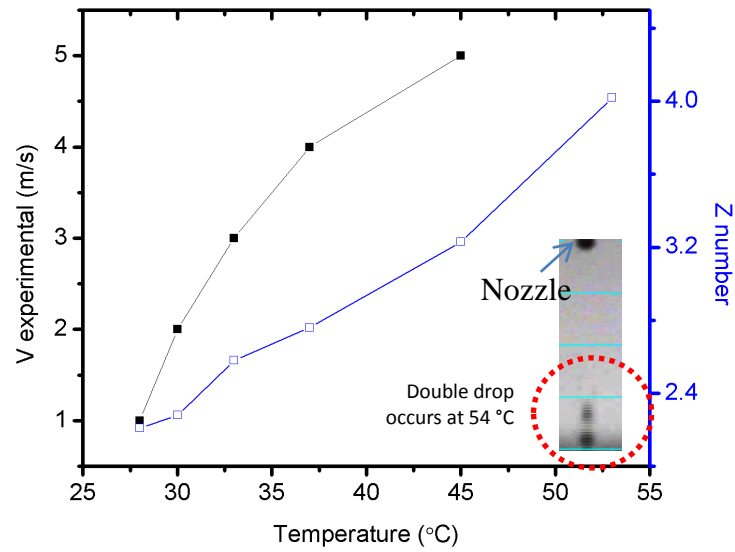
Figure 26. Influence of temperature on the $We_{critical}$ for nano copper (a) and nano particle silver inks (b).

To experimentally validate these predictions, the drop ejection at different cartridge temperatures was recorded using a fixed waveform and meniscus vacuum of 3 inches of H₂O. The conditions used were set based on the recommended standard values to achieve drop ejection for a Dimatix Model Fluid. The applied voltage was 40 V, the maximum value the DMP can generate. For the nano copper ink, jetting

began at 34 °C with a drop speed of 2.2 m/s (Figure 27a). This corresponds to a Z number of 1.16, which falls between Z number range of 1 and 10. Thus, there is good agreement between the dimensional analysis results and experimental data. A similar result was found for the nano particle silver ink, which required a Z number of 2.21. This Z number was achieved with a drop speed of 1 m/s at 28 °C and applied voltage of 40 V. It was also determined that, both jetting speed and Z number were proportional to the temperature applied and that, the size of the drops became finer as the drop speed was increased. The reason for the faster drop speed and smaller drop size with increasing temperature is due to the increase in We and Re numbers caused by the decrease in viscosity and surface tension of the inks.¹⁸ This is supported by the double drops generated at the 54 °C temperature for the nano particle silver ink as shown in Figure 27b. At first, the drop fired from the nozzle has a tail belonging to its main drop. Then, the satellite drop forms when the drop becomes 400 µm long because the intermolecular forces in the drop are weakened by the elevated temperature, resulting in the breaking of the drop.



(a)



(b)

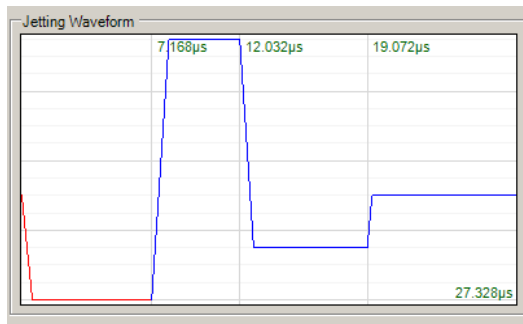
Figure 27. Change in drop ejection speed, V , and Z number with temperature for the nano copper (a) and nano particle silver inks (b).

2. Simulation of jetting evolution.

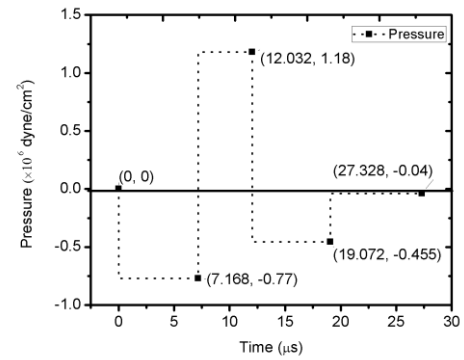
In order to determine the relationship between waveform and the pressure generated from the waveform¹⁹, the jetting evolution was simulated using *Flow-3D* commercial software. For the nano copper ink, the experimental data input into the program was 1 g/cm³ for the density, 28.8 dyne/cm for the surface tension and 18.3 cp for the viscosity at 34°C. Based on these factors, the drop speed was 2.2 m/s at a firing voltage of 40 V.

The applied waveform (Figure 28a) shows the four time intervals classified with displacement for the PZT as follows: first charging (up to 7.168 μ s), discharging (up to 12.032 μ s), second charging (up to 19.072 μ s) and equilibration (up to 27.328 μ s) with applied voltage (V). The first charging time interval is the negative displacement time zone of the PZT that draws fluid into the pumping chamber. Then, the firing pulse (positive displacement, discharging) is applied to the PZT, resulting in the ejection of the ink drop from the nozzle. As a final step to finish a one-cycle ejection, the PZT then returns back to its original position. In addition to the displacement of PZT, there are three main functions that are called; level, slew rate and duration to control the PZT displacement. Level indicates how far the piezo material is bent. Slew rate and duration show how fast the material is bent and how long it stays in that position, respectively. By adjusting these parameters, the ink ejection can be controlled properly. In Figure 28a, the up and down shape, tilting,

and time, indicates the level, slew rate and duration, respectively. However, one thing to note is that there is no universal waveform suitable for both inks due to the variations in their physical and chemical properties.



(a)



(b)

Figure 28. Experimentally applied jetting waveform (a) and simulated pressure in the ink chamber with time (b) for the nano copper ink.

In a piezo inkjet system, the pulse applied to the PZT generates a pressure wave inside the channel no matter how the main functions for displacing the PZT is in operation, leading to the ejection of the ink from the chamber. The resulting pressure for the waveform shown, generated from the simulation software, are shown in, Figure 28b. The pressure generated was obtained by applying various voltages with time. The agreement between these pressures with the experimental data was validated by comparing the drop velocity values with Figure 29 at a specific time.

Figure 29 compares the evolution of a simulated and experimental ejected droplet captured using the drop watcher on the DMP printer.

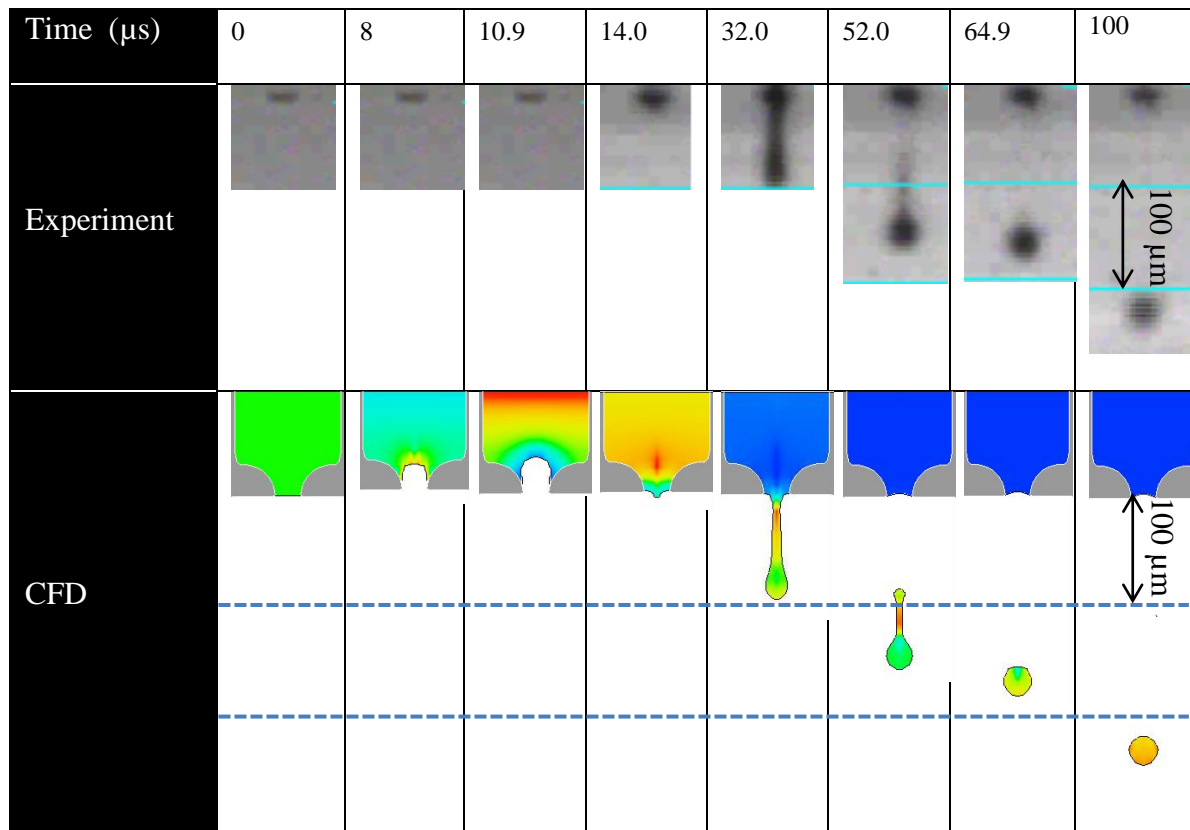
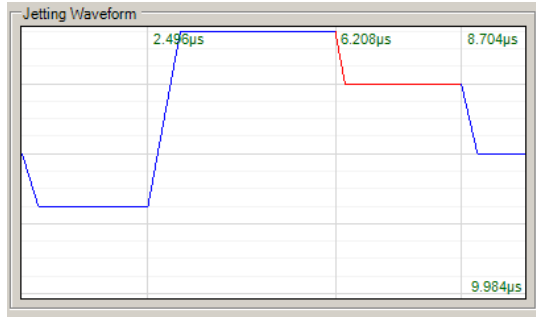


Figure 29. Comparison of drop evolution and drop ejection pictures droplet obtained experimentally and using CFD software for the nano copper ink.

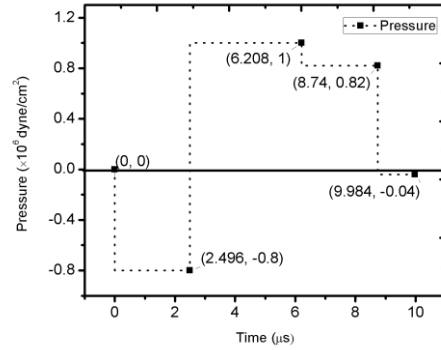
During the time that the reverse pulse (z direction pressure) was applied to the PZT for 7.168 μs in Figure 28b, the PZT was pulled up as much as the applied pulse at 10.9 μs , which resulted in an increase in ink capacity and pulling of the ink meniscus into the ink chamber. Since the PZT was originally pushed down toward the ink chamber, the first step was to apply a negative voltage causing the PZT to pull up,

Then, the PZT was pushed down into the chamber for the time period allowed by the waveform, from 7.168 to 12.03 μs , which led to the ejection of the ink from the nozzle at 13.98 μs . As the ink fell from the nozzle, the column of ejected ink formed a spherical droplet with a tail at 51.98 μs . In addition, the concave meniscus remained constant at the nozzle due to the capillary action within the nozzle. Although the time of z direction pressure began at 7.168 μs , the ejection did not occur simultaneously because the time for the transfer of the pressure waves through the ink was affected by the viscosity, surface tension and density of the ink. At the time of 64.9 μs the tail recoiled into the main droplet to form a complete droplet, as a result of surface tension. Finally, the tail was reunited with the main drop, where it proceeded in free flight before hitting the target at 100 μs .

For the nano particle silver ink simulation, the values of 1 g/cm^3 for density, 27.0 dyne/cm for surface tension and 11.5 cp for viscosity at 28 °C were input to the program. Based on these factors, the drop speed for the jetting waveform was 1 m/s at a firing voltage of 40 V. This corresponds to the condition optimized to bring about an initial ejection from the nozzle like that for the nano copper ink. The experimental waveform used is shown in Figure 30.



(a)



(b)

Figure 30. Experimentally applied jetting waveform (a) and simulated pressure in the ink chamber with time (b) for nano particle silver ink.

Unlike the waveform used for the nano copper ink, the applied waveform in Figure 30a, shows four PZT displacement intervals classified with time as follows: first charging (up to 2.496 μ s), discharging (up to 6.208 μ s), second discharging (up to 8.704 μ s) and equilibration (up to 9.984 μ s) with applied voltage. Since the viscosity of the nano particle silver ink (11.5 cp) was lower than that of nano copper ink (18.34 cp), less time was needed to form a drop, as shown in Figure 30b. Figure 31 shows the evolution of ink ejection with time for the nano particle silver ink. At 7.98 μ s, a high pressure was applied into the chamber, resulting in the pushing of the fluid out from the nozzle.

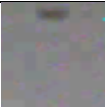
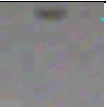
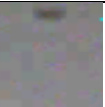

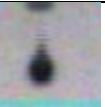
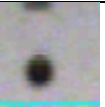
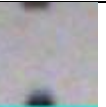
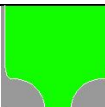
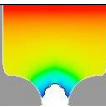
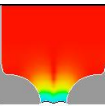
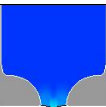
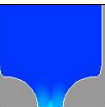
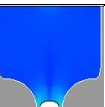
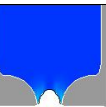
Time (μs)	0	5.01	7.98	51.02	53.98	77.97	100
Experiment							
CFD							

Figure 31. The evolution of an ejected droplet compared experiment with CFD for nano particle silver ink.

Figure 32 shows how the waveform applied for each ink impacted ink ejection.

The waveforms used for each ink were exchanged and the results were compared to the experimental data. The other factors affecting jetting evolution such as firing voltage, cartridge temperature and meniscus vacuum were fixed. The drop evolution simulation result for the nano particle silver ink is compared in Figure 32a to the experimental result obtained at 4.39 μs timing mark and 1.90 μs timing mark in Figure 32b. The evolution of the nano copper ink is based on the waveform used for the nano particle silver ink.

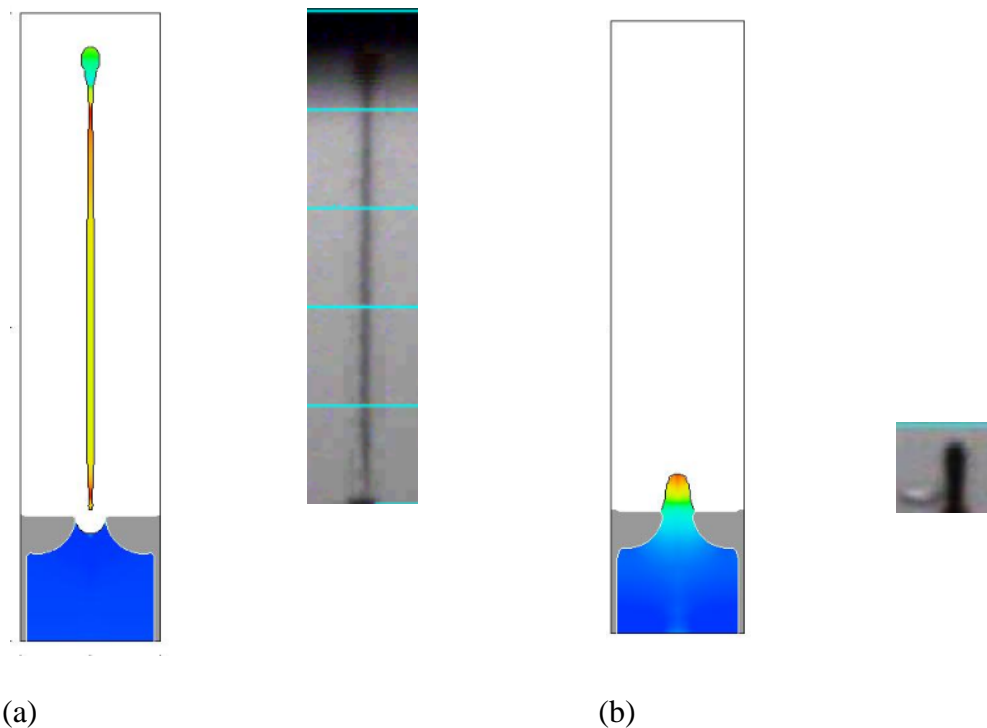


Figure 32. The comparison of simulation results with experimental data obtained by exchanging the waveforms used on each ink.

Although the ink ejection somewhat occurred for the nano particle silver ink with the use of the nano copper waveform, Figure 32a, a long tail tending to be a satellite drop remained during ink flight. For the nano copper ink, there was no ink ejection but instead only a fluctuation in the ink as shown in Figure 32b. Thus, it was verified that the waveform used for a specific ink does not produce the same jetting behavior as when waveforms determined for other inks are used. Instead, a new waveform must often be determined for a given ink used. In addition, the simulation for the nano particle silver ink was in good agreement with the experimental results,

where there was about a 20 μm extension error for the nano copper ink, as shown in Figure 32b.

Conclusion

In order to predict the inkjettability of a nano copper ink and nano particle silver ink, the Z and Oh numbers were calculated at different temperatures. In addition to performing these calculations, a CFD simulation was performed. Based on the results, the CFD piezoelectric inkjet printing results showed reasonably good agreement with the Dimatix inkjet printer. The results demonstrate the relationship between the requirements for pressure and displacement of the PZT element for ink ejection to the viscosity and surface tension of an ink. The evolution and formation of ink drops from a nozzle were clearly depicted by the visualization simulation results obtained.

References

- 1 Ryoichi Ohigashi and Katsunori Tsuchiya, IEEE MEMS 2001, pp.389, (2001).
- 2 A. Rida, L. Yang, R. Vyas, and M. M., “Conductive Inkjet-Printed Antennas on Flexible Low-Cost Paper-Based Substrates for RFID and WSN Applications”, IEEE Antennas and Propagation Magazine, Vol. 51, No.3, (2009).
- 3 Sung-Jun Park, Wonchul Sim, Youngseuk Yool and Jaewoo Joung 1-4244-0140-2/06, IEEE. (2006).
- 4 F. Pan, J. Kubby and J. Chen, “Numerical simulation of fluid- structure interaction in a MEMS diaphragm drop ejector”, IOP publishing Ltd, 0960-1317, (2002).
- 5 Donald J. Hayes et al., SPIE Con. on Micro and Microfab., pp.1. (2001).
- 6 Fromm, J. E., “Numerical Calculation of the Fluid Dynamics of Drop-on-Demand Jets”, IBM Journal of Research and Development, Vol 28, pp. 322 – 333, (1984).
- 7 Shield, T. W., Boggy, D. B., Talke, F. E., “Drop formation by DOD ink-jet nozzles: A comparison of experiment and numerical simulation”, IBM Journal of Research and Development, Vol 31, pp.96-110, (1987).
- 8 V. Fakhfouri, G. Mermoud, J. Y. Kim, A. Martinoli and J. Brugger, “Drop-On-Demand Inkjet Printing of SU-8 Polymer”, Micro and Nanosystems, 1, 63-67, (2009).
- 9 Thomas, G. O. “The aerodynamic breakup of ligaments”, Atomization Sprays, 13(1), 117-129 (2003).
- 10 Reis, N.; Ainsley, C.; Derby, B., “Ink-jet delivery of particle suspensions by piezoelectric droplet ejectors”, J. Appl. Phys., 97(9), 094903-6, (2005).
- 11 Pilch, M.; Erdman, C. A., “Use of breakup time data and velocity history data to predict the maximum size of stable fragments for acceleration-induced breakup of a liquid-drop”, Int. J. Multiphase Flow, 13(6), 741-757, (1987).

- 12 S. M. Lim, J. T. Youn and K. H. Kim, “Computer simulation of ink flow in the conventional gravure cell”, J. Korea Printing Society, vol. 25(1), pp. 109 ~ 120 (2007).
- 13 Chen PH, Peng HY, Liu HY, Chang SL, Wu TI, Cheng CH, “Pressure response And droplet ejection of a piezoelectric inkjet print head”, Int. J Mech. Sci. 41:235–248, (1999).
- 14 Wijshoff H, “Free surface flow and acousto-elastic interaction in piezo inkjet, Proc. Nanotechnol, 2:215–218, (2004).
- 15 J. T. Youn and S. M .Lim, “Computer simulation of dot formation on paper in the gravure”, Korean Society for Imaging Science and Technology, Vol. 14 (1), pp. 62 – 70, (2008).
- 16 Hua Hu, G. Ronald Larson, J. Phys. Chem. B 106, 1334–1344, (2002).
- 17 Tong-Min Liou, Chia-Yen Chan, Kuan-Cheng Shin., Effects of actuating waveform, ink property, and nozzle size on piezo electrically driven inkjet droplets, Microfluid Nanofluid DOI 10, 1007/s 10404-009-0488-4, (2009).
- 18 Ibrahim E, Przekwas A. “Impinging jets atomization. Phys. Fluids A 3(12):2981-2987, (1991).
- 19 Sayama T, Yonekubo S., “Device for driving inkjet print head”, US Patent 6,074,033, (1998).

CHAPTER V

INKJET PRINTABILITY OF AN AMBIENT SATABLE ORGANIC SEMICONDUCTOR

Sooman Lim, Erika Rebrosova and Bradley J. Bazuin

Department of Paper Engineering, Chemical Engineering, and Imaging,

Western Michigan University

4601 Campus Dr. # A-217

Keywords: Inkjettability, Organic Semiconductor, OTFTs

Abstract

The focus of this research was to compare the inkjet printability of two organic semiconductors, P2TDC17FT4 (poly[(3,7-diheptadecylthieno[3,2-b]thieno[2',3':4,5]thieno[2,3-d]thiophene-2,6-diyl)[2,2'-bithiophene]-5,5'-diyl] dissolved in 1,2-dichlorobenzene and P3HT (poly-3 hexylthiophene). The properties of both inks were characterized by measuring their surface tension, viscosity and surface energy after printing. The Z number for each ink was calculated to predict the jetting performance through the orifice of a Dimatix, drop on demand (DOD), inkjet printer (DMP-2800, Fujifilm). The relation between drop speed, drop volume and

firing voltage was studied, as well as, the influence of drop spacing and substrate temperature on print quality. From the results, the printability and print quality of P2TDC17FT4 was sufficient to realize a fully inkjet printed top gate OTFT. The performance of the P2TDC17FT4, printed under ambient conditions, has important implications to the realization of low cost fully printed OTFTs.

Introduction

The printing of electronic inks offers the possibility of producing low-cost, flexible electronic devices.^{1,2} Of particular interest is the use of organic polymers and nanoparticle based inks to produce low temperature processable organic thin film transistors (OTFTs). OTFTs are the basic components of various electronic devices, such as RFID, various sensors and displays.^{3,4} To date, most of the work done has focused on the printing of polymeric semiconductors^{5,6} or solution processable inorganic semiconductors⁷. The regioregular P3HT (poly(3-hexylthiophene)) is the most widely used polymeric semiconductor due to its affordability, solubility and film forming properties, as well as, its controllable electrical properties⁸. The main drawbacks of P3HT are its sensitivity to oxygen and moisture. Therefore, its best performance is typically achieved when processed in an inert atmosphere⁹. The most common solvents used to dissolve P3HT are chlorinated solvents (tetrahydrofuran (THF), chloroform, chlorobenzene, etc.) and some aromatic hydrocarbons (toluene, p-

xylylene, etc.), most of which are not environmentally friendly and may prohibit the use of P3HT on a large manufacturing scale. Although low cost, due to high throughput, is one of the advantages of printing, it rarely reflects the majority of the costs of an end product. Major costs can be incurred if special environmental, processing or drying conditions are needed, i.e., class 100 clean room processing, inert atmosphere. These requirements not only affect capital costs, but also largely affect the speed and cost of the process. Thus, the printing of ambient stable, low temperature, solution processable materials are of great interest.

Inkjet printing technology has improved since its first applications in graphic printing. In recent years, this technology has been adapted in a number of areas of technology as a fabrication tool such as displays¹⁰, plastic electronics¹¹, tissue engineering¹² and 3D printing¹³. The main advantage of inkjet printing is its ability to generate consistent drop volumes in a desired place. This advantage is distinguishable from other conventional deposition methods such as spin coating, spray deposition and dip coating. With this controllable deposition method, various types of electronic components requiring multiple layers such as OLEDs and TFTs can be fabricated.¹⁰ In OTFT fabrication with inkjet, all materials must meet the requirements of chemical stability, good solubility in common solvents, low-temperature processing, and for fully printed devices¹⁴, excellent jetting properties.¹⁵ As for the source and drain (S/D) electrodes, there must be a sufficiently small gap between them to obtain a high

mobility. Doggart, et al.¹⁵ reported the ability to inkjet print an S/D of a transistor with a channel length of 40 μm using a silver based ink. However, the ability to print a channel length less than 30 μm was found to be very difficult without masking. In addition to these requirements, a highly uniform ink film is desired to assure good uniformity within the sequential layers to be deposited. To accomplish this, there are some factors regarding drop properties that must be controlled to obtain good print quality; more specifically drop speed, drop volume and drop spacing.¹⁶ Furthermore, the dot shape printed on the substrate has to be uniform and void of satellite drops, which are controlled by the waveform. It is also important that the droplets fall in a straight path towards the substrate. Thus, overall, the productivity of a high quality image depends on the stability and setup of the jetting process⁸

The purpose of this research was to correlate print conditions to layer formation and image resolution. The work was performed using a new ambient stable organic semiconductor (OSC)¹⁷ and a commercially available semiconductor, P3HT. Such a study has not yet been performed to-date on this OSC. Because this material is of high interest for use in the fabrication of a fully printed OTFT under ambient conditions, results are being sought to better understand the process parameter requirements needed for good print quality to assist in the future fabrication of fully printed OTFT using this new semiconductive material.

Experiment

Properties of Materials

A new semiconductor (P2TDC17FT4 (OSC), Corning) and P3HT (SP001, Merck, UK)) were used as the organic semiconductor materials used in the inkjet printability studies. The OSC ink is from the Alkyl substituted Thienothiophene chemical family. Prior work has shown it to be oxidatively and thermally stable in a bottom gate OTFT structure fabricated under ambient conditions using different deposition methods and materials than reported herein.¹⁸ The P3HT ink was prepared according to the manufacturer's recommended ink formulation procedure. Both inks were degassed prior to printing. The concentration of the P3HT in the ink was 1.0 % by weight and the concentration of the OSC was 0.25% by weight. The properties of the materials were characterized by performing rheology, surface tension and dynamic contact angle measurements. The rheological properties were measured because they are known to be important to achieving proper solution flow, transfer and leveling of the ink during the deposition process. The rheological measurements were performed with an AR 2000 Advanced Rheometer (TA Instruments) using a double couette geometry at 25 °C. The surface tension and wetting properties of the inks and surface energy (Owens-Wendt model)¹⁹ of the PET substrate (Melinex ST505, DuPont Teijin Films) were measured using a First Ten Angstroms (FTA)

dynamic contact angle measuring device. The surface energy of the nano particle silver ink was also measured after printing and drying of the ink on the PET because this is the surface over which a semiconductive material would be printed in the fabrication of a bottom gate of OTFT. The PET film was rinsed with isopropanol and dried before performing all measurements. A thermal gravimetric analyzer, TGA, was used to demonstrate the drying properties of the OSC ink. The drying conditions used for all remaining experiments with this ink were based on the results obtained from these experiments.

Design of Experiment for Inkjetability of OSCs

Both of the inks were printed with a laboratory scale piezo inkjet printer (Dimatix Materials Printer, DMP-2800, Fujifilm) onto PET using a 10 pl cartridge with a nozzle diameter of 21 μm . The relationship between drop speed and drop volume was researched by observing the drops being ejected from the nozzle with a drop watcher camera and drop volume measurement tool installed on the printer. The printed drop diameter was measured after drying in order to determine how the drop speed and drop volume of the ejected ink affected the print properties at different drop spacings. The three drop spacings used were 20, 35 and 50 μm . These spacings were used to print a line of a nominal width of 100 μm . While printing the lines with these drop spacings, the drop height, temperature of the cartridge and plate, drop

frequency and voltage applied to the cartridge remained constant. The print quality of the layers and widths of the printed semiconductor lines were analyzed with an ImageXpert image analysis system. After completion of the inkjettability and printability studies, two-hundred micron nominal lines were printed, using the same drop spacings as above, between the silver electrodes previously printed on the PET to create active channels. A dimensional analysis of the printed samples was performed to determine the amount of drop spreading that occurred during the printing process.

Printed OTFTs

After printing the OSC and P3HT on the silver source and drain (S/D) electrodes, the output characteristic of the OTFT was measured. The silver ink consisted of nano silver particles (InkTec, Korea). To complete the OTFT device, a copper plate was used for the bottom gate and the PET served as the dielectric layer. The structure printed is shown in Figure 33, where the light blue, orange, purple and pink, indicate the copper plate, PET, sub nano silver particle ink and semiconductor, respectively. The order of color indicates the sequence of deposition. An interdigitated channel type of S/D was printed to provide a large active area for the transistor as compared to a single channel design. The Drain current (I_D) vs. Source-Drain voltage (V_{DS}) and Gate voltage (V_G) was measured under a range of voltages

using a Model 2602A Dual-channel System Source Meter Instrument (Keithley Instruments).

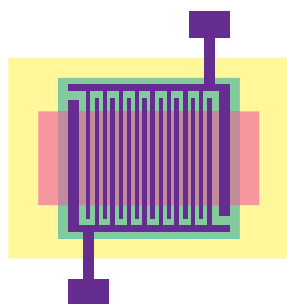


Figure 33. Schematic design of a top gate structure of an OTFT where, light blue, orange, purple, pink, indicate the copper plate, PET, nano particle silver and semiconductor, respectively.

Results and Discussion

1. Ink formulation testing

Table 1 shows the surface tension and surface energies of the OSC and P3HT inks at room temperature. The table also includes the results for the nano particle silver ink used to print the source and drain electrodes.

Table 1. Comparison of Surface Tension Properties of the Inks Used and Surface Energies of the Printed Ink Films

Unit: dyne/cm

Sample	Surface Tension (at 25 °C)	Surface Energy	Polar	Dispersive
Organic Semiconductor Ink	26.7 ±1	36.5	0.4	36.1
P3HT	29.9 ±1.2	33.0	0	33.0
Nano Particle Silver Ink	27.0 ±1	43.9	2.5	41.4
PET	-	43.8	2.3	41.8

The suggested range of ink surface tension for printing with the 10 pl nozzle of the Dimatix printer is 28 – 33 dynes/cm. Thus, as shown in Table 1, the materials were close to the required range. For an ink to wet a substrate, its surface tension should be 10 dyne/cm lower than the surface energy of the substrate.²⁰ Based upon this understanding, good wetting was expected between the inks and PET substrate. Figure 34 shows a comparison of the rheological properties of the semiconductive inks used.

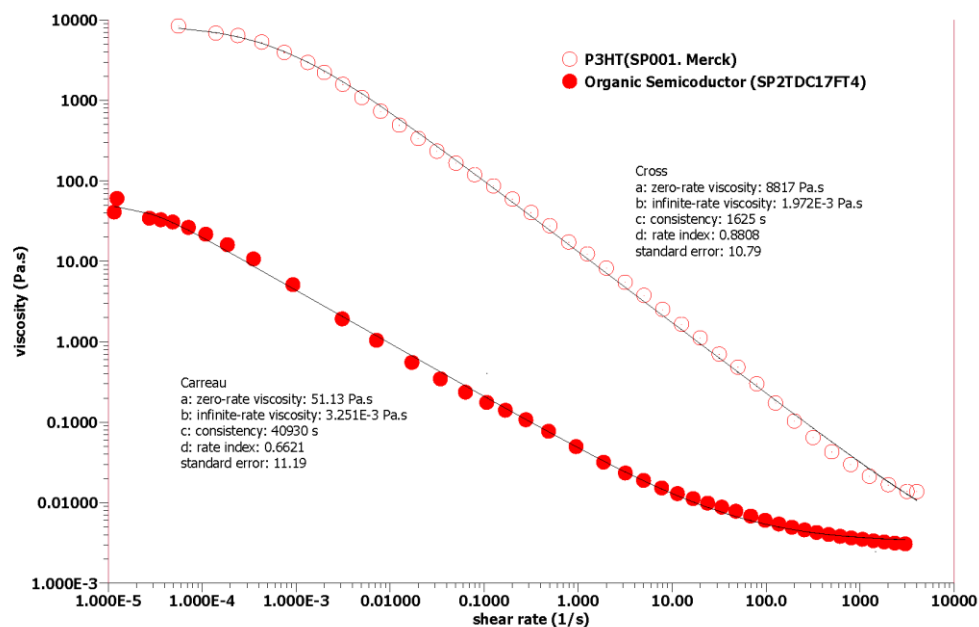


Figure 34. Comparison of the steady state flow sweep profiles for the OSC and P3HT inks.

Among the various types of flow models that can be used, the best fit for each ink was found using the Cross and Carreau model for the P3HT and OSC inks, respectively.^{21,22} These models combine the low shear viscosity, η_0 , high shear viscosity, η_∞ and shear thinning portions of the curve with a two parameter power law relationship. Other parameters of the model, shown below, include K, known as the characteristic time of the material and m, degree of shear thinning. Results from the Cross model (10) and Carreau (11) model fits are summarized in Table 2.

$$\eta = \frac{\eta_0 - \eta_\infty}{[1 + (K\dot{\gamma})^m]} + \eta_\infty \quad (10)$$

$$\eta = \eta_\infty + (\eta_0 - \eta_\infty)[1 + (\lambda\dot{\gamma})]^{m-1/2} \quad (11)$$

Table 2. Parameters of Cross Model and Carreau Models

Sample	η_0 [Pa.s]	η_∞ [Pa.s]	$K(\lambda)$ [s]	m	Standard Error (%)
P3HT	8817	1.972E ⁻³	1625	0.8808	10.79
OSC	51.13	3.151E ⁻³	40930	0.6621	11.19

For good jetting, a shear thinning behavior, as found, is desired.²³ As shown, the viscosity of the P3HT is higher than the OSC viscosity over the entire shear regime. This indicates that more kinetic energy will be needed to eject the P3HT ink from the ink chamber than for the OSC ink. The viscosity of P3HT and OSC was 10.3 and 4.8 cp at a shear rate of 200 s⁻¹, respectively, which is close to the onset point of the second linear plateau shear region for the OSC ink.

In order to predict the jetting stability of the inks, the Z numbers were calculated. The Z number (or Oh number) is a dimensionless expression (14) derived from the Reynolds (*Re*) number (12) and Weber (*We*) numbers (13).²⁴

$$Re = d \cdot v \cdot \rho \cdot \eta^{-1} \quad \text{Eq. (12)}$$

$$We = \text{Inertial force} / \text{Surface tension force} \quad \text{Eq. (13)}$$

$$= d \cdot v^2 \cdot \rho \cdot \sigma^{-1}$$

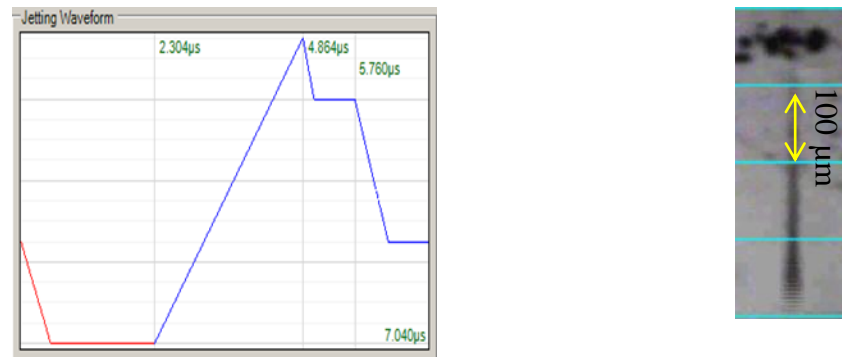
$$Z = (\rho \cdot \sigma \cdot d)^{1/2} / \eta = Oh^{-1} \quad \text{Eq. (14)}$$

Where, ρ , η and σ are the density, dynamic viscosity and surface tension of the fluid respectively, v is the velocity, and d is a characteristic length.

Using a drop jetting speed of 6 m/s, nozzle size of 21.5 μm , and the measured densities, viscosities and surface tension values obtained for each ink at room temperature, the following Z numbers were found: 2.46 for P3HT and 4.95 for OSC ink. Both of these values fall within the recommended range of $10 > Z > 1$ for stable jetting.

2. Jetting Performance

Figure 35 shows the waveform optimized for each ink and captured images of the ink drops as inks are ejected from the nozzle at a drop speed of 4 m/s at 20 KHz. During jetting, it was observed that the P3HT drops had shorter tails. This is due to its higher surface tension. It was also observed that this ink needed a longer jetting period for generating ink drops. This can be attributed to the higher viscosity of the ink requiring more kinetic energy to overcome the static resistance energy in the ink chamber.



(a) OSC waveform and captured image of fired drop



(b) P3HT waveform and captured image of a fired drop

	P2TDC17FT4	P3HT
Firing voltage (V) at 4 m/s	18.7	21.2
Temperature of cartridge(°C)	28	28
Meniscus vacuum (Inches H₂O)	4	4
Jetting Frequency (KHz)	20	20

Figure 35. Waveforms and specific parameters used in each waveform to optimize the jetting of the OSC (a) and P3HT (b) semiconductors inks.

Drop-volume was controlled by the waveform and change in drop speed used. The ideal drop volume depends on the application under consideration since the volume must meet the performance requirements of the printed layer. Drop volumes for most printed electronic applications typically range from 2 to 32 picoliters.²⁵ For large areas where coverage is needed, large drops (high volume) are desired, while for high resolution printing small drops (low volume) are desired. Figure 36 shows that by increasing the voltage amplitude faster drop speeds and larger drop volumes were obtained since the piezoelectric displacement is proportional to the applied

electric field. Although both materials produced similar drop volumes, it was observed that satellite droplets occurred with the P3HT ink during ink firing at and above a drop speed of 6 m/s. This could be due to the higher concentration of the P3HT (1.0 %) in comparison to the OSC (0.25 %). Previous studies have shown similar effects where it had been reported that a lower concentration ink helped to stabilize the tail of a drop, enabling it to retract back to its main body, resulting in the deposition of a single drop.²⁶ Generally, higher surface tension requires more voltage to generate a droplet, whereas low surface tension values can lead to undesirable dripping from the nozzles.²⁷ In this case, the OSC required less voltage than the P3HT to generate a drop from the drop speed range of 4 m/s to 8 m/s.

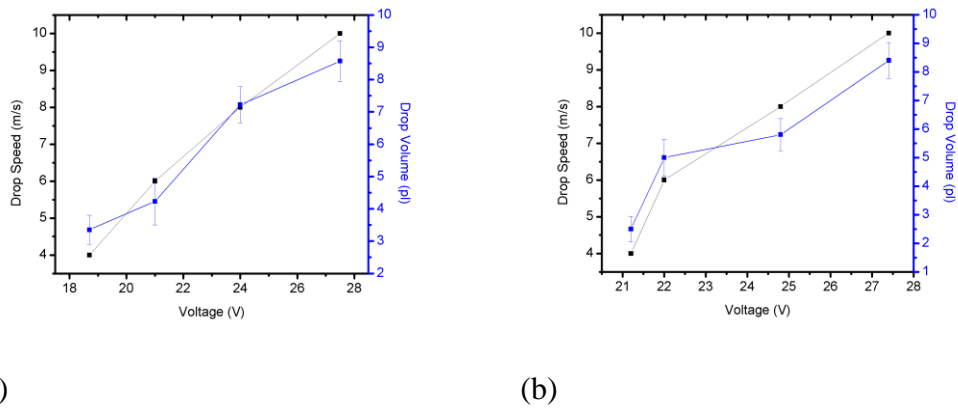


Figure 36. The influence of the firing voltage driving the piezoelectric actuator on the ejected drop volume and velocity. Data for the OSC (a) and P3HT (b) inks jetted at a frequency of 20 kHz are shown.

3. Ink Drying Test

Although the OSC jetted and printed well on the PET, it was observed that after drying the ink rub-off resistance was very poor. Since the manufacturer's recommended drying conditions were followed, it was unclear if the ink had failed to completely dry or if it had failed to adhere. Thus, extensive drying studies were performed by TGA analysis.

Figure shows the loss in mass obtained at a temperature rate of 5 °C/min. As shown, a rapid decrease in ink weight is observed between the temperatures of 112.5°C and 142°C. Beyond the 142°C temperature point, no significant loss in weight is observed. Based on these results, it was concluded that a temperature between 112 °C and 140°C was needed to dry the ink. Since a temperature of 140 °C is too high for PET use, additional drying experiments were performed at 130 °C to determine the additional time requirement to dry the ink at this temperature.

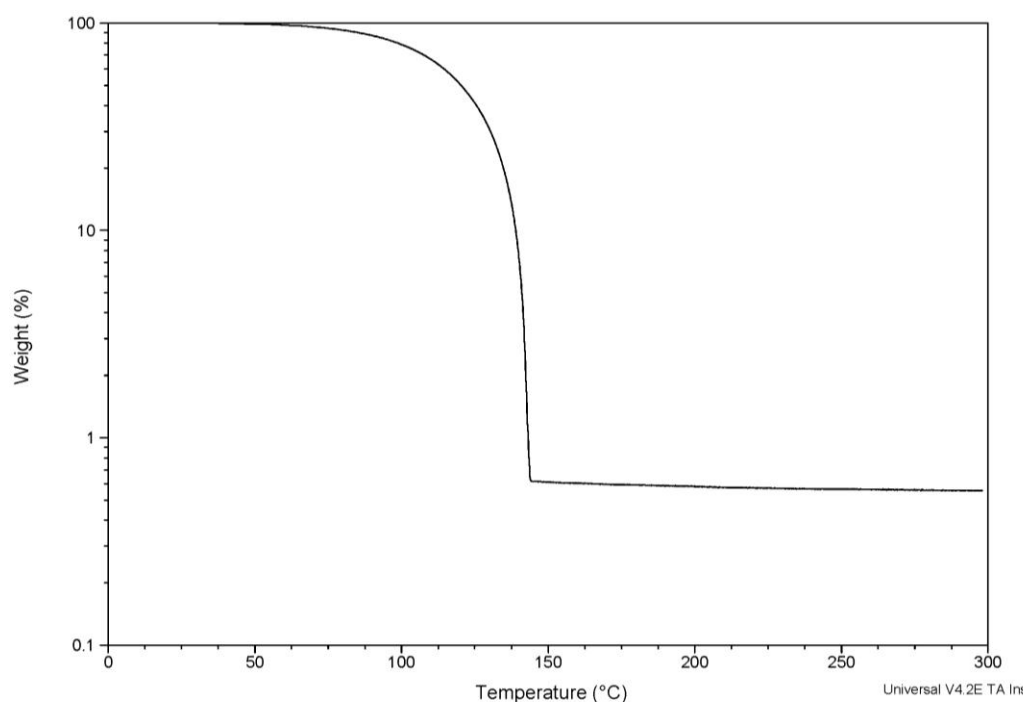


Figure 37. Results from the TGA testing of the OSC ink.

These results are shown in Figure . The red section of the chart indicates where the temperature is increased to 130 °C at a rate of 5 °C/min. The blue section indicates where the temperature is held constant at 130°C. The results indicate that after 23 min. (time needed to reach temperature 130 °C), 59% of the initial weight of ink is lost. The weight of the ink then dramatically dropped (over a 9 min. period) to a constant weight of 0.25% of the initial weight.²⁸ Based on these findings, a drying condition of 130 °C for 10 min was adopted. Under these conditions of drying, the ink rub-off resistance significantly improved, but further improvements will be needed if

this material is to be commercially adopted. As is, a printed ink film of this ink would not survive without damage if run on a press.

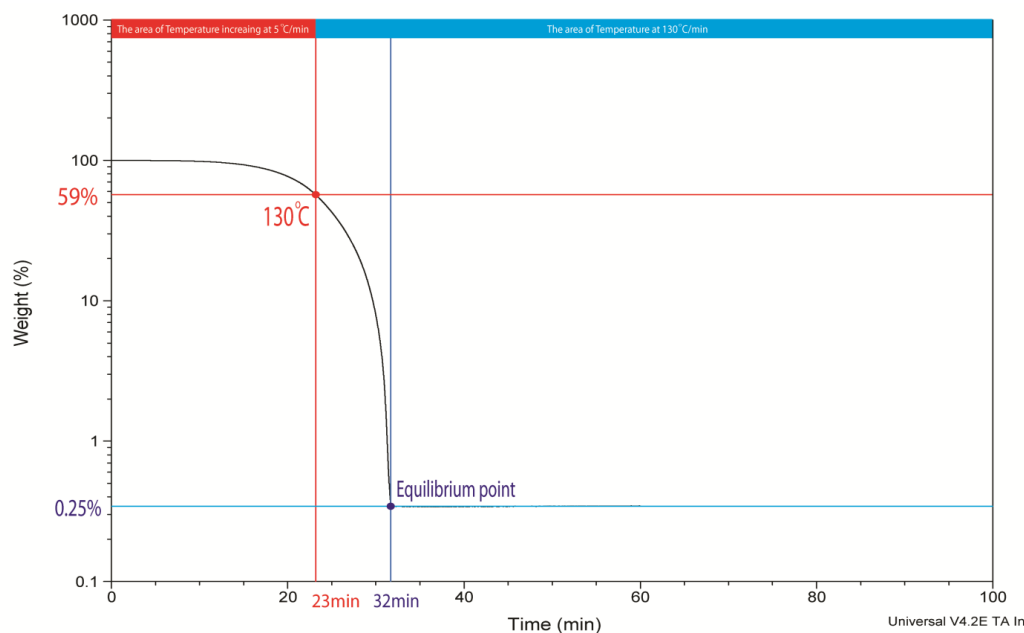


Figure 38. The result of second TGA test with constant temperature 130°C.

4. The effect of drop spacing and substrate temperature on printed line width.

Using the best waveform and drying conditions found for each ink, a nominal pattern, $100\mu\text{m} \times 104\mu\text{m}$, was printed on the PET substrate. Figure 39 shows the drop diameter for the two inks with an increase in drop speed from 4 to 10 m/s. Since the Bond number²⁹, $Bo = \rho g a / \sigma$, is much less than 1, the drop behavior on the substrate is capillary driven. This resulted in the drop diameter of the P3HT being

smaller than the OSC. The drop diameter for the OSC was ranged from 61 to 68 μm and from 59 to 67 μm for the P3HT for the drop speeds reported.

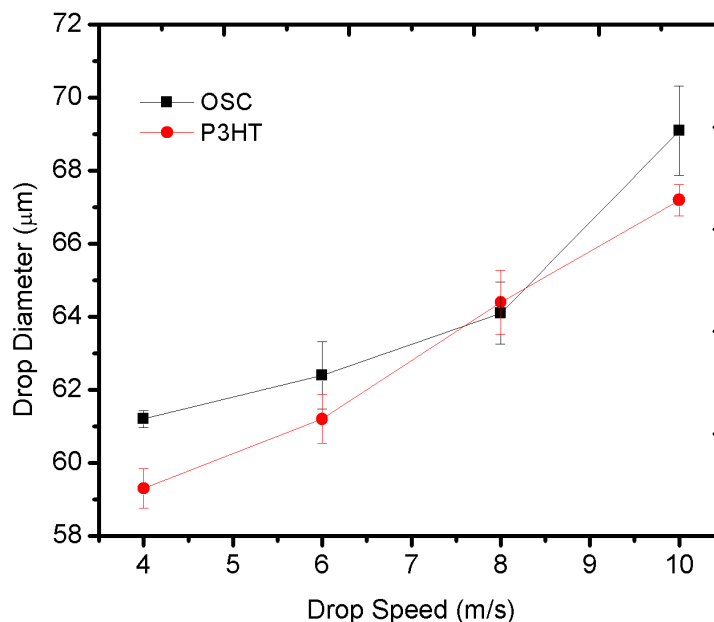


Figure 39. Comparison of drop diameters measured after printing the OSC and P3HT inks with different drop speeds.

The line widths obtained for the different drop spacings at a drop speed of 6 m/s are shown in Figure 40. As the drop spacing increased, the line width decreased due to less overlap between droplets¹⁶. At the 100 μm drop spacing, the drops were all isolated.

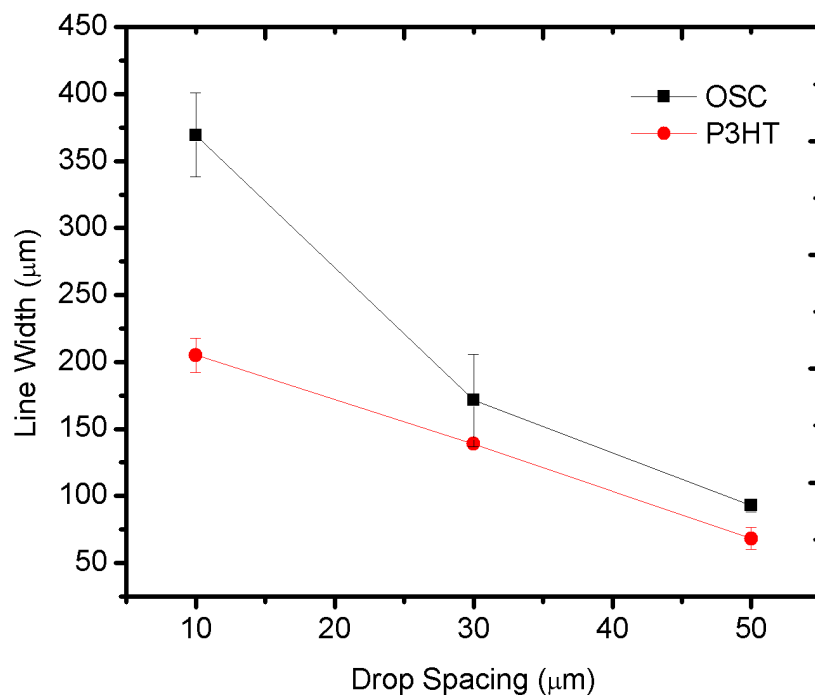


Figure 40. Line widths for different drop spacings at 6 m/s.

In Figure 41, for the OSC bulging drops are observed along the length of the line. Duineveld³⁰ explained this phenomenon by stating that when an additional drop is added to existing beads of ink drops because of the narrow drop spacing, between drops, the drops tend to exceed the bead's equilibrium contact angles, resulting in rounded bulges. No bulging drops were found in the P3HT printed lines, although the drop diameters at 6 m/s were smaller than the diameters of the OSC drops.

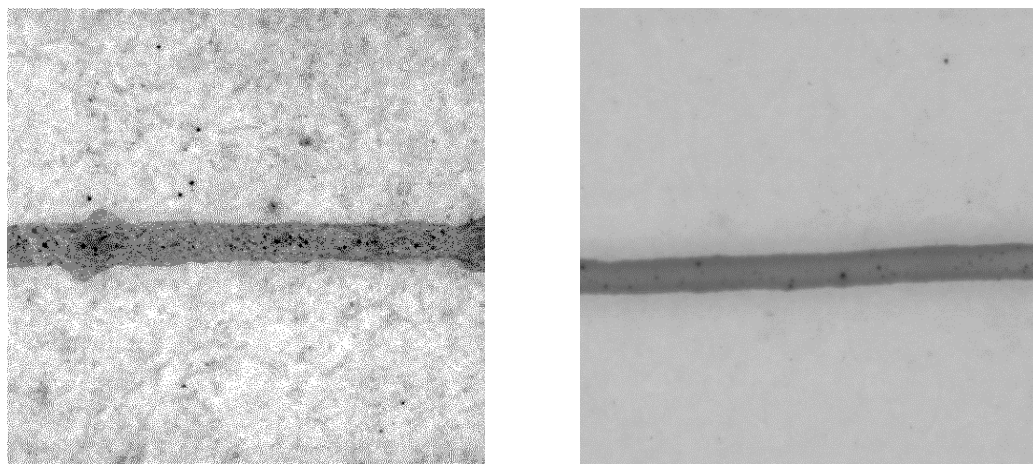


Figure 41. Captured pictures for OSC (left) and P₃HT (right) printed at a drop spacing 30 μm and a drop speed of 6 m/s. (*The picture for OSC was retouched in Adobe Photoshop to increase the contrast between the printed line and background. Due to its lower concentration, the thickness of the OSC film is lower than the P3HT film).

Overall, the line widths of the P3HT printed lines were narrower than the OSC printed lines. These findings can be explained by the lower viscosity and surface tension of the OSC ink. Upon drop impact with the substrate, ink spreading for the OSC would be larger than for the P3HT ink. The greater spreading of the OSC ink increase the chances for drops overlap, leading to the same effect found for decreasing the drop spacing. Regarding the proper drop spacing required to print a uniform line, D. Soltman¹⁶ experimentally showed that y , the ratio of drop spacing to landed drop radius, should equal 1.1. To obtain this value, the proper drop spacing was determined to be 28 μm based on a drop radius of approximately 30 μm for both inks at a drop speed of 6 m/s. However, the line formations for both inks were

different 30 μm drop spacing, even if consideration that there was 2 μm off the calculated drop spacing. Thus, other factors in the inks must be affecting line formation such as particle size, molecular weight or polymer concentration.

Figure 42 shows how heating the substrate affected the width of the printed lines. As a whole, line width decreased with increased temperature. There was also a significant decrease in line width at the 10 μm drop spacing from $369 \pm 31 \mu\text{m}$ at room temperature to $94.1 \pm 7.6 \mu\text{m}$ (Figure 42a) for the OSC ink and from $205 \pm 13 \mu\text{m}$ to $177 \pm 10 \mu\text{m}$ for the P3HT ink, respectively. For the P3HT ink, individual ink drops are observed at the 50 μm drop spacing (Figure 42b), but the ink drops merged at the 30 μm drop spacing (not shown). Since the printed drops dried faster on the heated substrate, due to the transfer of heat energy from the substrate to the ink, the time available for drop spreading decreased, resulting in narrower line widths. In regards to this, the boiling point of the main solvent for each ink contributed to considerably the line widths obtained because toluene (b.p: 110 – 111 $^{\circ}\text{C}$), the solvent for the OSC ink, has a much closer boiling point to 60 $^{\circ}\text{C}$ than the solvent 1-Methylnaphthalene (b.p: 240 – 243 $^{\circ}\text{C}$), the solvent for the P3HT ink. This resulted in the quicker evaporation and drying of the OSC printed line.

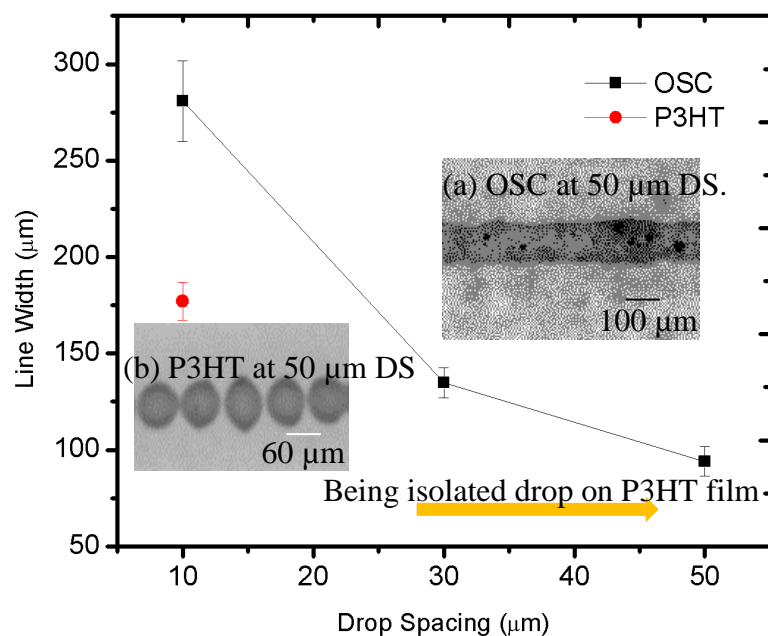


Figure 42. Line widths and pictures of P3HT and OSC printed lines. The line widths at different drop spacings are shown (printing was performed at a substrate temperature of 60 °C and drop speed of 6 m/s).

5. Fabrication of OTFT

The electrical performance of the OSC inks was measured after overprinting the ink onto previously inkjet printed nano silver electrodes on PET. A picture of the printed electrodes and print pattern used is shown in Figure 43.

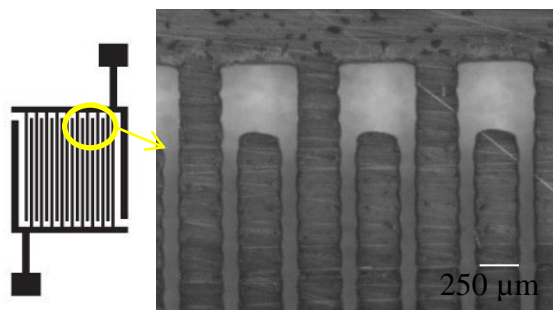


Figure 43. Interdigitated Channel S/D (Line width 238 μm , Channel width 10mm, Channel length 79.7 μm).

The applied voltage range for the gate voltage and source and drain was set to $\pm 30\text{V}$ and $\pm 45\text{V}$, respectively. Since the dielectric layer and gate electrode were not printed at this stage, a copper plate was placed underneath the sample to simulate the gate electrode. The PET substrate played the role of the dielectric layer (bottom gate type structure). After depositing three layers of the OSC ink onto the interdigitated nano-silver structure sufficient coverage was obtained to produce an IV curve for the device (Figure 44). Because of the high thickness of the dielectric layer (PET film, 127 μm), the performance of the printed structure was very low. However, by introducing a proper printed dielectric layer into the system, it is believed that a working fully inkjet printable TFT device could be realized. As for the performance of P3HT printed under ambient conditions, it failed to work.

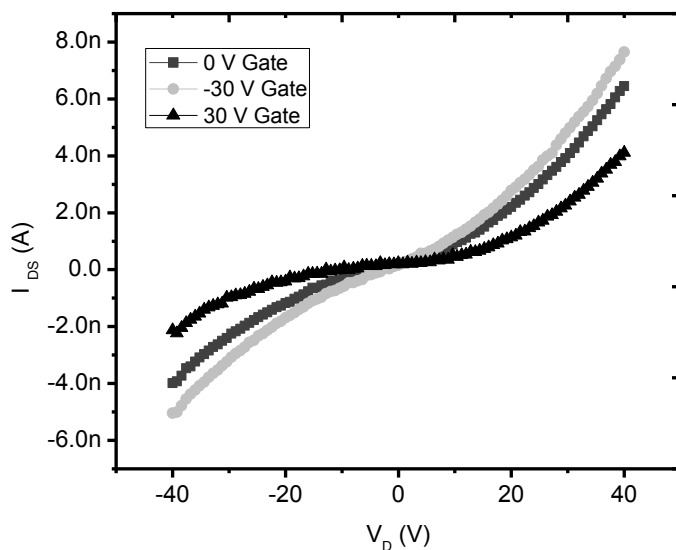


Figure 44. Output characteristics of OTFT printed with OSC ink.

Conclusion

The inkjet ability and print ability of a new ambient stable OSC chemistry was compared to a commonly used semiconductive ink, P3HT. Both inks were characterized according to their surface tensions in the wet state, surface energies in the dried state and rheological properties under various conditions of shear. A, dimensional analysis was performed by calculating the Z (Oh) numbers for the inks using the ink properties measured. From the Z (Oh) numbers enabled the process conditions for good ink formation were determined. The drying property of the OSC ink was determined through TGA analysis. The relationship between drop speed, drop volume and drop voltage was studied and the influence of drop spacing and

substrate temperature on print quality determined. Using the inkjettability and printability results, a top gate OTFTs was realized. The performance of the P2TDC17FT4, printed under ambient conditions, has important implications to the realization of attaining low cost fully printed OTFTs.

References

- 1 T. Hasegawa, et al., “Thin Solid Film”, doi: 10.1016/j.tsf, (2009).
- 2 F. Eder, H. Klauk, M. Halik, U. Zschieschang, G. Schmid, and C. Dehm, Appl., Phys. Lett., vol. 84, no. 14, pp. 2673-2675, (2004).
- 3 P. F Baude, D. A. Ender, T. W. Kelley, M. A. Haase, D. V. Muires, and S. D. Theiss, in IEDM Tech. Dig., pp. 8.1.1-8.1.4, (2003).
- 4 B. Crone, A. Dogabalapur, A. Gelperin, L. Torsi, H. E. Katz, A. J. Lovinger, and Z. Bao, Appl. Phys. Lett., vol. 78, no. 15, pp. 2229-2231, (2001).
- 5 C. D. Sheraw, J. A. Nichols, D. J. Gundlach, J. R. Huang, C. C. Kuo, H. Klauk, T. N. Jackson et al., Proc. 58th Device Res. Conf., pp. 107-108, (2000).
- 6 J. Lee and V. Subramanian, “Organic transistors on fiber: A first step towards electronic textiles”, in IEDM tech. Dig., pp.8.3.1-8.3.4, (2003).
- 7 Y. Wu, H. Yan, M. I. Huang, B. Messer, J. H. Song, and P. Yang, Chem. Eur. J, 8, No. 6, (2002).
- 8 G. Horowitz, “Organic thin film transistors: From theory to real devices”, J. Mater., Vol 19, (2004).
- 9 D. A. Lyashenko, b, Alexander A. Zakhidov, V. A. Pozdin, G. G. Malliaras, Vol 11, Issue 9, pp 1507–1510, (2010).
- 10 Bharathan J, Yang Y. Appl. Phys. Lett. 72:2660–62, (1998).
- 11 Sirringhaus H, Kawase T, Friend R.H., Shimoda T, Inbasekaran M, et al. Science 290:2123–26, (2000).
- 12 Nakamura M, Kobayashi A, Takagi F, Watanabe A, Hiruma Y, et al. Tissue Eng. 11:1658–66, (2005).
- 13 P. Calvert, “Inkjet Printing for Materials and Devices”, Chem. Mater., 13 (10), pp 3299–3305, (2001).

- 14 He Yan, Zhihua Chen, Yan Zheng, Christopher Newman, Jordan R. Quinn, Florian Dotz, Marcel Kastler and Antonio Facchetti, *Nature*, doi: 10.1038, Vol. 457, (2009).
- 15 J. Doggart, Y. Wu and S. Zhu., *Applied Physics Letter* 94, 163503, (2009).
- 16 D. Soltman and V. Subramanian, “Inkjet-Printed Line Morphologies and Temperature Control of the Coffee Ring Effect”, *Langmuir*, 24, 2224-2231, (2008).
- 17 M. He, J. Li, M. L. Sorensen, F. Zhang, R. R. Hancock, H. H. Fong, V. A. Pozdin, D. M. Smilgies, and G. G. Malliaras, “ Alkylsubstituted Thienothiophene Semiconducting Materials: Structure-Property Relationships”, *J. AM. CHEM. SOC.*, 131, 11930–11938, (2009).
- 18 M. He, J. Li, M. L. Sorensen, F. Z, R. R. Hancock, H. H. Fong, V. A. Pozdin, M. Smilgies, and G. G. Malliaras, “Alkylsubstituted Thienothiophene Semiconducting Materials: Structure-Property Relationships”, *J. AM. CHEM. SOC.*, 131, 11930–11938, (2009).
- 19 Owens D. K., Wendt R. C., “Estimation of the Surface Free Energy of Polymers”, *J. Appl. Pol. Sci.*, 13, p 1741, (1969).
- 20 B. Thompson, *Printing Materials: Science and Technology*, Pira International, Edition, year , pp
- 21 J. Koszkuł, J. Nabiale, *Journal of Materials Processing Technology* 157–58, 183–187, (2004).
- 22 http://www.rheologyschool.com/cross_model.html
- 23 B. J. de Gans, P.C. Duineveld, U. S. Schubert, Vol. 16, Issue 3, p.p 203–213, (2004).
- 24 Reis N, Derby B. *MRS Symp. Proc.* 624:65–70, (2000).
- 25 H. E. Katz, *J. Mater. Chem.* 7, 369, (1997).
- 26 Xu D, Sanchez-Romaguera V, Barbosa S, Travis W, de Wit J, et al. *J. Mater. Chem.* 17:4902–7, (2007).

- 27 P. Calvert., Chem. Mater., 13, 3299-3305, (2001).
28. R. Bollstrom, D. Tobjork, P. Dolietis, T. Remonen, C. J. Wikman, S. Viljanen, J Sarfraz, P. Salminen, M. Linden, C. E. Wilen, J. Bobacka, R. Osterbacka and M. Toivakka, "Roll to roll printed electronics on paper, PaperCon, New Orleans, (2012).
- 29 Hua Hu, G. Ronald Larson, J. Phys. Chem. B 106, 1334–1344, (2002).
- 30 Duineveld, P. C. J. Fluid Mech. 477, 175-200, (2003).

CHAPTER VI

INKJET PRINTING AND SINTERING OF NANO COPPER INK

Sooman Lim, Margaret Joyce and Paul D. Fleming

Center for the Advancement of Printed Electronics, Department of Paper Engineering, Chemical Engineering and Imaging, Western Michigan University

Keyword: nano copper, inkjet printable, intensive pulse light, Xenon sintering

Abstract

An alternative low cost replacement for silver and gold conductive inks is of great interest to the printed electronics industry. Nano particle copper inks and silver coated nano copper inks are some of the alternative materials being tested for use, especially in applications where low temperature flexible substrates are favored. Although the inkjettability of nano copper ink influence on print quality has been reported, information regarding the relationship between ink film thickness and energy required for sintering by intensive pulse light is not yet understood. In this study, an inkjettable nano copper ink was printed on PET (PolyEthyleneTerapthalate) and glass and the samples were sintered using bursts of high intensity pulsed light. The amount of energy applied determined the degree of sintering among particles.

The greater the number of sintered nanoparticles, the higher is the conductivity of the printed traces. A comparison of energy levels required for sintering on glass and PET in relationship to ink film thickness is reported and the thermal contribution of the substrate to the processing energy requirements of this ink is revealed.

Introduction

Inkjet printing is an attractive printing technology for the deposition of functional inks, due to its advantages of low-cost, ability to print fine lines and thin layers, and due to the wide range of available materials available for printing by this method. Although the inkjet printing of silver and gold is already being practiced, their high costs have limited their use, especially in low cost flexible electronic applications. As a result, low cost alternative materials are of interest. The use of conductive organic polymers, organo-metallic compounds, metal precursors and metal-based nano inks have all been reported, with different print methods being employed for their deposition. Although conductive polymers meet the requirements in terms of being used in soluble deposition printing, their low conductivity and instability to the air are significant shortcomings.¹ Metal precursor and organo-metallic compounds require a heat treatment for reduction, which leaves residual organic matter in the fabricated film that may adversely affect the product performance.² For metal-based nano inks, the requirement for low-temperature, in-

situ sintering of the inks is an issue.³ Kim et al.⁴ sintered Ag nano ink at 200 °C for 30 min. in a thermal oven and found that the conductivity was changed based on the sintering temperature and size of the nano Ag particles applied. Ko et al.⁵ used a localized sintering technique to sinter nano Au particles on polyimide films, but found that the sintering technology used was not useful over a large area. The thermal sintering of an inkjet printable nano copper ink developed through a polyol process has also been studied.¹ However, this technology required the ink to be sintered under vacuum to avoid the oxidation of the copper particles. High temperatures and long cycle times (an hour or more) were also needed, which are not process conditions conducive to high speed R2R printing for low cost flexible printed electronic applications. To address the high throughput needs for R2R processing and desire for a low cost alternative to Ag and Au inks, the use of intensive pulsed light (IPL) generated from a Xenon lamp source, to sinter nano copper ink particles under ambient conditions, was examined.⁶ IPL delivers a quick burst of intense near UV energy to the printed surface. The intensity of energy, duration of the pulse and distance from the printed surface can all be varied to alter the amount of energy applied. Due to the short time interval (milliseconds) of the light pulses, the nano particles can be sintered without damage to the underlying substrate layer. This makes it appropriate for use with PET film and paper for flexible printed electronic applications. For copper based inks, conductivity is achieved through either the conversion of CuO nano particles to Cu, or vaporization of a protective coating layer

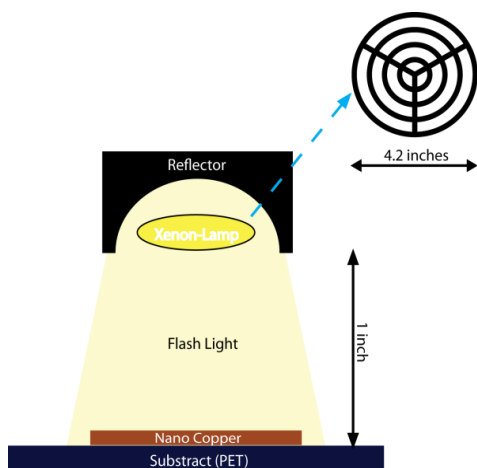
applied to the Cu nanoparticles to prevent oxidation prior to sintering. Some of these inks may also benefit from a pretreatment thermal step to drive off carrier solvent in the ink prior to sintering. The mechanism for achieving Cu conductivity depends on the commercial source of the ink used. Though the mechanism for conversion of these inks from the non-conductive to the conductive state is understood, until now, the relationship between ink film thickness and amount of irradiated energy required for sintering has not yet been examined.

In the present work, the inkjet printability and print quality of a new commercially available nano particle copper ink was studied on PET and glass. The inks were printed using a Dimatix DMP-2800 inkjet printer. Sintering was performed using a Xenon Sinteron 2000 unit. All sintering was performed under atmospheric conditions without first preheating the printed samples. The amount of energy applied was controlled by varying the applied voltage, duration of pulse and number of pulses. The electrical resistances of the samples were measured before and after treatment with the Sinteron 2000. The extent of particle sintering was examined under high magnification with a scanning electron microscope (SEM).

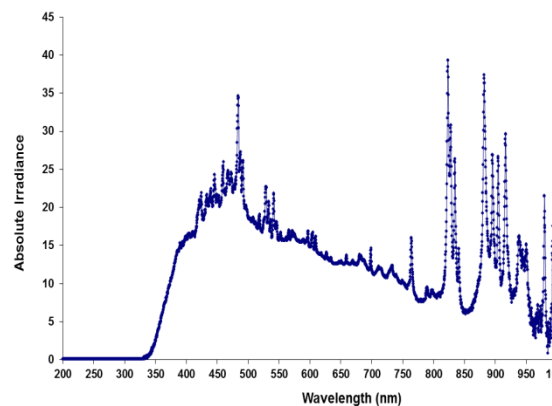
Experiment

A commercial nano copper ink, CI-002, (Intrinsiq Materials, UK) containing 45 nm diameter of particles (10 % Wt.) uniformly dispersed in a mixture of Ethane-1,2-diol and n-Butanol (as reported by the supplier) was used to print multiple 1 cm × 0.5 cm rectangular samples. The samples were printed at different drop spacing intervals (10, 20 and 30 μm) using a Dimatix DMP 2800 inkjet printer (Fujifilm, CA). Prior to printing the inks were characterized by measuring the surface tension and rheological properties with a FTA 200 (First Ten Angstroms, Inc., VA) dynamic contact angle measuring device and RA 2000 dynamic stress rheometer (TA Instruments, DE), respectively. The surface energy of the ink was determined at room temperature using the Owens-Wendt Model⁷ with high purity water and methylene iodide as test fluids. Since the jetting performance of an inkjet ink strongly depends on its dimensionless Z-number, this value was calculated from viscosity, surface tension, density and drop diameter (nozzle orifice) measurements.⁸ Viscosity measurements were performed at a fixed shear rate of 10 s^{-1} , which was determined to be in the second linear plateau region of the steady flow curve obtained for this ink. Surface tension was measured by the pendant drop method. Prior to printing, the ink was placed into an ultrasonic bath for one hour to ensure homogeneity and degassing of the ink. The ink was then injected into a 10pL cartridge and loaded into the DMP, where it was allowed to equilibrate for 30 minutes. The waveform and temperature

range of cartridge (from 28 to 70 °C), were then adjusted by observing the ink jetting behavior and the drop formation of the ink through a drop watcher camera until satisfactory jetting was achieved (no satellite drops or puddling at the nozzle). Two substrates were printed – a 127 µm PET film Melinex ST505 (DuPont Teijin Films, Delaware) and a 614 µm glass film (Alkaline Earth Boro-Aluminosilicate type). After printing, the samples were immediately sintered (Sinteron 2000, Xenon Corporation, MA). The least amount of energy required to obtain the lowest electrical resistance without damage to the ink film or substrate was determined by inspecting each sample after sintering and measuring its electrical resistance using a 4 point probe. The IPL system consisted of a 15 cm diameter xenon spiral Type B lamp⁹, power supply, capacitors, lamp flash control panel and air cooling system, as illustrated in Figure 45a. The spiral lamp irradiated over a wide wavelength spectrum in the range from 330 nm to 1,050 nm as shown in Figure 45b.



(a)



(b)

Figure 45. Schematic of intensive pulsed light sintering system (a), spectral distribution of the Xenon lamp at 3600 V - 15 Hz setup (b).

Using equation 15, the electrical energy per pulse was calculated,

$$\frac{\{C \times (V)^2\}}{2} = \text{Electrical Energy / pulse} \quad \text{Eq. (15)}$$

Where C and V refer to capacitance and voltage applied to the system, respectively. The pulse energy was varied from 5175 to 10909 J while the capacitance and pulse duration was fixed at 115 F and 500 μ s, respectively. During printing of the samples, it was observed that the ink was not wetting the PET film well, resulting in incomplete coverage and poor uniformity of the ink film. To improve wetting, the

film was treated with UV/Ozone (Jelight Inc., CA) for up to 275 sec. The UV/Ozone treatment raised the surface energy of the film promoting better wetting which improved the quality of the printed ink film.

As a first step, after printing each sample received a single pulse flash, after which the sheet resistance was measured using a 4 point probe sensing mode (Keithley multimeter model 2400, OH). If the sample was non-conductive, the IPL treatment procedure was repeated. Based on the results, changes were made to the increase the pulse energy by adjusting the lamp voltage in order to minimize the number of pulses required. Once the number of pulses and voltage required to obtain the lowest resistance for each sample was determined, on average, 3 samples for each substrate were treated and 3 resistance measurements per sample taken. The quality of the printed pattern was analyzed using an ImageXpert, Inc. image analyzer. Next, the surface of sintered samples was examined under a scanning electron microscope and Wyko white light interferometry microscope. And, adhesion tests performed using a Friction / Peel Tester Model 225 (Thwing Albert instrument company, PA). The Friction/Peel tester was equipped with a diamond tip attached to a sled containing 1 kg weight, which was dragged across the surface of the samples at 0.1 cm/s. Once the test was completed, the scratches were measured using the ImageXpert image analyzer.

Results and Discussion

1. Dimensional analysis.

In order to predict the inkjettability of the nano copper ink on the Dimatix DOD inkjet printer, the Z number was calculated according to Eq (16). This number is the reciprocal of the Ohnesorge number¹⁰.

$$Z = \frac{Re}{We} = (d\rho\sigma)^{\frac{1}{2}} \frac{1}{\eta} = Oh^{-1} \text{ (Ohnesorge number)} \quad \text{Eq. (16)}$$

where η , ρ , and σ are the viscosity, density (g/cm³), and surface tension of the liquid, respectively, and d is the diameter of the nozzle aperture (21.5 μ m). The Z number is important, because it predicts the drop formation quality through an inkjet nozzle.

As a first step to calculate the Z and Oh numbers, the change in surface tension and viscosity of the ink with temperature was measured. As shown in Figure 46a, the temperature of the ink was increased from 25 °C (room temperature) to 70 °C (maximum attainable cartridge temperature adjustable). The properties of the ink were measured at elevated temperature because it was determined that elevated temperatures were needed for good jetting. The change in Z number and Oh number with temperature are shown in Figure 46b. As a consequence of heating, both the

surface tension and viscosity of the ink decreased, which consequently resulted in the lowering of the Z number. According to Reis,⁸ et al., for best jetting the Z number should fall between 1 and 10. As shown in Figure 46b, the Z number does not meet this criterion at 25 °C, but this criterion is met at any temperature over 27 °C. However, in practice, it was found that a minimum cartridge temperature of 34 °C at an applied voltage of 40 V was needed to jet the ink. Under these conditions, a drop speed of 2 m/s is accomplished with good jetting characteristics.

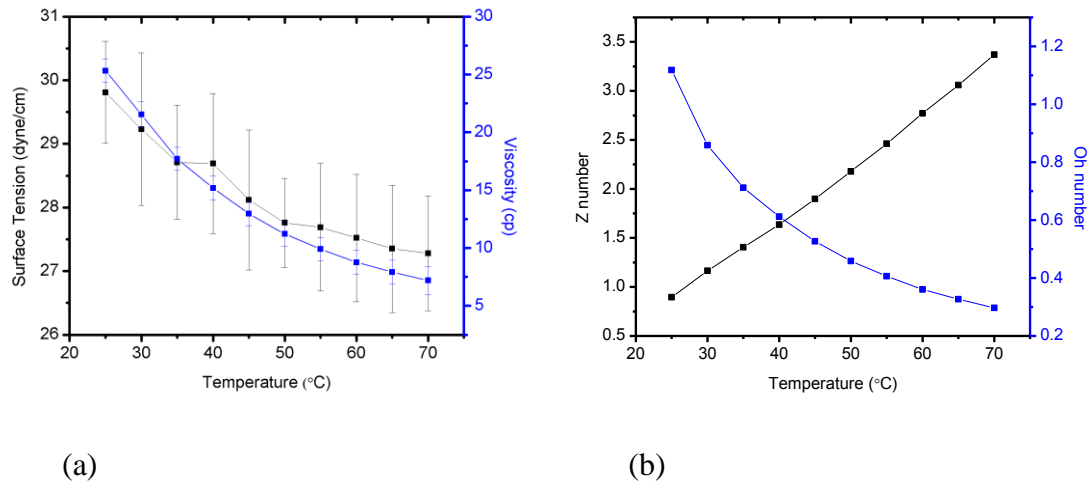
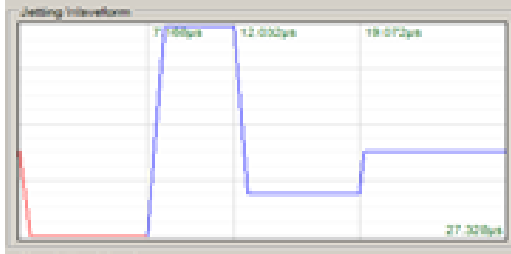


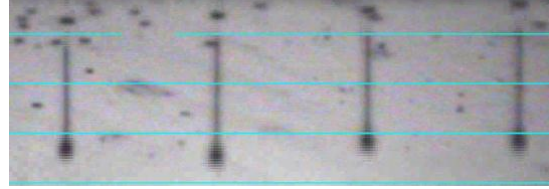
Figure 46. Change in surface tension and viscosity (a), Z number and Oh number (b).

Although the 34 °C temperature was higher than what was expected to be needed for good jetting, at this temperature, the Z number (1.35), does fall within the theoretical Z number range for good jetting. In general, for good jetting the kinetic energy applied to the drop needs to be higher than the surface tension energy of the liquid and the viscous dissipation of the liquid for drop ejection to occur. This means

that a high surface tension and viscosity ink will require more kinetic energy, to expel it from the cartridge.¹¹ Based on this reasoning, the ink did not jet well at room temperature due to its viscosity and surface tension being higher than the kinetic energy that could be generated by the waveform. Practically, the measured viscosity of 28.3 cp at room temperature was much higher than the 1 ~ 12 cp range recommended by Dimatix. Increasing the cartridge temperature reduced the surface tension and viscosity low enough for the kinetic energy to be sufficient to promote jetting. However jetting is not the only characteristic that needs to be controlled, drop speed is also important. If the drop speed is too slow, the ink volume delivered to the substrate could be too low, leading to incomplete coverage or an insufficient ink film thickness to meet the desired electrical property requirements. Furthermore, a slow drop speed often results in the misdirection of the ink droplets as they travel towards the substrate. Thus, to obtain good print quality, the cartridge temperature and drop speed must be properly adjusted. Drop speed is adjusted by altering the firing voltage. Drop volume is adjusted by altering the waveform. For this ink, the best jetting and print quality was accomplished at a drop speed of 4 m/s and cartridge temperature of 47 °C. Using this set-up, a 1 cm by 0.5 cm pattern, was printed at three different drop spacings (10 µm (2540 dpi), 20 µm (1270 dpi) and 30 µm (847 dpi)) to obtain ink films of different thicknesses. The waveform used and picture of the jetting evolution are displayed in Figure 47.



(a) Waveform for nano copper ink



(b) Ink ejection from the nozzles

Figure 47. The waveform and ink ejection for nano copper ink.

The shear thinning properties of the ink are shown in Figure 48. As shown, the rheological properties of the ink are well fitted by the Cross¹² Model (equation 17), which combines the low shear viscosity (η_0), the high shear viscosity (η_∞), and the shear thinning part of the curve by a two parameter power law relationship. From the Cross Model, K, the characteristic time of the material and m, degree of shear thinning, are obtained. These values are provided in Table 1.

$$\eta = \frac{\eta_0 - \eta_\infty}{[1 + (K\dot{\gamma})^m]} + \eta_\infty \quad \text{Eq. (17)}$$

The standard error is well below 20, meaning the fit is very good. The results from the Cross model fits are summarized in Table 3.

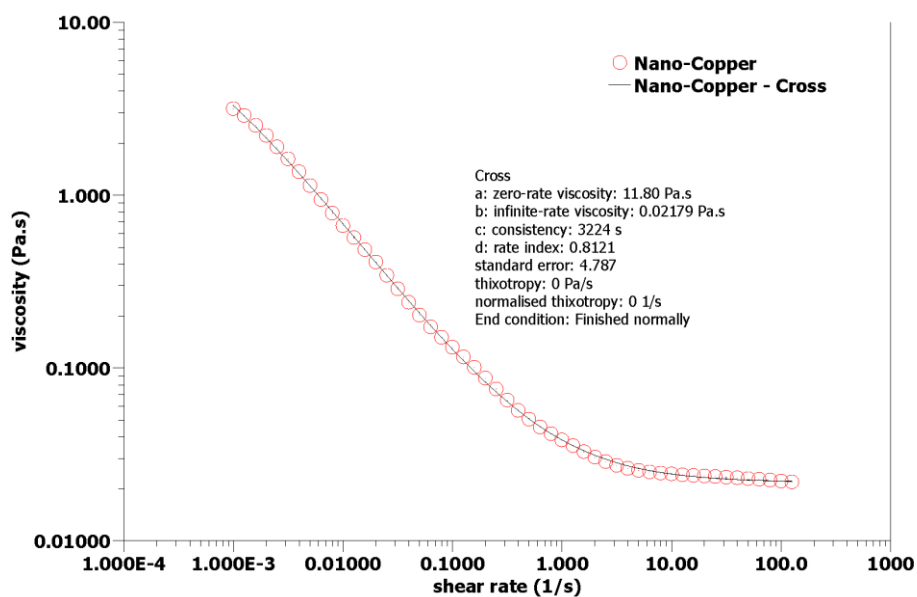


Figure 48. The result of rheological behavior for nano copper ink.

Table 3. The Results of Cross-Model Analysis

Sample name	η_0 [Pa.s]	η_∞ [Pa.s]	K [s]	m	Standard Error (%)
Nano Copper	11.8	0.0217	3224	0.8121	4.787

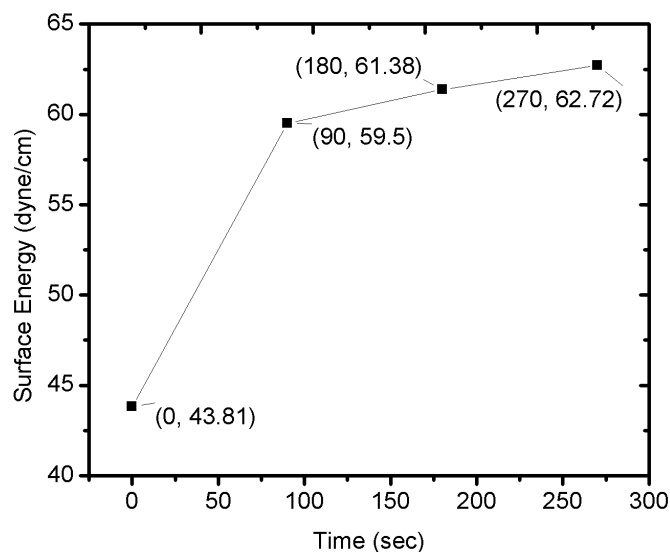
The initial deposition of the ink onto the PET film did not result in good ink wetting or ink adhesion. Instead, the ink beaded-up forming a discontinuous string of pearls. On the other hand, the ink printed well on the glass. The differences in results can be explained by the differences in the surface energy of the two substrates. As shown in Table 4, the surface energy of the glass, 63.7 dyne/cm, is much higher than the PET film, 43.8 dyne/cm.

Table 4. Surface Energy Values of Substrates

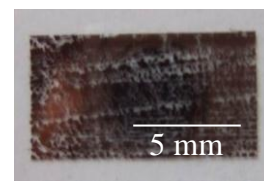
Unit: dyne/cm

Name	Surface Tension	Surface Energy	Dispersive	Polar
Nano copper ink	29.8 ±1.2	-	-	-
PET	-	43.8	2.3	41.8
PET with UV/Ozone treatment for 275 sec	-	62.7	46.2	16.5
Glass	-	63.7	47.4	16.4

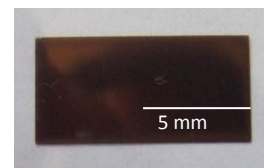
To alleviate the problem, the surface energy of the PET was increased to 62.7 dyne/cm by application of a UV/Ozone treatment. Before and after treating the film with the UV/Ozone the film was cleaned with Isopropyl alcohol (IPA). The change in surface energy of the film with UV/Ozone exposure time is shown in Figure 49a. The surface energy of the film greatly increased after 100 s of exposure. Only a slight difference in surface energy is observed above the 150 s time of exposure. The differences in the uniformity of the printed surfaces resulting from the UV/Ozone treatment are shown in Figure 49b. Before treatment, the ink film is rough and beaded ink drops are observed. After treatment, the ink film is smooth.



(a)



Printed copper ink
on untreated PET



Printed copper ink on
UV/Ozone treated
PET for 275 s

(b)

Figure 49. Influence of UV/Ozone treatment on PET with time (a) and pictures of printed nano copper ink films (b).

Application of the UV/Ozone treatment for 275 seconds increased the surface energy from 43.8 to 62.7 dyne/cm. The treatment especially affected the dispersive energy component of the surface energy value (Table 2). This is in agreement with Ton-That et al.¹³ who reported that the π bonding of phenyl groups in the PET is broken by absorbing UV energy absorbed, which leads to an increase in the number of ester groups at the surface. The greater the exposure time, the greater the number of ester groups through which the oxidization readily takes place, resulting in larger grains at the surface of the treated PET than that of untreated PET. The grain size is

proportional to roughness. Therefore, exposure of the film to UV/Ozone roughens the surface of the film, which for a hydrophilic substrate raises the surface energy in accordance with the Young-Laplace equation.^{14,15} The increase in PET film surface energy improved the print quality of the nano copper ink.

The experimental design followed for sintering the substrates is shown in Table 5. The energy applied was altered by changing the voltage of the lamp and time of printed sample exposure. As shown, the total energy applied was varied from 5175 to 10909 J.

Table 5. The Experimental Design Followed for Altering the Amount of Energy Applied to the Nano Copper Printed PET Film.

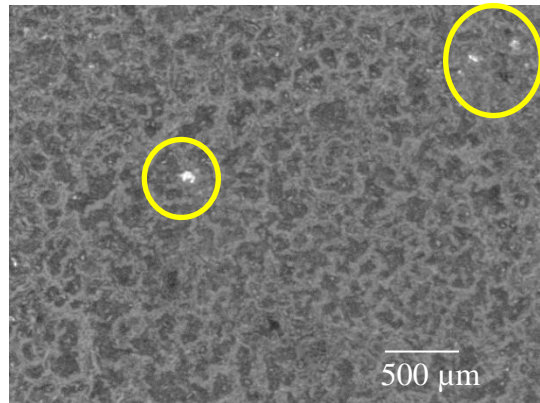
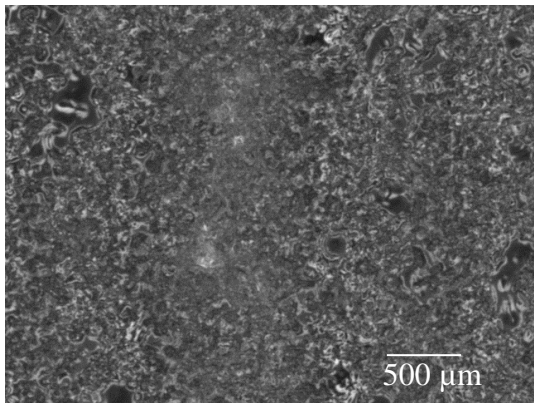
Sample No.	Drop Spacing (μm)	Pulse Width (μs)	Capacitance (μF)	Applied Voltage (V)	Applied times (sec)	Distance (inch)	Total Electrical Energy (J)	Resistance (Ω/□)
1	10	500	115	3080	10	1	10909	1.4 ± 0.2
2	10	500	115	3080	5	1	5455	Not dried
3	10	500	115	3000	5	1	5175	Not dried
4	20	500	115	3080	10	1	10909	>105M*
5	20	500	115	3080	5	1	5454.6	6.18 ± 0.42
6	20	500	115	3000	5	1	5175	47k ± 6k
7	30	500	115	3080	10	1	10909	>105M*
8	30	500	115	3080	5	1	5455	>105M*
9	30	500	115	3000	5	1	5175	20.0 ± 0.3

*Greater than the measurable impedance of the instrument used.

The optimized total electrical energies for the samples printed at 10, 20 and 30 μm drop spacings were 10909 J, 5455 J and 5175 J, respectively. Under these conditions, the lowest resistance obtained was 1.4 ± 0.2 Ω/□. Since sample No.1 was

printed with a drop spacing of 10 μm , it had the highest ink film thickness (595 nm) prior to exposure to the xenon lamp. So, this was the sample used to approximate the needed conditions for sintering the other samples (No. 5 and 9) of thinner ink film thicknesses (110 and 62 nm, respectively). Likewise, the sintering condition for sample No. 9 printed at a drop spacing of 30 μm was used to estimate the energy required for sintering the No.6 printed sample with a drop spacing of 20 μm drop. The amount of energy applied for sample No. 1 and 5 caused damage to the No. 7 and 8 samples.

Figure 50 shows the damaging affect the IPL can have on the ink film if too much energy is applied. The pin holes present (highlighted in yellow) are most likely due to out gassing.

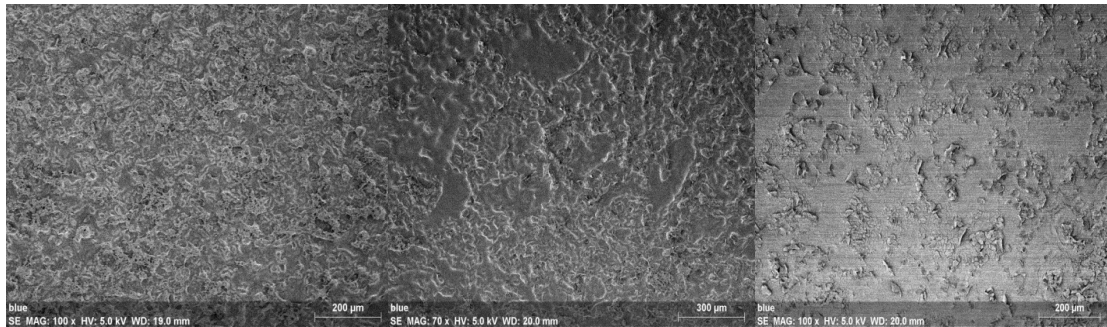


Sintered at 5455 J on 20 μm drop spaced sample, sample No. 5 (a)

Sintered at 10909 J on 20 μm drop spaced sample, sample No. 4 (b)

Figure 50. Optical micrographs of nano copper ink sintered at different applied Xenon lamp energy intensities.

The influence of IPL energy on the morphology of the inks can be seen from the SEM images shown in Figure 51. The SEM pictures were taken from samples cut from the printed copper line shown below in the SEM micrographs, which was sintered under the spiral Xenon lamp.



(a). Applied energy:
5454 J

Resistance: $6.18 \Omega/\square$

(b). Applied energy:
4800 J

Resistance: $7.2 \Omega/\square$

(c). Applied energy:
3709 J

Resistance: $> 105 M \Omega/\square$



Figure 51. SEM micrographs of sintered samples (Magnification $\times 100$).

As shown in Figure 52 the energy intensity of the spiral lamp decreases the further the sample is away from the center of the lamp.

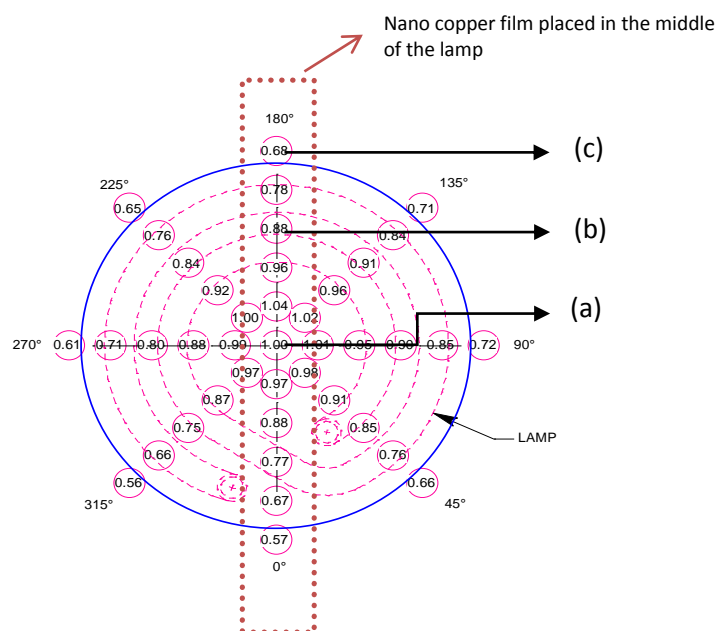


Figure 52. Energy mapping of the 4.2 inch spiral Xenon lamp used.¹⁶

Thus, by placing the nano copper printed strip under the lamp in the direction indicated by the red box, the influence of lamp energy on particle sintering could be obtained. From the SEM pictures, it is clear that as the energy applied increased, fewer individual nano particles are present as a result of particle sintering. The applied energies to (a), (b) and (c) in Figure 51 were calculated from the energy values provided in Figure 52.

Figure 53 shows the XRD pattern for the copper ink before and after sintering. The sintered XRD pattern shows two characteristic peaks at 43.56 and 50.80° for the all printed samples. The peaks verify the presence of the face-centered cubic (FCC) copper phase without any oxidization or other impurity phases being present after IPL

sintering. And, the more the drop spacing decreased, the higher the intensity. The increase in Cu peaks after sintering with decrease in drop spacing indicates the coalescence of Cu due to the increased amount of particles. Comparison of the surface roughness of the sintered and un-sintered samples indicates that the roughnesses of the printed ink films were affected by this result. The average of measured roughness (Ra) of the unsintered film printed at the 10 μm drop spacing was 11.49 nm and 4089, 84.0, 20.6 nm for the sintered samples at the 10, 20 and 30 μm drop spacings, respectively.

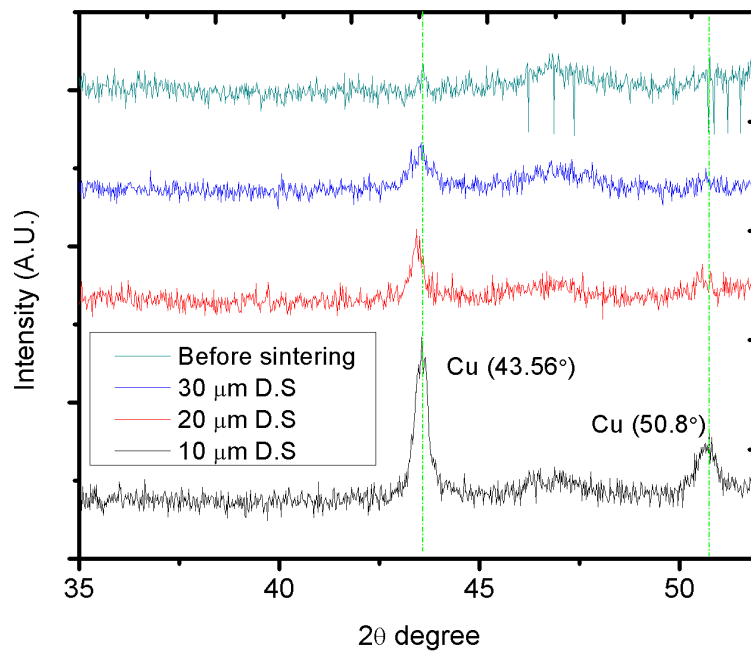


Figure 53. XRD patterns of nano copper ink printed with different drop spacing (D.S).

The surface topography of the printed samples before and after sintering is shown in Figure 54. Since the surface roughness of base film (PET) is less than 10 nm (as reported by the manufacture), the vacuum oven dried ink film is very smooth (Figure 54a). After sintering, the roughness is shown to dramatically increase, Figure 54b, due to the movement and cohesion of the nano Cu particles and burn off of carrier solvent within the ink and other ink components.

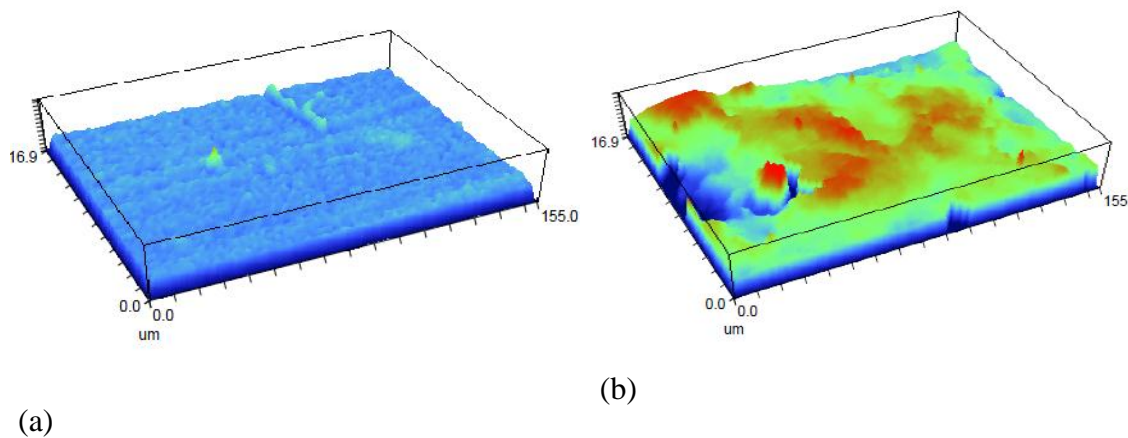


Figure 54. Surface morphology of unsintered ink film (a) and sintered film (b). All films were printed using a drop spacing of 10 μm .

Figure 55 shows the relationship between ink film thickness and sintering energy requirements. The relationship between sintering energy and resistance is also shown. The energy required for sintering is proportional to the ink film thickness while the resistance is inversely related to the ink film thickness. Resistance decreased with ink film thickness as a result of more nano copper particle-to-particle

contact in the printed ink film.

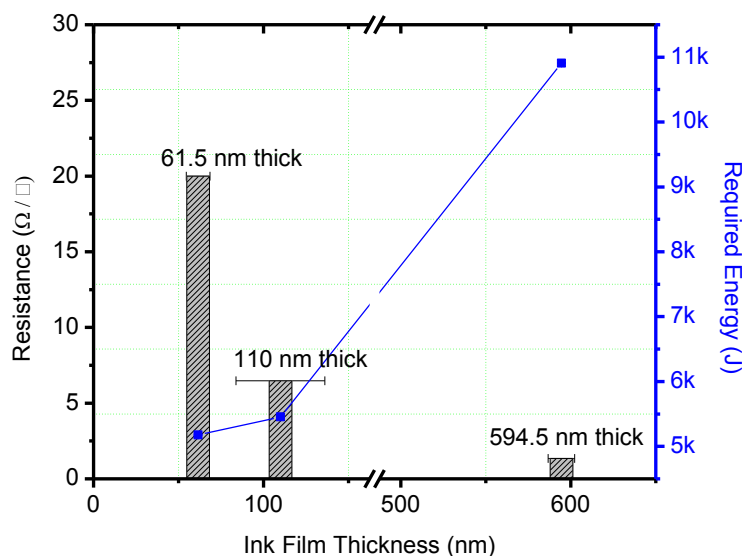
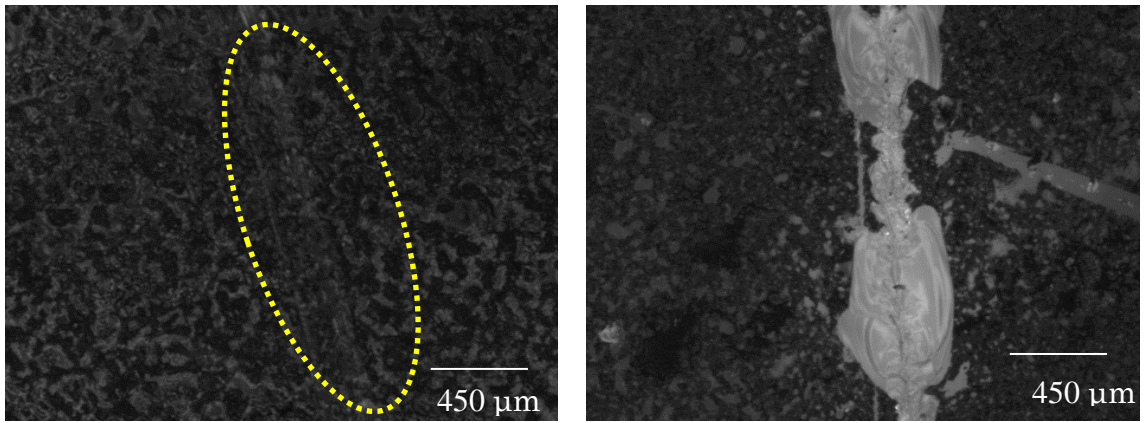


Figure 55. Relation between average ink film thickness and required energy for sintering nano copper ink on PET.

In addition to determining the influence of ink film thickness on sintering energy requirements, the influences of the substrate thermal properties on sintering energy requirements were also determined by comparing the energy required to sinter the nano copper ink on a transparent 614 μm thick glass and 127 μm thick PET. Since the glass had a similar surface energy to that of the UV/Ozone treatment PET, it did not have to be treated before printing. Both substrates were printed at a drop spacing of 20 μm . Application of 5455 joules (Sample 5 in Table 2) of energy was insufficient to sinter the particles on glass. Instead, significantly more energy (about

10 times higher) was needed. This application of higher energy resulted in a resistance of $68.9 \pm 9.5 \Omega/\square$. Unfortunately, as shown by the scratch resistance test results in Figure 56, the adhesion of the copper ink on the glass was poor.



(a) Line width of scratch : $90.9 \pm 4.4 \mu\text{m}$ (b) Line width of scratch : $372 \pm 165 \mu\text{m}$

Figure 56. Adhesion testing for the sintered nano copper film on PET (a) and glass (b).

The reason for this finding can be explained as follows:

Suppose an IPL with 1 J/cm^2 is irradiated onto a $10 \mu\text{m}$ thick nano copper ink film printed over $127 \mu\text{m}$ thick PET film and $614 \mu\text{m}$ thick glass film. Assume further that all of the light energy is absorbed into both layers without scattering and reflection. Then, based on these assumptions, the increase in temperature for all the materials can be estimated by use of the lumped mass method as follows⁴,

$$\Delta T = \frac{E}{\rho C_p V} = \frac{E}{\rho C_p A t} = \frac{\text{Energy Density}}{\rho C_p t} \quad \text{Eq. (18)}$$

where ρ , C_p , and t are the density, the heat capacity and the ink film thickness.

Using the thermal properties of the materials provided in Table 3, sintering produces an increase in the copper, PET and glass film temperatures to 297, 43.5 and 8.9 °C, respectively. Since the PET and glass are both poor thermal conductors, as shown in Table 6, the copper plays an important role in the adhesion between the substrates by melting the substrate at the ink interface. For the glass, there was only 8.9 °C increase in temperature, which is about 5 times lower than that of the PET. This temperature difference explains the poor adhesion of the copper to glass in comparison to the PET.

Table 6. Thermal Properties of Materials^{317,18}

Material	Thermal conductivity (W/mK)	Heat capacity (J/g/K)	Density (g/cm ³)	Melting temperature (°C)
Copper	170	0.386	8.71	1084
Polyethylene terephthalate (PET)	0.14	1.3	1.39	255
Glass	0.01	0.768	2.38	No data

Conclusion

In order to sinter the nano copper ink printed onto a PET film under ambient conditions, an Intensive Pulsed Light (IPL) treatment was applied. The effect of inkjetting conditions and sintering, without preheating, was studied. The relationship between ink film thickness and required energy for sintering the nano copper ink particles was determined. SEM micrographs of the sintered copper ink film show the bridging of the ink particles. The amount of bridging present increased with the amount of energy applied. Overexposure of the samples to the Xenon lamp resulted in damage to the printed samples and loss in electrical properties. The influence of the thermal conductivity properties of the substrate on sintering energy requirements for the nano copper ink was also determined by use of the lumped mass method.

References

- 1 B. K. Park, D. J. Kim, S. H. Jeong, J. H. Moon, J. S. Kim, Thin Solid Films 515, 7706-7711, (2007).
- 2 T. Cuk, S. M. Troian, C.M. Hong, S. Wagner, Appl. Phys. Lett. 77 2063 (2000).
- 3 H. S. Kim, S. R. Dhage, D. E. Shim, Appl. Phys. A 97: 791-798 (2009).
- 4 D. J. Kim, J. H. Moon, Electrochem. Solid-State Lett. 8 (11), J30-J33, (2005).
- 5 S.H. Ko, H. Pan, C. P. Grigoropoulos, C. K. Luscombe, M.J. Frechet, D. Poulikakos, Appl. Phys. Lett. 90, 141103 (2007).
- 6 W. S. Han, J. M. Hong, H. S. Kim and Y. W. Song, Nanotechnology 22 395705 (6pp), (2011).
- 7 Owens D. K., Wendt R. C., "Estimation of the Surface Free Energy of Polymers", J. Appl. Pol. Sci., 13 (1969), p1741
- 8 Reis, N. Ainsley, C. Derby, B. Ink-jet delivery of particle suspensions by piezoelectric droplet ejectors. J. Appl. Phys., 97(9), 094903-6, (2005).
- 9 http://xenoncorp.com/uv_spectrums.html
- 10 V. Fakhfouri, G. Mermoud, J. Y. Kim, A. Martinoli and J. Brugger, "Drop-On-Demand Inkjet Printing of SU-8 Polymer", Micro and Nanosystems, 1, 63-67, (2009).
- 11 V. Fakhfouri, G. Mermoud, J. Y. Kim, A. Martinoli, and J. Brugger, Micro and Nanosystems, 1, 63-67, (2009).
- 12 http://www.rheologyschool.com/cross_model.html
- 13 C. Ton-That, D.O.H. Teare, P.A. Campbell, R.H. Bradley, Surf. Sci. 433, 278, (1999).
- 14 T. Young, in Miscellaneous Works, G. Peacock, ed., J. Murray, London, 1855, Vol. I, p. 418.

- 15 P. S. de Laplace, *Mechanique Celeste*, Supplement to Book 10, 1806.
- 16 By private correspondence with Ray Hathaway, Xenon Corporation.
- 17 http://www2.dupont.com/Displays/en_US/products_services/films/PET_films.html
- 18 http://psec.uchicago.edu/glass/Corning_Eagle_XGdisplayglass.pdf

CHAPTER V

CONCLUSION

This study examined the inkjettability and print quality of materials important to the fabrication of OTFTs using a Dimatix DOD inkjet printer. In order to understand jetting evolution based upon ink characteristics, simulations were performed with nano copper and nano particle silver inks. To predict the inkjettability of the nano copper ink, the Z and Oh numbers were determined at different temperatures. The results from the simulation studies correlated well to the experimental results.

For semiconductor material interests, the inkjettability and print quality of two organic semiconductors, P2TDC17FT4 (poly[(3,7-diheptadecylthieno[3,2-b]thieno[2',3':4,5]thieno[2,3-d]thiophene-2,6-diyl)[2,2'-bithiophene]-5,5'-diyl] dissolved in 1,2-dichlorobenzene and P3HT (poly-3 hexylthiophene) were compared. The relationships between drop speed, drop volume and firing voltage, as well as the influence of drop spacing and substrate temperature on print quality were examined. Through this work, a fully inkjet printed top gate OTFT was accomplished. The performance of the P2TDC17FT4, printed under ambient conditions, has important implications to the realization of low cost fully printed OTFTs.

As a post processing study, a nano copper ink was sintered with IPL (Intensive Pulsed Light. Nano copper is of interest due to its low cost in comparison to silver. The focus of this study was to examine the relationship between ink film thickness and energy required for sintering. A comparison of the energy levels required to sinter the nano copper ink on glass and PET showed the glass transfers less energy to the printed ink film than the PET. As a result, the adhesion of the nano copper ink to glass was poorer than found for PET. The thicker the ink film, the more energy required to sinter the ink particles. SEM photographs verified the sintering of the nano copper ink particles on PET.

Overall, understanding jetting behavior of functional ink through simulation would be essential in order to use inkjet technology in fabrication of OTFTs. Especially, researching the deposition of inks used in fabricating OTFTs would take critical portion to improve the performance and fabrication of OTFT structure. Moreover, technology regarding sintering nano copper ink as an alternative material to noble inks, with IPL system in ambient condition is able to advance the use of material in OTFTs. Therefore, the findings of this research improve the current understanding of the material property needs and challenges to attaining a fully printed OTFT.

APPENDIX

LIST OF PUBLISHED WORK

- I S. M. Lim, P. D. Fleming and M. K. Joyce, “A Study on the Jetting Evolution of Nano Copper Ink and Nano Particle Silver Ink with Inkjet”, Revised for JIST, June, 2012.
- II S. Lim, M. K. Joyce and B. Bazuin. “Inkjet Printability of an Ambient Stable Organic Semiconductor”, in preparation.
- III S. M. Lim., M. K. Joyce and P. D. Fleming, “A Study on the Jetting Evolution of Nano Copper Ink and Nano Particle Silver Ink with Inkjet”, Proceedings of the IS&T DF12 Conference, Sept. 9-13, 2012.
- IV J. T. Youn and S. M. Lim “Computer simulation of dot formation on paper in the gravure”, Korean Society for Imaging Science and Technology, Vol. 14 (1), pp. 62 ~ 70, (2008)
- V S. M. Lim, J. T. Youn, Y. S. Lee, and Y. B. Seo and J. Yang, “ A study on the printability of paper made from red algae pulp (RAP)”, J. Korea Printing Society, ISSN : 1229-4012, pp.129 ~ 134, (2008)
- VI S. M. Lim, J. T. Youn and K. H. Kim, “Computer simulation of ink flow in the conventional gravure cell”, J. Korea Printing Society, vol 25(1), pp. 109 ~ 120, (2007)
- VII S. J. Park , S. M. Lim and J. T. Youn, “ Simulation of ink transfer in the printing nip”, J. Korea Printing Society, vol 25(1), pp. 53 ~ 64, (2007)
- VIII J. S. Mok, J. T. Youn and S. M. Lim, “ A study on the void free vacuum printing method in PCB ”, submitted to Korean Society for Imaging Science and Technology

Paper I focuses on understanding jetting evolution of nano copper and nano particle silver inks with simulation. The results from the simulation studies correlated

well to the experimental results. To predict the inkjetability of these inks, the Z and Oh numbers were determined at different temperatures.

Paper II considers the inkjetability and print quality of two organic semiconductors, P2TDC17FT4 (poly[(3,7-diheptadecylthieno[3,2-b]thieno[2',3':4,5]thieno[2,3-d]thiophene-2,6-diyl)[2,2'-bithiophene]-5,5'-diyl] and P3HT (poly-3 hexylthiophene). The relationships between drop speed, drop volume and firing voltage, as well as the influence of drop spacing and substrate temperature on print quality were examined. Through this work, a fully inkjet printed top gate OTFT was accomplished.

Paper III deals with sintering a nano copper ink with IPL (Intensive Pulsed Light). The thicker the ink film, the more energy required to sinter the ink particles. And, a comparison of the energy levels required to sinter the nano copper ink on glass and PET showed the PET showed the glass to transfer less energy to the printed ink film. As a result, the adhesion of the nano copper ink to glass was poorer than found for PET.

Paper IV shows how the ink in a gravure cell is transferred to the substrate (paper) with three-dimensional transient methods on the Navier-Stokes equation. Especially, the effect of printing speed of gravure on the transfer of the ink was researched.

Paper V reported on the printability of paper made from red algae pulp. With studying printability on this paper, the possibility of the paper to be used in printing area was demonstrated.

Paper VI show how the ink contained in the gravure cell is transferred into substrates according to variable size and depth of gravure cell. The importance of this paper is that the amount of ink from cell has a great effect on the quality of final printed products.

Paper VII considers the ink flow in the conventional gravure cell. Various nip pressure and speed applied into the gravure cell was simulated to predict ink transfer from the ink cell with poly-flow simulation software and the results was compared to the results gained through experiments with IGT printability tester.

Paper VIII focuses on printing PCB with “dry printing” method newly developed from screed printing. Using this system has great potential to reduce materials and printing steps required for printing PCB.